Optimizing High Density Lipoprotein Compositions for Modulation of Vascular Inflammation.

by

Emily Morin

A dissertation submitted in partial fulfillment
of the requirements for the degree of
Doctor of Philosophy
(Pharmaceutical Sciences)
in the University of Michigan
2019

Doctoral Committee:

Associate Professor Anna Schwendeman, Chair
Professor Y. Eugene Chen
Associate Professor Wei Cheng
Associate Professor James J. Moon

Emily Morin

emmorin@umich.edu

ORCID iD: 0000-0001-5253-2074

© Emily Morin 2019

Dedication

To my late grandparents, Ray and Milly. Thank you for always reminding me that I can, indeed, do anything I set my mind to.

With love, always.

Acknowledgements

First and foremost, I would like to thank my parents, Daniel and Nan Morin. Without the unconditional love and support you have demonstrated throughout my life I would not be here today. Thank you for always pushing me to be my best, even when I wanted to give up. I would also like to thank my step-mother, Nancy, for loving me like her own; your strength has inspired me. And to my sister, Stephanie. I cannot imagine going through life with anyone else. Thank you for always having my back. Finally, to my grandparents, Ray, Milly, Eleanor, Robert, and my dear friend Margueritte for inspiring me to change the lives of others through science.

Next, I would like to extend great thanks to my mentor, Dr. Anna Schwendeman. The last five years have been filled with laughter, life advice, and of course science. You are a true role model, and now, someone I am glad to call a friend. Thank you for believing in me. I would also like to thank the rest of my committee; Dr. Y. Eugene Chen, Dr. Wei Cheng, and Dr. James Moon for their time and invaluable guidance throughout the course of my research, as well as Dr. Steven Schwendeman for his thoughtful input throughout my studies.

I would also like to thank the College of Pharmacy and NIH for funding me over the course of my studies, as well as our collaborators and lab members for all of their help and support. First, to our collaborators Dr. Yanhong Guo for her guidance with cardiovascular studies and Dr. Xiang-An Li at the University of Kentucky for his contributions to our sepsis work. Second, I would like to thank Dr. Wenmin Yuan for her

mentorship which was instrumental throughout my doctoral studies—I will miss sharing my lab bench with you. And of course, to my lab managers, Rose Ackermann and Karl Olsen, without whom my research would have never been possible. It has been a pleasure working with and getting to know you over the past five years and I will truly miss our conversations. And to the members of the Schwendeman group(s), past and present, thank you for making the lab a fun and enjoyable place to be: Dr. Dan Li, Sang Kim, Jukyung Kang, Minzhi Yu, Alexander Benet, Maria Fawaz, Lindsay Scheetz, Jia Zhou, Jenna Walker, Justin Hong, Jason Albert, Jenny Shenkar, Dr. Hiren Patel, Dr. Yayuan Liu, Dr. Ling Mei, Dr. Hongliang He, Dr. Jie Tang, Dr. Wenmin Yuan, Dr. Rui Kuai, Dr. Gergely Lautner, Dr. Tina Li, Dr. Karthik Pisupati, Dr. Morgan Giles, Dr. Amy Doty, Dr. Max Mazzara, Dr. Rae Sung Chang, Dr. Brittany Bailey, and Dr. Kari Nieto. I have learned so much from you all and wish you the best of luck in your careers.

Finally, I would like to thank everyone who has made my time in Ann Arbor so special; I would never have made it through grad school without you. I would especially like to thank my dear friends, Alex Yu, Xiaole Sun, Phil Rzeczycki, Patrick Sinko, Morgan Giles, Lindsay Scheetz, and Allyson Job. I am so happy to have met all of you. To my boyfriend, Joe, for all of your support, encouragement, and reminders that you still have more degrees than I. To the Humane Society of Huron Valley for allowing me the opportunity to pursue my passion of animal rescue. And finally, anyone who knows me knows that I could not go on without acknowledging my babies, Stella, Lucy, and Flash. I know my lab mates will all miss the daily cat stories, endless photos, and my high-pitched voice when talking about you. You are the loves of my life.

Table of Contents

Dedication ii

Acknowledgements iii

List of Figures vii

List of Tables xi

Abstract xii

Chapter 1: Introduction 1

1.1 High-Density Lipoproteins 1

1.2 HDL Structure and Composition 2

1.3 Physiological Roles of HDL 8

1.4 Disease Implications 15

1.5 Synthetic HDL: Peptides, Particles, and Clinical Evaluation 18

1.6 Research Scope 25

1.7 Thesis Overview 25

Chapter 2: Synthetic high-density lipoprotein—A potential therapy for sepsis 28

2.1 Abstract 28

2.2 Introduction 29

2.3 Materials and Methods 31

2.4 Results 42

2.5 Discussion 59

2.6 Supplemental Information 65

Chapter 3: Synergetic effect of rHDL and LXR ligand co-administration on induction of cholesterol efflux and reduction of atherosclerosis. 67

3.1 Abstract 67

3.2 Introduction 68

3.3 Materials and Methods 70

3.4 Results 76

3.5 Discussion 87

Chapter 4: Synthetic high-density lipoproteins containing sphingosine-1-phosphate for modulation of endothelial function 94

4.1 Abstract 94

4.2 Introduction 95

4.3 Materials and Methods 98

4.4 Results 102

4.5 Discussion 113

Chapter 5: Conclusions and Perspective 117

Bibliography 122

List of Figures

Figure 1-1 HDL Subclasses. HDL is highly heterogeneous and can be classified based on shape **(A),** apolipoprotein content **(B),** density and size **(C),** and electrophoretic mobility **(C, D).** Figure taken from [25]..... 6

Figure 1-2 Reverse Cholesterol Transport (RCT) pathway. The process involves the formation of discoidal HDL **(1),** formation of cholesterol esters by LCAT **(2),** transfer of cholesterol esters and triglycerides between HDL and LDL/VLDL **(3),** uptake of cholesterol by the liver **(4),** and secretion of cholesterol into the bile **(5).** Figure taken from **[19]** 9

Figure 2-1 Septic patients have lower HDL levels, which is associated with poor survival. At time of intake (Day 0), there is a significant difference between plasma concentrations of HDL-C (**A**) and ApoA-1 (**B**) in expired sepsis patients versus non-sepsis controls. Patients entering the ICU with HDL-C levels <10 mg/dL had a higher incidence of death than those with HDL-C levels >10 mg/dL (**C**); those with ApoA-1 levels <30 mg/mL also had a higher incidence of death than those with ApoA-1 >30 mg/mL (**D**); HDL-C (**E**) and ApoA-1 (**F**) levels over 14 days in septic patients with HDL-C <10 mg/dL at day 0; statistical significance determined by one-way ANOVA with Tukey's multiple comparison test. 44

Figure 2-2 sHDL preparation and characterization. Schematic of sHDL preparation procedure (**A**); Transmission electron microscopy (TEM) image shows nanosized, discoidal sHDL particles (**B**); gel permeation chromatography (GPC) profile of sHDL indicates >99% purity (**C**); Size distribution of sHDL particles is 10.43 ± 3.28 nm with a PDI of 0.112 as determined by dynamic light scattering (DLS) (**D**). 46

Figure 2-3 sHDL protects CLP-induced animal death and attenuates CLP-induced organ injury and inflammatory cytokine production. B6 mice were subjected to CLP (21G needle, 2/3 ligation). 2h post CLP, mice were treated with 100 μl of PBS or sHDL containing 7.5 mg protein/kg body weight (i.v.). Plasma and lung were collected 18 h post CLP and HDL was prepared by sequential ultracentrifugation (1.5 ml plasma from 5 mice were used to make one HDL preparation); HDL-cholesterol concentrations (**A**); 7d Survival (**B**); Body temperature (**C**). Organ injury was detected by quantifying plasma ALT (**D**), lung wet/dry ratio (**E**), and plasma BUN (**F**). Plasma cytokines TNF-α **(G**), IL-6 (**H**) and IL-10 (**I**) were quantified with ELISA kits. 48

Figure 2-4 Modeling of sHDL binding to endotoxins. The initial state of the lipid-only particle (**A**), all lipid (colored in cyan) are randomly distributed. The positively charged choline head and the negatively charged phosphoric acid group are colored in blue and gold, respectively. The X, Y, and Z axes of the coordination system are showed by red, green, and blue arrows, respectively. The final state of lipid-only particle (**B**), its self-assembly to a discoid nanodisc in 3 μs simulation. The hydrophilic surface of the Nanodisc is aligned with XY plane. LTA (**C**) and LPS (**D**) are showed in stick-ball style and colored in red and can insert into the lipid-only particle. The initial state of ETC-642 particle (**E**) , 22A peptides are showed in cartoon style and colored in green. ETC-642 particle also forms a nanodisc (**F**)

with all peptides arranged around the lipid. LTA (**G**) and LPS (**H**) can also insert into the ETC-642 particle, however, they favorably localize near the 22A peptides. PMF calculated binding free energy of (**I**) LTA and (**J**) LPS binding with lipid-only (blue) or ETC-642 particle (red) show ETC-642 particles have more favorable binding energy for both LPS and LTA over lipid-only particle. 50

Figure 2-5 sHDL suppresses LPS/LTA/TNF-α-induced NF-κB activation. HEK-Blue cells expressing TLR4, TLR2 or TNF-α receptors were cultured to 70% confluency and treated with LPS at 1ng/ml (**A** and **B**) or LTA (**D**) in the presence of sHDL ETC642 for 16 hours. Alternatively, cells were pre-treated with sHDL ETC642 at 60 µg/ml for 6 h and stimulated with the corresponding ligands (**C** and **E)**. Then, 100µl of the culture supernatant was mixed with 100µl HEK-Blue™ Detection and the activation of NF-κB reporter was quantified by measuring absorption at 650nm. Data was analyzed by one-way ANOVA (**B and D**) or student's t-test (**C and E**). 52

Figure 2-6 sHDL suppresses LPS and LTA-induced cytokine production in macrophages. Raw 264.7 cells were cultured to 70% confluency and treated with LPS (**A** and **B**) or LTA (**C**) in the presence of sHDL ETC-642 for 16 hours. The concentrations of TNF-α and IL-6 in the supernatant were measured by ELISA. 54

Figure 2-7 sHDL inhibits LPS/TNF-α-induced endothelial cell activation and inflammatory cytokine production. Human umbilical vein endothelial cells (HUVEC) were treated with LPS in the presence of sHDL at the concentrations indicated in the figure. Fold change in gene expression of VCAM-1 (**A**), ICAM-1 (**B**), E-selectin (**C**), and eNOS (**D**) were determined by RT-qPCR and normalizing to endogenous GAPDH expression. Concentrations of cytokines IL-6 (**E**) and IL-8 (**F**) in the supernatant were measured by ELISA. 56

Figure 2-8 sHDL suppresses TLR4 lipid raft targeting. For (**A**) and (**B**), RAW 264.7 cells were cultured to 70% confluency and pre-treated with sHDL at 60 µg/mL for 12 h, stimulated with LPS at 2 ng/ml (k12) for 10 min. (**A**) The cells were harvested and the subcellular fractions were isolated with Opti-Prep method and TLR4 or SR-BI in each fraction was analyzed by Western blot. Post-nuclear supernatant (PNS), cytosol (CYT), intracellular membrane (IM), plasma membrane (PM) and lipid raft (LR) fractions. (**B**) Cells were harvested and total cellular cholesterol was extracted and quantified using Wako Diagnostics total cholesterol reagent kit using the FPLC method. (**C-D**) RAW 264.7 cells were loaded with [^{3}H]-cholesterol for 24 hours followed by incubation with sHDL for 18 h at 0, 15, 30, 60, or 120 µg/mL (**C**) or 6h incubation with sHDL or 22A peptide at 15 µg/mL (**D**) . Percent cholesterol efflux was determined by dividing radioactive counts in media by the sum of counts in media and cellular fraction. Average blank values were subtracted to yield net cholesterol efflux due to sHDL; data are expressed as mean +/- SD. 58

Figure 3-1 sHDL reduces ABCA1 and ABCG1 expression in vitro. J774A.1 murine macrophages treated for 24 h with clinically-mimicking rHDLs CER-001 (ApoA-I-SM 1:2.7 w/w), CSL-112 (ApoA-I-POPC 1:1.5 w/w), or ETC-642 (22A-DPPC-SM 1:1:1 w/w) exhibit decreased levels of ABCA1 (**A**) and ABCG1 (**B**) mRNA relative to PBS treated controls, as measured by RT-qPCR. sHDL concentration is expressed in terms of peptide or protein. Data represented as mean ± SEM. *p<0.05. 77

Figure 3-2 Effect of sHDL individual components on ABCA1 and ABCG1 expression in vitro. ABCA1 and ABCG1 expression in J774A.1 murine macrophages treated for 24 hr with

22A peptide or ApoA-I protein (**A-B**) or lipid emulsions of SM, DPPC, or POPC (**C-D**). Effect of peptide/protein and lipid composition on whole-particle induced ABCA1 and ABCG1 expression probed by incubating J774A.1 cells for 24 hr with rHDL prepared from either 22A peptide or ApoA-I protein complexed with SM, DPPC, or POPC lipids (all at 1:2 protein:lipid ratio by weight) (**E-F**). Expression values were determined relative to PBS treated controls. Data represented as mean ± SEM. *p<0.05 79

Figure 3-3 Effect of LXR agonist on ABCA1 and ABCG1 expression and cholesterol efflux in vitro. Levels of ABCA1 and ABCG1 mRNA in J774A.1 murine macrophages (**A-B**) treated with different combinations of rHDL (100 µg/mL), T1317 (1 µM), GW3965 (1 µM), or LXR623 (1 µM) for 24 hours. ABCA1 protein levels in J774A.1 macrophages were determined by Western Blot following 24h incubation rHDL (100 µg/mL 22A) in the presence/absence of T1317 (1 µM) (**C**). [^{3}H]-cholesterol efflux to sHDL acceptor (50 µg/mL) in J774A.1 cells incubated with or without T1317 (1 µM) for 24 hr (**D**). Data are expressed as mean ± SEM. *p<0.05, **p<0.001. 82

Figure 3-4 sHDL/T0 co-administration effect on ABCA1/ABCG1 expression in vivo. Macrophages were elicited I.P. in C57BL/6J mice with 3% thioglycolate broth for 48 hr prior to administration of PBS, rHDL (50 mg/kg), T1317 (5 mg/kg), or rHDL+T1317 (50 mg/kg and 5 mg/kg, respectively). Macrophages were collected 24 hr post-dose and ABCA1 (**A**) and ABCG1 (**B**) expression were calculated relative to PBS control. **p<0.01. 84

Figure 3-5 sHDL-T1317 anti-atherosclerosis effect in ApoE$^{-/-}$ mice. ApoE $^{-/-}$ mice were fed a high fat/high cholesterol diet to induce atherosclerosis prior to treatement. At week 7, animals were dosed by I.P. injection 3 times weekly for a duration of 6 weeks with PBS, rHDL (30 mg/kg), rHDL+T1317 (30 mg/kg rHDL and 1.5 mg/kg T1317), or T1317 (1.5 mg/kg). At the end of treatment mice were sacrificed and aortas were fixed and sectioned for plaque area visualization by Oil Red O staining (**A-D**). Plaque area was quantified using ImageJ (**E**). 85

Figure 3-6 Liver safety biomarkers following anti-atherosclerosis therapy. Liver safety biomarkers in ApoE$^{-/-}$ mice following 6 weeks of anti-atherosclerosis therapy with PBS, rHDL (30 mg/kg), rHDL + T1317 (30 mg/kg + 1.5 mg/kg, respectively), or T1317 (1.5 mg/kg) were measured. Activity of liver enzymes alanine aminotransferase (ALT) and aspartate aminotransferase (AST) were determined in the plasma (**A-B**), and gene expression of sterol response element binding protein 1 (SREBP1) and fatty acid synthase (FASN) were determined in liver lysates (**C-D**). *p<0.05, ***p<0.001 86

Figure 3-7 ABCA1 and ABCG1 expression in ApoE$^{-/-}$ mice after anti-atherosclerosis therapy. ABCA1 and ABCG1 expression in ApoE$^{-/-}$ mice following 6 weeks of anti-atherosclerosis therapy with PBS, rHDL (30 mg/kg), rHDL+T1317 (30 mg/kg + 1.5 mg/kg, respectively), or T1317 (1.5 mg/kg) were measured in the aortas (**A-B**) and livers (**C-D**) 48 hr after administration of the final treatment dose. 91

Figure 4-1 Characterization of sHDL containing S1P. sHDL was prepared with 22A peptide complexed with either POPC (**A,D**), DMPC (**B,E**), or DPPC (**C,F**) lipids at a 1:2 peptide:lipid weight ratio, containing 0, 0.05 (S1P-sHDL #1), 0.5 (S1P-sHDL #2), or 5 (S1P-sHDL #3) µM of sphingosine-1-phosphate. Dynamic light scattering was used to measure particle size (**A-C**) and gel permeation chromatography with detection at 220 nm was used to measure particle purity (**D-F**). Particles were imaged by TEM for further analysis of size and morphology (**G-I**). 105

Figure 4-2 sHDL toxicity screening in endothelial cells and macrophages. Primary human endothelial cells (HUVEC) or RAW 264 murine macrophages were incubated for 24 h in the presence of sHDL made from DMPC (purple bars) or DPPC (green bars) lipids containing 0, 0.05 (S1P-sHDL #1), 0.5 (S1P-sHDL #2), or 5 (S1P-sHDL #3) μM of sphingosine-1-phosphate. Cell viability was measured by MTS reagent and PBS-treated controls were set to 100%. Data is reported as mean ± SEM. 106

Figure 4-3 sHDL containing S1P promotes endothelial cell integrity through NO release via eNOS. Primary human endothelial cells (HUVEC) were incubated for 15 min with sHDL containing 0 (sHDL), 0.05 (S1P-sHDL #1), 0.5 (S1P-sHDL #2), or 5 (S1P-sHDL #3) μM. Nitric oxide release was quantified by ozone chemiluminescence measurement of nitrite in the media (**A,B**). Transendothelial electric resistance (TEER) was monitored over 48 h in HUVECs treated with sHDL or S1P-sHDL (**C**). eNOS activation in HUVECs treated with sHDL or S1P-sHDL was measured by Western blot for eNOS and phospho-eNOS-Ser1177 and normalized to GAPDH housekeeping control (D). Data are reported as mean ± SEM. *p<0.05 vs. PBS control; **p<0.01; ***p<0.001; #p<0.05 vs sHDL..... 109

Figure 4-4 sHDL containing S1P inhibits endothelial cell activation induced by LPS. Primary human endothelial cells (HUVEC) were pretreated with PBS, sHDL (0.2 mg/mL), S1P-sHDL (0.2 mg/mL sHDL and 0.1 μM S1P), or HSA-S1P (0.1 μM S1P) for 18 h, then challenged with (+) or without (-) LPS (1 μg/mL) for 6 h. mRNA levels in lysates were determined by RT-PCR and normalized to PBS (-) using the ddCt method (**A-D**). Cytokine levels in the supernatants were measure by ELISA (**E,F**). Data are represented as mean ± SEM. **p<0.01 vs PBS (+)..... 112

List of Tables

Table 1-1 Mimetic peptides of ApoA-I: sequences and desired clinical applications. 19

Table 1-2. Summary of findings from rHDL infusion clinical trials. Adapted from [106]..... 22

Table 2-1 Demographic and clinical characteristics of the patient population. 65

Table 2-2 ITC experiments data for different particle-LPS mixtures. The ΔH between ETC642-LPS and Lipids-LPS mixtures in 37°C is -16.31 kcal/mol..... 66

Table 3-1 Plasma lipid markers. Total cholesterol (TC), HDL-cholesterol (HDL-C), LDL-cholesterol (LDL-C), and triglycerides (TG) were measured in plasma collected from ApoE$^{-/-}$ fed a high fat/high cholesterol diet for 6 weeks followed by treatment with PBS, rHDL (30 mg/kg), rHDL+T1317 (30 mg/kg + 1.5 mg/kg, respectively), or T1317 (1.5 mg/kg) for 6 weeks. Blood was collected 48 hr following the administration of the final dose. Data are expressed as mean ± SEM. 92

Table 3-2 Primer sequences used for RT-PCR assays. 93

Table 4-1 Summary and comparison of size and purity of S1P-containing sHDL made from different phospholipids. sHDL was prepared with 22A peptide complexed with either POPC, DMPC, or DPPC lipids at a 1:2 peptide:lipid weight ratio, containing 0 (Blank), 0.05 (S1P #1), 0.5 (S1P #2), or 5 (S1P #3) μM of sphingosine-1-phosphate. Dynamic light scattering was used to measure particle size and gel permeation chromatography with detection at 220 nm was used to measure particle purity. Data represented at mean ± SEM. 107

Abstract

Synthetic high-density or reconstituted lipoproteins (sHDL/rHDL) are a novel class of therapeutics being developed for treatment of cardiovascular disease (CVD). Designed to mimic the athero-protective function of endogenous HDL, sHDLs are composed of apolipoprotein A-I (ApoA-I) protein complexed with phospholipids to form 8-10 nm nanodiscs. In clinical trials, rHDL infusions were shown to reduce atheroma volume, improve endothelial function and reduce systemic inflammation in patients. Known as the “good” cholesterol, endogenous HDL asserts its athero-protective properties through efflux of cholesterol from atheroma macrophages and maintaining vascular integrity. Given their proven safety in humans, we proposed that optimizing HDL infusion therapies for treatment of vascular dysfunction, specifically in the context of CVD and sepsis, could be an effective and rapidly translatable therapeutic approach.

In the first study we investigated the use of sHDL infusions as a potential therapy for sepsis. Given that multiple factors contribute to sepsis, targeting an endogenous factor with multi-protective effects against endothelial dysfunction may present a novel approach for sepsis therapy. Interestingly, we observed that HDL levels were 45% lower in septic patients compared with non-septic patients. To explore the significance of this finding, we tested the efficacy of sHDL in a murine cecal ligation and puncture model of sepsis. sHDL treatment significantly increased plasma HDL-cholesterol levels, improved 7d survival rate by nearly 40%, and decreased plasma BUN, IL-6 and IL-10 levels. *In vitro*, sHDL neutralized LPS/LTA, suppressed NF-kB signaling and inhibited endothelial

activation. Together, our findings suggest that sHDL therapy can be an effective therapy for sepsis.

In the second study, we investigated the potential synergetic effect of co-administering sHDL and a liver X receptor (LXR) agonist on atherosclerosis reduction. We hypothesized that synergy could exist due to the abilities of 1) LXR agonists to increase expression of cholesterol transporters ABCA1 and ABCG1 in foam cells, 2) sHDL to act as a functional cholesterol acceptor, and 3) LXR agonist to overcome sHDL-induced reduction of ABCA1/G1 expression. We show that strong dose-dependent reduction in ABCA1/G1 expression after sHDL treatment can be reversed *in vitro* by co-administering the LXR agonist T0901317 (T1317). In atherosclerotic mice, sHDL + T1317 combination therapy significantly reduced atheroma burden compared to vehicle-treated controls, while neither sHDL nor T1317 alone had a significant effect. Together, we show that synergetic effect of sHDL and LXR could lead to the lowering of minimal effective doses for each therapeutics resulting in reduction of side effects and lowering barriers for clinical translation.

Finally, we incorporated sphingosine-1-phosphate (S1P), a potent anti-inflammatory signaling lipid, in sHDL particles to improve endothelial delivery and barrier function. *In vitro*, S1P-sHDL treatment increased transendothelial electric resistance and induced a dose-dependent release of nitric oxide. Furthermore, S1P-sHDL was able to dampen endothelial activation after inflammatory insult, inhibiting expression of adhesion molecules and IL-6 and IL-8 pro-inflammatory cytokine production. Given these promising data *in vitro*, S1P-sHDL presents a viable strategy

for the delivery of S1P in an HDL-directed manner, warranting further evaluation *in vivo* for the treatment of endothelial dysfunction.

The findings from these studies have allowed us to develop a more comprehensive understanding of the role that HDL plays in inflammation and vascular disease, consequentially enabling us to rationally design sHDL formulations for potential treatment of inflammatory disorders including atherosclerosis and sepsis.

Chapter 1: Introduction

1.1 High-Density Lipoproteins

High-density lipoproteins (HDL) are small, nanosized protein-lipid particles that circulate throughout the body. Of its main physiological functions, HDL is most notably known for its role in cholesterol mobilization and inflammation. HDL, through a pathway known as reverse cholesterol transport, removes cholesterol from peripheral cells and transports it to the liver for excretion in the bile or transport to the adrenals, testes, or ovaries for hormone production [1-4]. This is particularly important in the case of atherosclerosis, in which HDL is able to accept effluxed cholesterol from overloaded macrophages within the plaques and remove it from circulation. In several clinical investigations, plasma HDL levels were shown to be inversely correlated with the occurrence of CVD, and many patients with severe CVD have very low levels of circulating HDL [5-7]. Thus, HDL has long been sought after as a possible therapy for the reversal of atherosclerosis and other cardiovascular diseases. In particular, synthetic HDL (sHDL) made from phospholipids and synthetic peptides has been investigated as a potential HDL replacement therapy. However, the exact properties of HDL and mechanisms by which it confers its anti-atherosclerotic activities has yet to be elucidated. This is mainly due to the vast heterogeneity and complexity of endogenous HDL.

1.2 HDL Structure and Composition

Lipoproteins are defined as soluble protein-lipid complexes that are synthesized by the liver and circulated throughout the bloodstream where they are involved in many critical metabolic processes. High-Density Lipoprotein (HDL) is an endogenous protein-lipid nanoparticle approximately 8-10 nm in diameter, made up of a membrane-like phospholipid bilayer "belted" by the amphipathic alpha-helical apolipoprotein A1 (ApoA-I). HDL takes on many forms, depending on the state of its maturation, ranging from small discoidal particles to larger spherical particles rich in cholesterol esters and other hydrophobic cargo. Although many apolipoproteins are associated with HDL *in vivo,* such as ApoE, ApoC, and ApoM, ApoA-I is the major protein constituent of both discoidal and spherical HDL [8, 9].

1.2.1 Apolipoprotein A-I

Human ApoA-I is a 243 amino acid protein with an average molecular weight of 28.1 kDa [9, 10]. To date, it is the only lipid-free human apolipoprotein in which there exists a high-resolution crystal structure [9, 10]. The primary sequence consists of four exons and three introns, of which the third and fourth exons encode for the entire protein. ApoA-I is highly alpha-helical in structure, with a predicted 80% of its amino acids taking on this secondary form. In this regard, ApoA-I contains two major alpha-helical domains, as determined by its crystal structure: the N-terminal/central domain, containing a highly-organized antiparallel 4-helix bundle, and the less organized and conservatively substituted C-terminal, consisting of a 2-helix domain [9]. While both the first (residues 44-65) and last (residues 121-186) repeat helices have the greatest lipid affinity, the hydrophobic C-terminus of ApoA-I is thought to be the initiator of lipid

binding, leading to formation of nascent and mature HDL particles endogenously. The overall structure of ApoA-I is depicted as a loosely folded, globular structure in which the N-and C-termini unfold independently, as indicated by the protein's biphasic melting curve[9]. The amphipathic nature of ApoA-I allows the solubilization of these protein-lipid complexes and provides a multifunctionality which enables HDL to interact with molecules of both hydrophobic and hydrophilic nature. This is critical, as HDL is involved in many metabolic processes which require both interaction and binding with other proteins and receptors, as well as transport and exchange of highly hydrophobic materials, such as lipids, hormones cholesterol esters, and triacylglycerides. These key metabolic functions of HDL will be reviewed later.

1.2.2 HDL Lipids

The lipid species present in HDL are important not only for providing overall structure to HDL but are also substrates for a variety of receptors and enzymes associated with HDL and its metabolic properties. Although we will simplify the lipid composition of HDL in this proposal, it should be recognized that endogenous HDL is a highly heterogeneous and can contains hundreds of different lipid species as well as steroids, cholesterol esters (making up 30-40 wt% of total HDL lipid), and triacylglycerides. That being said, however, phospholipids still predominate the HDL lipidome, accounting for 40-60 wt% of total HDL lipid [11]. Of the phospholipids, phosphatidylcholines (PC) are by far the largest population of HDL lipids, making up 33-45 wt% of total HDL lipid. Other phospholipids present in HDL include lysophosphatidylcholines (lyso PC), phosphatidylethanolamines (PE),

phosphatidylinositols (PI), phosphatidylserines (PS), phosphatidylglycerols (PG), plasmologens, cardiolipin, and phosphatidic acids.

In addition to PCs, sphingolipids make up roughly 5-10 wt% of total HDL lipid [11]. Sphingolipids, including sphingomyelin, ceramides, sphingosylphosphorylcholine, and sphingosine-1-phosphate, are important structural and signaling components of HDL, although they constitute only a minor portion of the overall lipid population. Of recent particular interest are both sphingosine-1-phosphate and ceramide, which are potent signaling lipids shown to be key players in HDL's ability to modulate inflammation.

1.2.3 HDL Formation and Solubilization

Nascent HDL is discoidal in nature, approximately 8-10 nm in diameter and 4.4 nm in thickness[9, 12, 13]. There are roughly 2 ApoA-I molecules per every 100 phosphatidylcholine (PC) molecules [14], although this number can greatly vary depending on the lipid nature of the HDL. The process of solubilization begins with lipid-free or lipid-poor ApoA-I, known as pre-β HDL, and a phospholipid bilayer structure. The rate of conversion to HDL is greatest at the gel to liquid-crystal phase transition temperature of the lipid (T_g), as this introduces lattice defects which create sites to which the helices of ApoA-I can bind, destabilizing the lipid bilayer and forming nascent HDL particles. The process of formation can be broken down into three major steps: 1) Initial Contact; 2) Insertion of α-helices; and 3) Rearrangement [9]: 1) Initial contact can be either direct or indirect. In direct contact, the α-helix makes the initial contact at a lattice defect, allowing the reaction to proceed immediately to step 2. Rather, indirect contact involves interaction at a non-defective site, in which case the protein must

diffuse over the surface of the lipid bilayer until it reaches a defective site to which it can bind. This type of initial contact limits the rate to which the reaction can proceed to step two and is known as a slow kinetic phase; 2) Once the protein has interacted with a defective site, the reaction can proceed to step 2, in which the α-helices insert themselves into the defective sites of the bilayer. Like Step 1, Step 2 is rate-determining due to the fast or slow insertion of the helices into the bilayer; 3) The insertion of ApoA-I's α-helices into the bilayer's lattice defects will continue until a critical concentration of ApoA-I α-helices adsorbed into the defects is reached. Upon reaching this threshold, the bilayer is disrupted and spontaneously rearranges to form a more thermodynamically stable nanodisc, in which the phospholipid head groups interface with the aqueous surroundings, while the amphipathic α-helices create an interface to stabilize the hydrophobic lipid side chains and the surrounding aqueous environment.

1.2.4 HDL Subclasses and Remodeling

As stated earlier, HDL is highly heterogeneous and is present in a variety of different forms depending on its size, shape, density, and lipid/protein composition. This is a result of HDL remodeling, which is a continuous process involving several endogenous enzymes. Put simply, HDL can be continually and reversibly recycled between lipid-poor ApoA-I, discoidal HDL, and small/large/larger spherical HDLs. These subsets of HDL are classified into two groups, HDL2 and HDL3, based on their densities [12, 13]. HDL2 is lipid-rich and less dense (1.063-1.125 g/mL) than its HDL3 counterpart, which is dense (1.125-1.21 g/mL) protein-rich in comparison [12]. Both HDL2 and HDL3 can be further divided into 2 and 3 subclasses, respectively, based on their size; HDL3 ranges in size from roughly 7-9 nm in diameter while HDL2 ranges

from about 9-12 nm [12]. To further complicate things, HDL can also be classified according to its surface charge and shape. Spherical, more neutral HDL particles are classified as α-HDL, while nascent, discoidal HDL particles, known as β-HDL, are poorly lipidated and more negative in overall charge (Figure 1).

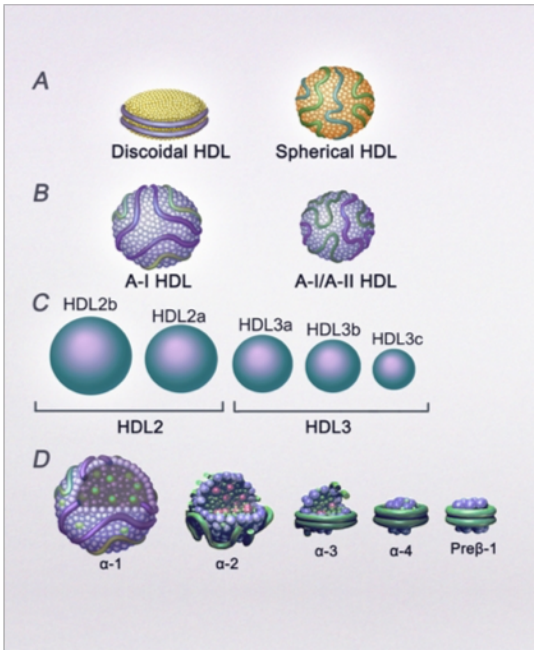


***Figure 1-1 HDL Subclasses**. HDL is highly heterogeneous and can be classified based on shape **(A),** apolipoprotein content **(B),** density and size **(C),** and electrophoretic mobility **(C, D).** Figure taken from [25]*

Initially lipid-poor HDL, pre-β HDL, is converted to α_4-HDL, or discoidal HDL, upon efflux of phospholipids and cholesterol to ApoA-I by the ATP-binding cassette transporter ABCA1. Once formed, α_4-HDL can bind lecithin cholesterol acyltransferase (LCAT) and form spherical α_3-HDL. LCAT is a 60 kDA, 416 amino acid protein which catalyzes a transesterification reaction. In this reaction, an unsaturated fatty acid (FA) is transferred from the sn-2 position of PC to the hydroxyl group of cholesterol via Serine 181 residue, forming cholesterol ester (CE) and Lyso-PC. The hydrophobic CE is buried

within the HDL lipid core, transforming discoidal α_4-HDL to the spherical α_3- and α_2-HDL, known as “mature” HDL, the former being the smaller of the two.

Spherical HDL particles contain not only ApoA-I, but also apoE, which facilitates the growing load of CE into the hydrophobic core since ApoA-I can only facilitate a limited amount of CE in the HDL core. ApoE is also useful in that it is a substrate for Low-density Lipoprotein Receptor (LDLR) and can deliver HDL cargo to hepatic LDLR for biliary excretion. This process will be covered in more detail in the sections to follow.

The process of HDL transformation from disc to sphere is reversible. Enzymes such as cholesterol ester transferase protein (CETP), phospholipid transfer protein (PLTP), hepatic lipase (HL) and endothelial lipase (EL), are all major contributors to these transformations. CETP is involved in the shuttling of CE and triacylglycerols (TAG) between HDL and VLDL. In this process, CETP forms a tunnel between HDL and VLDL which facilitates the exchange of CE from HDL to VLDL and TAG from VLDL to HDL. This exchange destabilizes HDL and causes ApoA-I to dissociate, forming smaller α_2-HDL spheres and pre-β HDL, which can then continue to grow via mechanisms mentioned above [13].

In addition to CETP, both HL and EL are capable of transforming larger HDL spheres into smaller spheres and pre-β HDL. HL is a lipase that hydrolyzes TAG and phospholipids associated with HDL. EL is a phospholipase whose preferred substrate are phospholipids. While TAG lipolysis due to HL encourages ApoA-I dissociation, phospholipid hydrolysis does not. This explains why HL knockout experiments show only a small increase in HDL-C plasma levels, while EL knockout studies show upwards of 50% increase in plasma HDL-C [1, 10].

PLTP, on the other hand, is capable of remodeling spherical HDL into both smaller and larger HDL spheres as well as pre-β HDL. This is due to phospholipid transfer between HDLs, HDL and VLDL, or via fusion of two HDL particles. As a result, PLTP knockout studies show up to a 50% reduction in plasma HDL-C [4, 13].

1.3 Physiological Roles of HDL

1.3.1 Reverse Cholesterol Transport

Reverse cholesterol transport (RCT) comprises the majority of research surrounding HDL to date. RCT, which is outlined in Figure 2, is defined as the process by which cholesterol is mobilized from the peripheral tissue and delivered to either the liver for biliary excretion, or to the adrenals, testes, or ovaries for hormone production [1]. HDL is the major transport vehicle for cholesterol, and defective or deficient levels of HDL *in vivo* are associated with many health complications, including diabetes, atherosclerosis, dyslipidemia, sepsis, and even cancer [15-18]. Cholesterol efflux from peripheral cells can be either active or passive, depending on the transporters involved [9].

The first step in the RCT pathway is cholesterol efflux from peripheral cells, mediated by the membrane-bound ATP-binding cassette A1 or G1 transporters (ABCA1, ABCG1). ABCA1 is a 2,261 amino acid protein consisting of two 6 trans membrane helices that mediate ATPase activity via cytosolic nucleotide binding domains. The two trans membrane domains form a channel by which phospholipids and free cholesterol can be transported from the cytosol to an HDL acceptor. ABCA1 expression is upregulated under cholesterol-rich circumstances. Cholesterol within the

cell is transformed to oxysterols under high cholesterol loading conditions. Increasing oxysterol levels induce activation of the liver X receptor (LXR), which then goes on to activate ABCA1 transcription. The induction of ABCA1 transcription and subsequent expression is crucial in order to prevent buildup of excess cholesterol in the cell, mainly in macrophages, which are quickly transformed into cholesterol-rich, pro-inflammatory "foam cells" which are key participators in development of aortic plaques most commonly associated with atherosclerosis and cardiovascular disease.

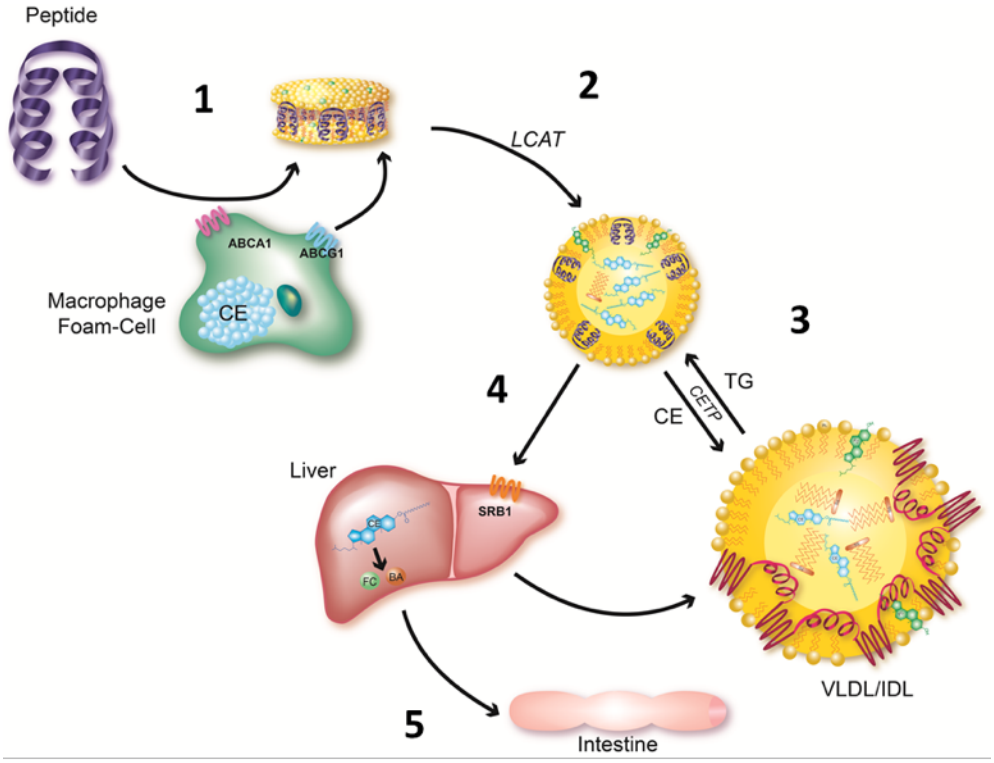


Figure 1-2 Reverse Cholesterol Transport (RCT) pathway*. The process involves the formation of discoidal HDL* ***(1),*** *formation of cholesterol esters by LCAT* ***(2),*** *transfer of cholesterol esters and triglycerides between HDL and LDL/VLDL* ***(3),*** *uptake of cholesterol by the liver* ***(4),*** *and secretion of cholesterol into the bile* ***(5).*** *Figure taken from* ***[19]***

Upon expression, ABCA1 can interact with HDL via ApoA-I binding to the receptor. It is then that free cholesterol and phospholipids can be transferred to the lipid-free or lipid-poor HDL in order to form pre-β or nascent HDL, respectively. Once bound to HDL, cholesterol is esterified by LCAT, which maintains the concentration gradient of free cholesterol between the cell and the plasma to prevent net efflux of cholesterol from reaching equilibrium. The esterified cholesterol is then buried within the hydrophobic core of HDL, and either transferred to LDL or VLDL or taken up by the liver via the scavenger receptor-B1 (SR-B1). If transferred to LDL or VLDL, the cholesterol can then be removed from circulation via low-density lipoprotein receptor (LDLR) uptake in the liver, and subsequently secreted into the bile.

Alternatively, cholesterol can be removed by SR-B1. SR-B1 was the first recognized HDL receptor and is responsible for mediating the flux of both free cholesterol and cholesterol ester between HDL and the plasma membrane [10, 13]. It is an 82 kDa membrane glycoprotein consisting of one large extracellular domain made up of 408 amino acid residues, as well as two trans-membrane domains. The cytoplasmic domain contains a PDZK1 binding motif that is responsible for modulating the relative abundance and localization within the plasma membrane. SR-B1 is expressed in many cell types, but hepatic SR-B1 is primarily responsible for the removal and excretion of cholesterol from circulation. SR-B1 interacts with HDL by recognition of amphipathic α-helices that are present in ApoA-I. That being said, SR-B1 can also accept lipid cargo from LDL and VLDL, as they also consist of amphipathic α-helix-containing lipoproteins, as well as efflux cholesterol from SR-B1 expressing cells, such as macrophages [9].

1.3.2 Modulation of Inflammation

More recently, HDL research has been growing in the field of inflammation. Specifically, HDL has been shown to exert anti-inflammatory properties both *in vitro* and *in vivo* [7, 14, 20-23] and levels of HDL in patients with inflammatory disorders such as sepsis, coronary artery disease, and atherosclerosis have been proven to be prognostic of clinical outcomes [24, 25]. HDL exerts these properties in a variety of manners. First, it can do so via maintaining cholesterol levels within localized cell membrane regions. Additionally, it is able to sequester the bacterial cell wall components LPS and LTA, neutralizing their proinflammatory activity as well as absorbing free radicals via ApoA-I and preventing further oxidation of lipid species in LDL and VLDL. Finally, HDL can modulate inflammation by the many exogenous species it carries, including signaling lipids, the antioxidative enzymes LCAT, PON, CETP, and others.

1.3.3 Cholesterol Efflux

Both HDL particles and the ApoA-I protein stimulate macrophage cholesterol efflux via ABCA1 and ABCG1 transporters, as described in the previous sections. This activity is crucial in maintaining the lipid composition of specialized membrane regions, known as lipid rafts, which house many important signaling proteins. Disruption of cholesterol levels within lipid rafts due to efflux by HDL/ABCA1 delocalizes proteins and reduces their cell surface expression [26, 27]. Therefore, both ABCA1/ABCG1 expression and HDL act as modulators of inflammation by regulating lipid-raft cholesterol levels.

Of the lipid-raft proteins are the Toll-like Receptors (TLR), which are the hallmark receptors of the inflammatory response. TLR4, for example, recognizes and binds

Lipopolysaccharides (LPS), also known as lipoglycan or endotoxin, which are lipid-polysaccharide molecules found in the cell membranes of Gram-negative bacteria [28]. Due to its origin, LPS elicits a potent inflammatory response by immune cells and can amplify this response by inducing TLR4 signaling [28]. Upon binding to LPS, TLR4 initiates a signaling cascade resulting in the increase of pro-inflammatory cytokine production, including TNF- α, interleukins IL-1β, IL-6, IL-8, IL-12 and others. By controlling the cholesterol content in lipid rafts, HDL is able to suppress the inflammatory cytokine cascade initiated by TLR4.

It should be noted that, in addition to delocalizing TLR4 from the plasma membrane, HDL is also able to bind and sequester circulating LPS in the plasma [28]. By doing so, it effectively neutralizes the immuno-stimulatory effect of LPS by inhibiting its ability to interact with TLR4 receptors. Once bound, HDL can then interact with hepatic SR-B1 to induce uptake of LPS by the liver leading to its eventual degradation and bile secretion. In addition to LPS, HDL is also able to sequester lipoteichoic acid (LTA), a cell wall component of Gram-positive bacteria structurally similar to LPS, in a similar manner to that of LPS [26, 28]. In this regard, HDL is a key host defense mechanism against bacterial infection.

1.3.4 Endothelial Function

HDL, in addition to its role in cholesterol efflux, is a potent regulator of endothelial function [24], exerting a wide range of vaso-protective effects. This is especially important, as endothelial dysfunction is one of the hallmarks of cardiovascular disease, atherosclerosis, and sepsis. This is most notably due to HDL’s ability to modulate endothelial nitric oxide synthase (eNOS) localization at the endothelial cell plasma

membrane [23, 29, 30]. eNOS is an important enzyme involved in the production and release of nitric oxide (NO) into the bloodstream [6, 31, 32]. NO causes relaxation of the blood vessels and is often dysregulated in patients with cardiovascular disease [33-35]. In endothelial cells, eNOS is anchored to cholesterol-rich caveola via palmitoylation and myristoylation. During periods of inflammation, oxidized LDL species can disrupt the lipid microenvironment of the caveola, causing delocalization and internalization of eNOS proteins, dampening the concentrations of NO in the blood. HDL is capable of maintaining the lipid environment of the caveola via lipid exchange with co-localized SR-B1 [23, 36]. Additionally, SR-B1 binding activates the Src family kinases PI3K and Akt, which can phosphorylate eNOS at serine 1177, increasing the enzyme's activity [36]. It should be noted that HDL-associated S1P signaling can also induce eNOS activity [37, 38], however it is not known whether this is due to a synergistic effect of both HDL and S1P signaling or whether one pathway is more potent than the other at eliciting this response.

1.3.5 Sphingosine-1-phosphate

HDL is also a carrier of many potent anti-inflammatory species including the signaling lipid sphingosine-1-phosphate (S1P) and the anti-oxidative enzyme paraoxonase-1 (PON1). PON1 is an important biological enzyme that is carried by HDL both prevents and reduces HDL and LDL associated lipid-oxidation through its calcium-dependent paraoxonase and arylesterase activity [39]. While PON1 activity is an essential anti-inflammatory enzyme, for the purposes of this proposal we choose to focus on S1P.

Sphingosine-1-phosphate is a lysosphingolipid present in the circulation at about 200 nM [20], its major carriers being serum albumin (35%) and apolipoprotein M of HDL (55%) [36]. S1P is formed by the hydrolysis of ceramide to form sphingosine, upon which sphingosine kinase phosphorylates sphingosine forming S1P [40]. S1P is then stored within platelets and erythrocytes, which lack S1P lyases and phosphatases that degrade S1P [36]. HDL, along with other acceptors, can then accumulate S1P however the mechanism by which it does so has yet to be elucidated [36]. Of the postulated mechanisms are those involving ABC transporters, specifically ABCC1 and ABCG2 [36], since HDL is well known to interact with other ABC transporters, ABCA1 and ABCG1. Regardless, HDL is the highest known carrier of S1P in the blood and exhibits an array of anti-inflammatory effects in the body.

Although S1P can take on many different biological functions, when bound to HDL it serves as a potent anti-inflammatory signaling lipid that preserves endothelial function, growth, and survival [20, 36]. HDL-associated S1P signaling can occur through 3 different G-protein coupled S1P receptors: the $S1P_1$, $S1P_2$ and $S1P_3$ receptors [36, 41, 42], however $S1P_1$ has been shown to have the greatest anti-inflammatory response in the endothelium. HDL-associated sphingosine-1-phosphate can elicit strong anti-atherogenic responses via $S1P_1$ signaling in endothelial cells, T cells, and macrophages [36]. This occurs, in part, by activation of extracellular signaling-regulated kinase (ERK), AMP-activated kinase (AMPK), and protein kinase B (PKB)/Akt [38, 43]. These signaling cascades lead to decreases in cell adhesion molecule expression, cell permeability, and an increase in NO-dependent vasorelaxation in endothelial cells. In macrophages, these signaling pathways trigger a decreased response to TLRs, lower pro-inflammatory

cytokine production, and an increase in anti-inflammatory cytokine production. A similar trend holds true for T cells, which exhibit a greater anti-inflammatory phenotype [36].

S1P has also been shown to stimulate a pro-inflammatory response under some circumstances, for example, studies both *in vitro* and *in vivo* have presented conflicting evidence for $S1P_3$ signaling, indicating that there may be both pro- and anti-atherogenic signaling cascades initiated by this receptor [38, 44, 45]. S1P has also been shown to have pro-inflammatory activity when freely circulating, but anti-inflammatory activity when bound to HDL or albumin [46, 47], however the current evidence remains to be conclusive. Nevertheless, S1P signaling mechanisms remain a hot topic of interest in the cardiovascular field.

1.4 Disease Implications

1.4.1 Cardiovascular Disease and Atherosclerosis

Cardiovascular disease is the leading cause of death in the western world [48, 49], atherosclerosis being the primary underlying cause of both heart disease and stroke [15]. Atherosclerosis is a chronic inflammatory disorder characterized by the buildup of fatty plaques within the major arteries, leading to endothelial dysfunction, stiffening of the arteries, and development of more serious cardiovascular conditions [15, 50]. While many cases can develop due to genetic pre-disposal, environmental factors such as smoking, lack of exercise, and high-fat diet are some of the major triggers of this disease [15].

The onset of atherosclerosis begins with retention of LDL particles within the sub-endothelial space. Once across the endothelial barrier, LDL becomes trapped by matrix

components and exposed to reactive oxygen species (ROS) that oxidize the lipid components of LDL [15, 50]. The oxidation of lipids induces an increase in expression of cell adhesion molecules, such as VCAM-1, ICAM, MCP-1, P- and E-selectins, as well as pro-inflammatory cytokine production by endothelial cells. This promotes migration and adhesion of monocytes to the vessel wall, where they can infiltrate the sub-endothelial space and differentiate into macrophages. These macrophages are able to recognize highly oxidized LDL particles via scavenger receptors that are expressed due to external stimulation by cytokines, such as tumor necrosis factor alpha (TNF-α) and interferon-γ (IFN- γ). Macrophages expressing these receptors can rapidly engulf oxLDL particles, forming foam cells, which are the hallmark cells of atherosclerosis. Upon foam cell death, a mass of extracellular lipids and cholesterol are left behind and contribute the formation and growth of fibrous plaques.

Inflammation is further induced by CD40 expression on the surface of macrophages and vessel endothelial cells which interact with CD40L of $CD4^+$ T-cells. This interaction leads to the upregulation of inflammatory cytokines, cell adhesion molecules, and matrix-degrading proteases [15]. These molecules are also stimulators for smooth muscle cell (SMC) migration and proliferation. Such stimulatory signals cause SMCs to invade the sub-endothelial space, proliferate, and secrete matrix, all of which contribute to the growth of the plaque and increased inflammation at the vessel wall. Over time, the plaques undergo calcification, hardening the vessel and reducing the volume of blood that is able to flow through at that site. Not only can this lead to heart attack or stroke, but also rupture of the plaque (thrombosis), all of which can lead to mortality.

HDL, however, is able to mediate the onset and progression of atherosclerosis by way of suppressing the inflammatory response. In this regard, if HDL is both functional and present in sufficient concentrations, it could lead to the reversal of plaque formation or prevent it all together. This makes HDL an intriguing focus of study in cardiovascular medicine.

1.4.2 Sepsis

Sepsis is a major health issue with a mortality rate exceeding 30% [51]. So far, therapeutic interventions blocking specific components of the inflammatory or coagulation pathways have had little impact on patient survival, and in some cases even increased overall mortality. There are no current therapies approved to treat sepsis, largely due to its rapid onset and progression, making treatment difficult and largely subjective. Endothelial activation and subsequent dysfunction are a common manifestation of sepsis, induced by a cascade of inflammatory events upon infection. Endotoxin released by bacteria activate immune effector cells to produce inflammatory cytokines and chemokines which can then activate the endothelium, resulting in endothelial dysfunction manifested by vascular leakage, increased leukocyte adhesion, and altered vascular tone, and leading to irreversible multi-organ failure and septic death [52-56]. Hence, therapies targeting the endothelium could be valuable in sepsis.

HDL levels in sepsis are a strong indicator of prognosis; clinically, septic patients present significant reductions in HDL-C and the extent to which these levels rise or fall is often predictive of survival rate [51, 57, 58]. Thus, the idea of HDL infusions to increase survival in sepsis patients with low circulating HDL-C is proposed in this thesis. HDL possess potent anti-inflammatory and endothelial protective effects that could be

exploited for sepsis therapy, notably via its abilities to bind and neutralize endotoxin, inhibit pro-inflammatory cytokine production in macrophages, and inhibit activation of endothelial cells [59-69]. Previous studies have shown that both ApoA-I mimetic peptides and rHDL infusions can improve outcomes in various animal models of endotoxemia [70-80] including one tested in humans following low-dose endotoxin challenge [80]. Considering that sHDL likely plays multi-protective roles in sepsis and that composition can significantly alter the properties of sHDL, further efforts are required to understand and tailor sHDL composition for increased efficacy in sepsis.

1.5 Synthetic HDL: Peptides, Particles, and Clinical Evaluation

1.5.1 ApoA-I Mimetic Peptides

Apolipoprotein mimetic peptides were initially used to investigate the structural features of the full-length ApoA-I protein [81]. However subsequent research sparked interest in these peptides as surrogates for ApoA-I in producing mimetic HDL particles, given their ability to recapitulate the biological functions of full-length protein *in vivo* [82-84]. Several ApoA-I mimetic peptides have been synthesized to date and are designed based on sequences homologous to the native protein [85]. These peptides have been optimized to maximize different functional outputs, such as cholesterol efflux capacity, lipid binding affinity, and LCAT activation [82, 85], and have been the focus of many recent clinical trials. Examples of such mimetic peptides and their applications are described in Table 1.

Table 1-1 Mimetic peptides of ApoA-I*: sequences and desired clinical applications.*

Peptide	Sequence	Company	Optimized Functional Output	Ref
ESP24218	P-V-L-D-L-F-R-E-L-L-N-E-L-L-E-A-L-K-Q-K-L-K	Esperion	• Lipid binding • LCAT activation • RCT	[83]
D4F	Ac-D-W-F-K-A-F-Y-D-K-V-A-E-K-F-K-E-A-F-NH_2	Novartis	• Same as L4F Chemical stability	[86]
L4F	Ac-D-W-F-K-A-F-Y-D-K-V-A-E-K-F-K-E-A-F-NH_2	Novartis	• RCT • Lipid binding • Inflammation reduction	[87]
Reverse 4F	K-L-K-Q-K-L-A-E-L-L-E-N-L-L-E-R-F-L-D-L-V-Inp Ac-F-A-E-K-F-K-E-A-V-K-D-Y-F-A-K-F-W-D-NH_2	Kos pharmaceuticals	• Lipid binding • Cholesterol mobilization	[88, 89]
5A	D-W-L-K-A-F-Y-D-K-V-A-E-K-L-K-E-A-F-P-D-W-A-K-A-A-Y-D-K-A-A-E-K-A-K-E-A-A	KineMed Inc.	• ABCA1 activation • Low hemolysis • Lipid binding	[84]
18A	Ac-E-W-L-E-A-F-Y-K-K-V-L-E-K-L-K-E-L-F-NH_2	N/A	• RCT	[90]
ATI-5261	Ac-E-V-R-S-K-L-E-E-W-F-A-A-F-R-E-F-A-E-E-F-L-A-R-L-K-S-NH_2	Roche	• Anti-oxidant properties • Promote ABCA1 dependent cholesterol efflux	[91]

1.5.2 Methods of Synthesis

Traditionally, HDLs prepared in the laboratory are made from plasma-purified human ApoA-I [92]. Once purified, the protein is reconstituted with phospholipids and often cholesterol to form “reconstituted” HDL (rHDL). This method, known as cholate dialysis, is a laborious task, as it involves the addition of detergents, such as cholate, followed by several days of dialysis to remove the detergent. There are many drawbacks to this methodology in addition to time consumption: incomplete detergent removal, endotoxin contamination of ApoA-I, particle heterogeneity, to name a few. Other methods, such as sonication of peptide and lipid mixtures have also been employed to prepare rHDL, but have similar drawbacks in that highly heterogeneous particles are difficult to make, especially in large scale [93]. Preparation of synthetic HDL particles by co-lyophilization, a technique developed and patented by Esperion Therapeutics [93], circumvents many of the issues described above. The process involves co-dissolving peptide and lipid constituents in organic solvent, freeze-drying, and subsequent hydration with an isotonic, neutral buffer. This process is easily scaled up and results in highly homogeneous sHDL particles.

1.5.3 Clinically Tested HDL

Several rHDL infusion products have been developed and tested in human clinical trials for both safety and efficacy in reducing follow up events in patients following an acute cardiac event [94-98]. A majority of rHDL products are made from full-length ApoA-I protein, either isolated from plasma or recombinantly expressed in *Escherichia coli,* complexed with soy phosphatidylcholine (soyPC), although the use of mimetic peptide has also been reported, such as for ETC-642 [99]. These cholesterol-

free particles are aimed to remove excess cholesterol from the periphery, and thus clinical biomarkers of efficacy include transient increases in both free and total plasma cholesterol levels. Overall, rHDL products have been proven safe and well-tolerated in both healthy and disease patients. A summary of clinically tested rHDL products, their composition and clinical outcomes can be found in **Table 1-2**. Given the differences in their protein and lipid composition, extrapolation between clinical results of rHDL products is somewhat difficult, as these properties can elicit variable pharmacodynamics, pharmacokinetics and toxicity [100-103]. Despite the lack of HDL infusion therapies on the market to date, a 17,400-patient Phase 3 trial is currently ongoing for CSL-112 to show reduction of major adverse cardiovascular events (MACE) in subjects with acute coronary syndrome (ACS) [104, 105].

***Table 1-2. Summary of findings from rHDL infusion clinical trials**. Adapted from [106]*

Drug	Composition*	Clinical Trial	Dose**	Pharmacokinetics	Safety	Ref.
SRC-rHDL (ZLB)	ApoA-I:sPC (1:4.2)	Phase I Single dose, healthy subjects (n = 7)	15 and 40 mg/kg	$T_{1/2}$ of ApoA-I> 24hr; $T_{1/2}$ of total PL ~ 8hr	No data reported	[101, 107]
		Phase I Single dose in hypercholesterolemic men (n = 24)	80 mg/kg	No data reported	No data reported	[108]
		Phase I Single dose in ABCA-$1^{+/-}$ and control subjects (n = 9)	80 mg/kg	No data reported	No data reported	[109]
CSL-111 (CSL Behring)	ApoA-I:sPC (1:4.2)	Phase I Single dose in type 2 diabetes patients (n = 7)	80 mg/kg	ApoA-I increased from 1.2 (baseline) to 2.8 g/L and returned to baseline on day 7	No data reported	[110]
		Phase I Single dose in patients with vascular disease (n = 20)	Placebo and 80 mg/kg	HDL-C increased by 20% after infusion of rHDL	No liver function changes	[111]
		Phase I Single dose in type 2 diabetes patients (n = 17)	Placebo and 20 mg/kg	$T_{1/2}$ of ApoA-I~ 72 hr	No data reported	[112]
		Phase II Multiple dose, ACS patients (n = 183)	4 weekly infusions of placebo, 40 and 80 mg/kg	No report	Liver function abnormalities in 80 mg/kg group	[98]
CSL-112 (CSL Behring)	ApoA-I:sPC (1:1.5)	Phase I Single dose, healthy subjects (n = 57)	Placebo, 5, 15, 40, 70, 105 and 135 mg/kg	T_{max} of ApoA-I = 2 hr; For doses >70 mg/kg; $T_{1/2}$ of ApoA-I=14.7 ~ 99.5 hr.	No safety issues	[100, 113]
		Phase I Multiple dose, healthy subjects (n = 36)	Four weekly infusion of placebo, 3.4 and 6.8 g/dose; Eight bi-weekly of 3.4 g/dose	T_{max} ApoA-I = 2hr; $T_{1/2}$ of ApoA-I = 19.3 hr ~ 92.8 hr	Safe and well tolerated	[100, 114, 115]
		Phase IIa Single dose in patients with stable atherothrombotic disease (n = 45)	Placebo, 1.7, 3.4 and 6.8 g/dose	T_{max} of ApoA-I ≈ 2 hr; $T_{1/2}$ of ApoA-I ≈ 12 hr.	Good safety	[116, 117]
		Phase IIb (AEGIS-I) Patients with acute MI (n = 1258)	Four weekly infusions Placebo, 2 and 6 g/dose	No report	Well-tolerated	[118]

		Phase III (AEGIS-II) Patients with ACS (n=17,400)	Currently recruiting	Currently recruiting	Currently recruiting	[104]
ProApoA-I-liposome (UCB)	ProApoA-I:sPC (1:1.25)	Phase I Single dose in patients with low HDL-C (male, n = 4) Phase I Single dose in FH patients (n = 4)	IV infusion for 1hr or 10 min 1.6 g/dose 4g by IV infusion over 20 min (~ 40-50 mg/kg)	$T_{1/2}$ of ApoA-I < 24 hr Transient increase in ApoA-I during the first 24 hr. C_{max} 64% and 35% above the baseline at 1 hr	No adverse events No safety issues	[119, 120]
ETC-216 (Esperion)	rApoA-I:POPC (1:1)	Phase I Single dose, healthy subjects (n = 32) Phase II Multiple dose, ACS patients (n = 57)	IV infusion of doses 0-100 mg/kg (males) and 0-50 mg/kg (females) Five doses; once per week by IV infusion; Placebo, 15 and 45 mg/kg	T_{max} of HDL free cholesterol level ≈ 30 min at 15 mg/kg and higher No report	Safe and well tolerated at all doses. Minor gastrointestinal adverse effects in 3 groups. 2 adverse events in high-dose group	[121] [94, 121]
CER-001 (Cerenis)	rApoAI:SM: DPPG (1:2.7:0.1)	Phase I Single dose, healthy subjects (n = 32) Phase II (CHI SQUARE) Multiple dose in ACS patients (n = 507) Phase II Multiple dose in patients with HoFH (n = 23) Phase II Multiple dose, FPHA patients (n = 7)	IV infusion of escalating doses of 0.25, 0.75, 2, 5, 10, 15, 30, 45 mg/kg. 6 weekly infusions of 0, 3, 6, and 12 mg/kg. 12 biweekly infusions at 8 mg/kg. IV infusion for 1hr; 20 infusions at 8 mg/kg for 6 months.	T_{max} of ApoA-IApoA ≈1-2 hr; $T_{1/2}$ ≈ 10 hr; C_{max} is dose-dependent and up to 0.9 mg/dL at 45mg/kg; No PK data ApoA-I increased by 13% from 114.8 mg/dL to 129.3 mg/dL during first hour T_{max}ofApoA-I≈4hr;$T_{1/2}$ ≈12hr	Safe and well tolerated at all doses; Well tolerated One serious adverse event reported to be drug related No serious adverse events	[102, 122] [97, 123] [124, 125] [126]
ETC-642 (Esperion)	ApoA-I peptide:SM: DPPC (1:1:1)	Phase I Single dose in patients with stable atherosclerosis (n = 28) Phase I Single dose in CVD patients (n = 24)	IV infusion of placebo and 0.1, 0.3, 1, 3 and 10 mg/kg IV infusion; 10, 20, 30 mg/kg	Dose proportional rise in peptide levels after infusion $T_{1/2}$ = 8.3 ~ 12.8 hr Dose proportional rise in the levels of peptide; $T_{1/2}$ of peptide = 10.2 ~13.8 hr. No data reported	Safe and well tolerated Asymptomatic elevations of liver function in one patient at 30 mg/kg No data reported	[83, 96] [95] [127]

		Phase I Multiple doses in patients with stable cardiovascular disease (n = 32)	4 weekly IV infusions of placebo 10, 20 and 30 mg/kg			
Abbreviations: sPC: soybean phosphatidylcholine; rApoA-I: recombinant ApoA-I; ACS: acute coronary syndrome; POPC: palmitoyloleoylphosphatidyl choline; SM: and sphingomyelin; DPPG: dipalmitoylphosphatidyl-glycerol; FH: familial hypercholesterolimea; HDL-C: high-density lipoprotein cholesterol; HoFH: heterozygous familial hypercholesterolemia; FPHA: familial primary hypoalphalipoproteinemia; DPPC: dipalmitoylphosphatidylcholine. * Indicates weight ratio, literature reported molar ratios were converted to weight ratios; **Dose of ApoA-I protein or peptide						

1.6 Research Scope

The preceding introduction discusses structure and function of high-density lipoproteins, their implications in inflammatory vascular diseases, and the development of synthetic versions of HDL to treat these diseases. Reconstituted and synthetic HDLs have been manufactured and tested clinically for their ability to minimize secondary cardiovascular events and reduce overall atherosclerotic plaque size in patients following an initial event. However, the main focus in developing these therapies has been on maximizing particle cholesterol efflux capacity while other functional aspects of the particles, i.e. anti-inflammatory and endothelial protective properties, have been overlooked. Given that vascular dysfunction is a hallmark of many diseases, the work presented here will demonstrate the utility of synthetic HDL to modulate and resolve vascular dysfunction in both atherosclerosis and sepsis settings.

1.7 Thesis Overview

The overall goal of this thesis is to explore the ability of sHDL to be tailored for treatment of vascular dysfunction. To do this, we will look at vascular inflammation in the context of both acute and long-term settings by using models of sepsis and atherosclerosis, respectively. This thesis consists of 5 chapters surrounding sHDL's ability to modulate inflammation at the vascular level.

Chapter 2 of this thesis focuses on the use of synthetic HDL to treat polymicrobial sepsis. This chapter first examines clinical relationships between endogenous HDL levels and septic mortality, and how such relationships could justify the use of sHDL as a sepsis therapy. This is accompanied by extensive *in vitro* and *in*

vivo characterization of sHDL in laboratory sepsis models and attempts to identify and understand the key mechanistic and compositional attributes of sHDL that confer its protective effects. Findings from this study can be used to further refine and optimize sHDL composition to maximize its therapeutic potential in sepsis.

Chapter 3 revisits the use of clinically-tested rHDL/sHDL products for treatment of atherosclerosis and explores the utility co-administration with liver X receptor (LXR) agonists. This chapter identifies key aspects of sHDL composition that lead to expressional changes in ABCA1/G1 transporters after treatment with sHDL and seeks to revive the clinical application of LXR agonists and augment the overall efficacy of sHDL therapy in atherosclerosis. The results from this study provide evidence for a synergetic effect between sHDL and LXR agonist therapies and could be used to direct future research and development strategies to improve therapeutic outcomes in patients with cardiovascular disease.

Chapter 4 utilized sHDL as a platform for delivery of sphingosine-1-phosphate. S1P is a well-known modulator of endothelial function and is essential is maintenance of endothelial barrier function. Although it also participates in immunomodulatory pathways, such as lymphopenia and lymphocyte egress, its actions in the vasculature are unique in that presentation by HDL elicits a tailored and specific response. These effects, including activation of eNOS and subsequent NO production, are probed by formulating S1P into sHDL particles and testing them in cellular models of endothelial activation. Findings from this work can be applied to in vivo models of vascular dysfunction and guide future development of S1P-based therapy.

Chapter 5 ties together the research by drawing final conclusions and discussing the future potential for this work, including study limitations and ongoing work. Each research chapter is written in manuscript format and will be submitted for publication.

Chapter 2: Synthetic high-density lipoprotein—A potential therapy for sepsis

2.1 Abstract

Sepsis is a major health issue with mortality exceeding 30%. So far, therapeutic interventions focused on blocking specific components of the inflammatory or coagulation pathways have had little impact on patient survival. Given that multiple factors contribute to sepsis, targeting an endogenous factor with multi-protective effects against endothelial dysfunction may present a novel approach for sepsis therapy. Here, we report that targeting high-density lipoprotein (HDL) with synthetic HDL provides effective protection against sepsis. We first measured HDL levels in septic patients and observed that HDL levels were lower by 45% in septic patients compared with non-septic patients. Importantly, HDL levels in non-surviving septic patients were significantly lower than those surviving. To explore the significance of this finding, we conducted studies in preclinical models using a new generation of synthetic HDL (sHDL), ETC-642, and tested its efficacy on cecal ligation and puncture (CLP)-challenged mice. Mice were administered sHDL 2h post-CLP. sHDL treatment significantly increased plasma HDL-cholesterol levels and, importantly, significantly improved 7d survival rate (76.2% survival in sHDL-treated versus 38.1% in PBS-treated mice). Additionally, septic mice treated with ETC-642 had significant decreases in BUN,

plasma IL-6 and IL-10 levels. To understand the mechanisms underlying sHDL protection, we investigated the effect of sHDL on endotoxin-induced inflammatory response in RAW264.7 and HUVECs, and in HEK-blue cells expressing TLR4- or TLR2-NF-kB reporters. sHDL not only neutralized LPS/LTA but also suppressed TLR4- or TLR2-NF-kB signaling, and inhibited LPS/LTA/TNF-α induced endothelial activation. Together, our findings suggest that sHDL therapy can be an effective therapy for sepsis.

2.2 Introduction

Sepsis is a major health issue with a mortality rate exceeding 30% [51]. So far, therapeutic interventions focused on blocking specific components of the inflammatory or coagulation pathways have had little impact on patient survival. Given that multiple factors contribute to sepsis, we propose that targeting an endogenous factor with multi-protective effects may present a novel approach for sepsis therapy.

Exogenous HDL or its synthetic analogs are potential candidates for sepsis treatment. First, endogenous HDL has a broad spectrum of activity highly pertinent to fighting sepsis, including neutralization of endotoxin, suppression of inflammatory signaling in immune effector cells and inhibition of endothelial cell (EC) activation [17]. Second, HDL levels drop markedly in septic patients and correlate with a poor prognosis [58, 128]. Third, consistent with the clinical evidence we recently demonstrated that HDL deficiency increases susceptibility to cecal ligation and puncture (CLP)-induced septic death using Apolipoprotein-I (ApoA-I) null mice as an HDL deficient model [129]. Importantly, increasing HDL levels by over expressing ApoA-I improved the survival in mice following CLP [129]. Based on these clinical and

experimental findings we recently hypothesized that a decrease in HDL levels is a risk factor for sepsis mortality, and that raising circulating HDL levels may present an efficient sepsis therapy [17].

To test our hypothesis, we utilized a new generation of synthetic HDL (sHDL), ETC-642, made up of a 22 amino acid ApoA-I mimetic peptide (ESP24218 or 22A) and phospholipids. ETC-642 was previously developed for the treatment of cardiovascular disease [130]. Specifically, it was optimized to effectively remove and eliminate excess cholesterol from atheromas. ETC-642 offers a competitive advantage in that it has already been tested in several single- and multiple-dose clinical trials, showing safety at doses ranging from 1 – 30 mg/kg in humans [95, 96]. The purity and homogeneity of ETC-642 sHDL particles is well controlled. Its clinical manufacturing is established and toxicology complete. Hence, it could be rapidly translated to the clinic for evaluation as a sepsis treatment.

In this study, we demonstrate that administration of sHDL after the onset of CLP-induced sepsis both increases effective HDL-C levels and is highly protective against septic death. We further demonstrate that, different from the earlier approaches that block the inflammatory pathway or simply neutralize LPS, sHDL therapy provides multiple protective mechanisms through promoting LPS/LTA detoxification, suppressing inflammatory signaling in macrophages and inhibiting endothelial activation. Together, our findings support further development of sHDL therapy for effective treatment of sepsis.

2.3 Materials and Methods

2.3.1 Reagents

22A peptide (PVLDLFRELLNELLEALKQKLK) was synthesized by Genscript (Piscataway, NJ) and purity was determined to be >95% by HPLC. Egg sphingomyelin (SM) and 1,2-dipalmitoyl-*sn*-glycero-3-phosphocholine (DPPC) were purchased from Avanti Polar Lipids (Alabaster, AL) and Nippon Oil and Fat (Osaka, Japan). LPS (*E. coli O111:B4*) and fluorescent LPS (*E. coli 055:B5*, Alexa Fluor® 488 Conjugate) were purchased from Sigma Aldrich (St. Louis, MO). LPS (*E. coli K12*) was purchased from InvivoGen (San Diego, CA). The serum against scavenger receptor B-I (SR-BI) was custom made by Sigma-Genosys using a 15 amino acid-peptide derived from the C-terminal of human SR-BI. The authentication of the antibody was verified by western blot using SR-BI null tissues [131]. Anti-TLR4 was purchased from Santa Cruz (cat # sc-293072, CA). All other reagents were obtained from commercial suppliers and were of analytical grade or higher.

2.3.2 Patients

Patients were recruited at the University of Michigan Medical ICU at the onset of sepsis, between September 2001 and April 2004. Sepsis was defined as described by the American-European Sepsis Consensus Conference (see inclusion/exclusion criteria below). Prior to entry into the study, an informed consent was properly obtained from the patient or the patient's legally acceptable representative. The study was approved by the institutional review board of the University of Michigan Medical School, Ann Arbor, MI. At the time of entry, a complete medical/sepsis history and physical examination were obtained from each subject. The following data were recorded:

APACHE III (Acute Physiology, Age, Chronic Health Evaluation) score, results of chest X-ray, electrocardiogram, ventilator parameters, positive culture, antigenic or nucleic acid assay results from any suspected source of sepsis, urinary output, administration of neuromuscular blocking agents, antibiotics, vasopressors and sedatives during the preceding 24 h. The APACHE III score was assigned once a day by a trained nurse at the ICU unit based on the previous 24 h of evaluation. From the laboratory studies we recorded arterial blood gases, most recent pulmonary artery systolic, diastolic, and wedge pressure (where available), blood profile, serum electrolytes, glucose, bilirubin, and albumin.

2.3.3 Patient Inclusion/Exclusion Criteria

For the sepsis patients, we enrolled subjects of both sex and aged ≥18 years who had at least two signs of systemic inflammatory response syndrome (SIRS). SIRS was defined by core, rectal, axillary, or oral temperature ≥ 38^{o}C or otherwise unexplained core or rectal temperature of ≤ 36^{o}C; heart rate ≥ 90 beats per minute; respiratory rate ≥ 20 per minute or PaC02 ≤ 32 mmHg or the subject was on a ventilator; WBC ≥ 12,000/mm^3 or ≤ 4,000/mm^3 or ≥ 10% immature neutrophils (bands). The source of sepsis was documented by culture, Gram stain or nucleic acid assay of blood, or normally sterile body fluid positive for a pathogenic microorganism that constituted the reason for systemic therapy with anti-infectives; chest radiography consistent with a diagnosis of pneumonia that constituted the reason for systemic therapy with anti-infectives; clearly verifiable focus of infection identified, e.g. perforated bowel with the presence of free air or bowel contents in the abdomen found at surgery; and/or wound with purulent drainage. We also enrolled patients with septic shock

(hypotension despite adequate fluid resuscitation (systolic BP ≤ 90 mmHg, mean arterial BP ≤ 65 mmHg) and need for vasopressors) or with organ dysfunction/hypoperfusion as a result of sepsis (e.g. pulmonary dysfunction - $Pa0_2/FI0_2$ < 250, or < 200 in the presence of pneumonia or other localizing lung disease; metabolic acidosis – pH ≤ 7.30 or increased plasma lactate levels; oliguria - urine output < 0.5 ml/kg/h for a minimum of two consecutive hours in the presence of adequate fluid resuscitation; thrombocytopenia - platelet count of <100,000 cells/mm^3 without other causes of thrombocytopenia; acute alteration in mental status). Subjects were excluded for the following criteria: pregnancy confirmed by urine or serum test; significant liver disease as defined by fulfillment of Child-Pugh Grade C or known esophageal varices; HIV infection with CD4+ count < 200; Prednisone therapy > 20 mg/day (or equivalent), cytotoxic therapy within 3 weeks prior to screening; confirmed, clinically-evident acute pancreatitis; extracorporeal support of gas exchange at the time of study entry; or receipt of an investigational drug within 30 days prior to study enrollment. For the non-septic control group we enrolled subjects of either sex and age >18 years admitted to the ICU for disorders other than sepsis, who did not have any of the exclusion criteria outlined above.

2.3.4 Patient Characteristics

A total of 124 patients from the CCMU at the University of Michigan Medical Center were recruited in this study, from whom 85 were patients with sepsis and 38 without sepsis. The demographic characteristics of the enrolled patients are presented in **Table 2-1**.

2.3.5 Blood Sampling and Analysis

Blood samples (15-20 ml) were taken in heparinized tubes within 24 hours from the onset of sepsis, and 1, 3, 7 and 14 days post entry. Plasma was separated by centrifugation at 4^{o}C, aliquoted and stored at -80^{o}C before analysis. HDL cholesterol (Roche kit 3030067), total cholesterol (Roche kit 450061), triglycerides (Roche kit 1488899), ApoA-I (Wako, Richmond, VA kit 991-27201), aspartate aminotransferase (AST; Roche kit 450064), were analyzed on a Hitachi 912 clinical chemistry autoanalyzer (Roche Diagnostics Corporation, Indianapolis, IN).

2.3.6 sHDL Preparation

Discoidal ETC-642 sHDL nanoparticles were made by co-lyophilization followed by thermal cycling as described previously [19, 132]. Briefly, 22A peptide and phospholipids were combined and dissolved in glacial acetic acid at a 22A:SM:DPPC ratio of 1:1:1 by weight. The resulting solution underwent rapid freezing in liquid nitrogen and was immediately placed on a shelf freeze-dryer (Labconco) overnight to remove the acid. Once dried, the lyophilized powder was reconstituted in 1X phosphate buffered saline (PBS) to the desired final peptide concentration and vortexed to completely dissolve, forming a cloudy white suspension. The resulting solution was subjected to 3 heat/cool cycle, each cycle consisting of 10 minutes heating at 55 °C and 10 minutes cooling at room temperature (above and below the transition temperature of the lipids, respectively). By the end of 3 cycles the solution had turned from cloudy to clear, indicating formation of sHDL nanoparticles. The pH of the sHDL solution was adjusted to 7.4 using NaOH and 0.2 μm sterile-filtered.

2.3.7 sHDL Characterization

Quality of ETC-642 sHDL particles was assessed using the following analytical techniques. Size distribution was determined by dynamic light scattering (DLS) on a Malvern Zetasizer Nano ZSP (Westborough, MA), and particle purity was determined by gel permeation chromatography (GPC) with UV detection at 220 using a Tosoh TSK gel G3000SWxl column (Tosoh Bioscience, King of Prussia, PA) on a Waters HPLC, as previously described. Transmission electron microscopy (TEM) images were obtained as previously described [133], by diluting samples with 1% uranyl acetate negative stain solution. Images were acquired on a JEM 1200EX electron microscope (JEOL, USA) equipped with an AMT XR-60 digital camera (Advanced Microscopy Techniques Corp.). Endotoxin levels in the final sterile formulations were determined using the Pyrotell® Limulus Amoebocyte Lysate (LAL) Assay (Associates of Cape Cod, Inc., Falmouth, MA #GP5003).

2.3.8 Cell Culture

Primary Human Umbilical Vein Endothelial Cells (HUVEC) from pooled donors (Lonza, C2519AS) were grown in 0.2% gelatin Type B (Sigma) coated tissue culture vessels containing Clonetics™ EGM-2 Complete Media (Lonza). Cells between passages 3-5 were used in all experiments. RAW 264.7 murine macrophages (ATCC® TIB-71™) were cultured in Dulbecco's Modified Eagle Medium (DMEM) containing 10% fetal bovine serum. HEK-Blue cells, which stably express CD14, MD2, NF-κB reporter and TLR4 or TLR2, were from InvivoGen. The cells were cultured in 96-well plate in complete DMEM medium containing 10% Endo-low FBS to 70% confluency and treated with LPS or LTA for 16 hours. Then, 100µl of the culture supernatant was mixed with

100µl HEK-Blue™ Detection Medium and incubated at 37ºC for 1 hour. LPS or LTA activates TLR4 or TLR2, respectively, resulting in induction of NF-κB reporter expression, which catalyzes the HEK-Blue™ Detection medium to blue. The blue color was quantified by measuring absorption at 650nm. All incubations were performed in a 37 °C incubator under 5% CO_2 atmospheric conditions.

2.3.9 In Vivo Efficacy Analysis

CLP (21G needle, 2/3 ligation) was performed on 10–12-week-old C57BL/6J (B6) mice as described previously [131]. Survival was monitored for a 7-day period. B6 mice were subjected to CLP (21G needle, 2/3 ligation). 2h post-CLP, mice were treated with 100 µl of PBS or sHDL containing 7.5 mg peptide/kg body weight (i.v.). 18h post CLP, body temperature was recorded and the plasma and lung were harvested. HDL was isolated from plasma by sequential ultracentrifugation as previously described[134, 135] (1.5 ml plasma from 5 mice were used to make one HDL preparation) and total HDL cholesterol was measured by Wako Diagnostics kit (Richmond, VA). Organ injury was determined by quantifying plasma ALT, lung wet/dry ratio and plasma BUN levels. Plasma cytokines TNF-α**,** IL-6, and IL-10 were quantified by ELISA (Biolegend or eBioscience).

2.3.10 LPS/LTA-induced NF-κB Expression in HEK-Blue Cells

HEK-Blue cells expressing TLR4 or TLR2 were cultured to 70% confluency and treated with LPS (K12, 1 ng/mL) or LTA (40 ng/mL) in the presence of ETC-642 for 16 hours. Alternatively, cells were pre-treated with sHDL ETC-642 at 60 µg/ml for 6 hours followed by stimulation with LPS or LTA. 100µl of the culture supernatant was mixed

with 100µl HEK-Blue™ Detection and the activation of NF-κB reporter was quantified by measuring absorption at A_{650nm}.

2.3.11 Macrophage LPS/LTA-induced Cytokine Expression Analysis

RAW 264.7 cells were cultured to 70% confluency and treated with LPS (K12, 2 ng/mL) or LTA (40 ng/mL) in the presence of ETC-642 (0, 15, 30, 60 or 120 µg peptide/mL) for 16 hours. The concentrations of TNF-α and IL-6 in the supernatant were measured using ELISA.

2.3.12 Endothelial LPS/TNF-α-induced Cytokine Expression Analysis

HUVECs were seeded into well-plates and grown to 90% confluency. Cells were washed twice with 1X PBS and incubated with LPS (K12, 100 ng/mL) or TNF-α (1 ng/mL) in the presence of ETC-642 (15, 30, 60, or 120 µg/mL peptide), or matching concentrations of 22A peptide, SM-DPPC liposomes, or PBS 16 hours. The concentrations of cytokines IL-6 and IL-8 in the supernatants were quantified using ELISA.

2.3.13 Gene Expression Analysis

HUVECs were seeded into well-plates and grown to 90% confluency. Cells were treated with LPS (100 µg/mL) in the presence of either ETC-642 (15, 30, 60, or 120 µg/mL peptide), or matching concentrations of 22A peptide, SM-DPPC liposomes, or PBS for 16 hours. After incubation, cells were washed twice in PBS and cells lysed in radioimmunoprecipitation buffer (50 mM Tris, 150 mM NaCl, 1% SDS, 0.5% sodium deoxycholate, 1% Triton X-100) containing cOmplete™ EDTA-free protease inhibitor cocktail (Roche). Total RNA was extracted using RNeasy mini kit (Qiagen) and reverse transcribed to cDNA using iScript cDNA synthesis kit (BioRad). Gene expression was

determined by RT-qPCR on a StepOnePlus™ Real-Time PCR System (Applied Biosystems) using TaqMan Gene Expression assays for ICAM-1 (Hs00164932_m1), VCAM-1 (Hs01003372_m1), eNOS (Hs01574659_m1), and E-Selectin (Hs00174057_m1) (Thermo Fisher). Data was normalized to endogenous GAPDH (Hs03929097_g1) expression and fold change in gene expression was calculated using the $\Delta\Delta C_T$ method.

2.3.14 Isolation of Lipid Rafts

Lipid rafts and other subcellular fractions were isolated with Opti-Prep method as previously described [136]. We used SR-BI as a marker protein in lipid rafts. TLR4 and SR-BI in each fraction were analyzed by Western blot.

2.3.15 Determination of Total Cellular Cholesterol

Total cellular cholesterol was determined by treating RAW264.7 cells with ETC-642 (60 μg/mL) or vehicle for 12 hr. Cells were then scraped, collected, and cholesterol was extracted and quantified using the Wako total cholesterol reagent kit (Wako Diagnostics, Richmond, VA).

2.3.16 Cholesterol Efflux

Cholesterol efflux studies were performed using RAW 264.7 cells. Briefly, cells were cultured in DMEM media containing 10% fetal bovine serum (FBS, heat inactivated) and 1% penicillin-streptomycin antibiotic in a humidified incubator at 37°C with 5% CO_2. Cells were labeled for 24 h with 1 μCi/ml of [^{3}H] cholesterol (Perkin Elmer) in serum-free DMEM supplemented with 0.2 mg/ml of fatty acid-free BSA and 1% penicillin-streptomycin antibiotic (DMEM/BSA). The cells were then washed with PBS twice and sHDL was added at concentrations ranging from 15-120 μg/mL peptide in

DMEM/BSA media. After either 6 or 18 h of incubation, media were collected and centrifuged at 10,000 rpm for 3 min to remove any floating cells. Finally, remaining cells were lysed with 0.5 ml of 0.1% SDS and 0.1 N NaOH. Radioactive counts in media and cell fractions were measured by liquid scintillation counting (Perkin Elmer), and percent cholesterol effluxed was calculated by dividing the media count by the sum of the media and cell counts and then multiplying this number by 100%.

2.3.17 Isothermal Titration Calorimetry

Microcalorimetric measurements of the binding of sHDL to LPS were performed on a VP isothermal titration calorimeter (Microcal Inc.) at 37°C. Typically, 20 consecutive 15 μL aliquots of sHDL at a concentration of 0.4 mM (1.05mg/ml) were injected into the cell (1.5 mL) filled with 2 μM (0.03 mg/ml) LPS solution. Both sHDL and LPS solutions were degassed under vacuum immediately before use. Injections were made at 400 s intervals. A constant stirring speed of 310 rpm was maintained during the experiment to ensure proper mixing after each injection. Data were analyzed using the software available for uptake assay.

2.3.18 CG Model of ETC-642 Nanoparticle

The atomistic initial model of 22A was constructed with an α-helical secondary structure by using PyMol [137]. The atomistic model was then transformed to a CG model by applying the MARTINI v2.2 force field for protein [138, 139]. For the CG model of solvent molecules, four water molecules were represented as a single CG bead. Ions in the CG model were represented as charged CG beads with their first hydration shell implicitly included [139]. Parameters for SM and DPPC lipids in the CG model were adopted from the MARTINI force field for lipids [140]. The GC parameter for LTA was

generated based on the parameter of galactosyldiacylglycerol (DGDG) from the MARTINI force field for glycolipids [141, 142]. An additional Q_a bead was added to represent the additional phosphate group found on LTA. Bond and angle parameter for the new Q_a bead was adopted from the parameter of phosphatidylinositol (PI) in the MARTINI force field for glycolipids. Parameterization for LPS was generated by iteratively fitting the CG model with an all-atomistic model, following a protocol similar to Lopez's work [142]. The initial model simulation system for ETC-642 (S_1) was constructed with a random distribution of 20 ETC-642 peptides, 75 PPCS molecules, and 75 DPPC molecules, following the 1:3.75:3.75 molar ratio of corresponding components in the ETC-642 particle. A total of 20 α-helical peptides (equivalent number of α-helices for 2 Apo A-I lipoproteins in the double-belt model) and 150 lipids in the system is approximated to the composition of reported models of discoidal HDL particles [143-146]. The initial model simulation system for the lipid-only particle (S_0, control) was also constructed with a random distribution of 75 PPCS molecules and 75 DPPC molecules, without the addition of ETC-642 peptides. CG beads of water and ions (0.15 M NaCl) were added to both systems for the simulation of physiological environment. Simulations totaling 3 μs with a 30 fs integration at a temperature of 323 K were performed for each system using Gromacs v4.6 [147]. A temperature of 323K in the CG simulation was used to reproduce the results of the all-atom simulation at temperatures ranging from 300-315 K [140, 148, 149].

2.3.19 Binding Model and Free Energy Calculation for ETC-642 Binding with LPS/LTA

In order to simulate the binding conformation of LTA/LPS with the ETC-642 particle, one LTA/LPS molecule was randomly added into solvent of the two previously

equilibrated simulation systems, i.e., S_0 and S_1. The combined four systems were termed S_0-LTA, S_0-LPS, S_1-LTA, and S_1-LPS, respectively. Solvent beads overlapped with LTA/LPS were removed, while the charge introduced by LTA/LPS was naturalized by adding counter ions (Na^+) in each of the four systems. Then, simulations totaling 1 μs with a 30 fs integration time step at 323 K were performed for each system using Gromacs v4.6 [147]. The potential of mean force (PMF) was calculated by using the pull code and WHAM method [150, 151], implemented in Gromacs v4.6, to estimate the binding free energy of LTA/LPS with the ETC-642 particle. Based on the previously equilibrated LTA/LPS binding simulation systems, the reaction coordinates of LTA/LPS binding with ETC-642 was obtained by pulling the center of mass (COM) for LTA/LPS 8 nm away from the COM for the ETC-642 particle in 80 ns simulations with a time step of 30 fs. Then, 40 sampling windows were subjected to an additional 10 ns equilibration (30 fs time step) and 10 ns (5 fs time step) umbrella sampling based on the reaction coordinates with an interval of 0.2 nm. The binding free energy of LTA/LPS with the lipid-only particle was also estimated in the same way. Three independent PMF calculations were performed for each system to average the fluctuations.

2.3.20 Statistics

Data are presented as mean ± SEM or mean ± SD. Significance in experiments comparing two groups was determined by 2-tailed Student *t*-test. Comparison of more than two groups was evaluated by one-way ANOVA, followed by post hoc analysis using Tukey's test. Means were considered different at $p < 0.05$. Survival analysis was analyzed with Log-Rank x^2 test using SPSS software. Unless otherwise specified, all other experiments were statistically evaluated using GraphPad Prism Software.

2.4 Results

2.4.1 HDL Levels are Reduces in Septic Patients

To better understand the role of HDL in sepsis, a clinical observation study was conducted in one hundred twenty-four patients admitted to the University of Michigan Hospital Intensive Care Unit. For analysis, patients were broken up into 3 groups: non-sepsis controls (n = 38), sepsis survivors (n = 69), and patients who had not survived sepsis (n = 16, also termed “sepsis expired”). HDL-cholesterol (HDL-C) levels at time of admission to the ICU (Day 0) and for the duration of ICU stay were measured (**Fig. 2-1A**). Interestingly, HDL-C levels were markedly lower in patients with sepsis versus non-sepsis controls on Day 0, with sepsis-expired individuals displaying significantly lower HDL-C (15 ± 10 mg/dL) than both sepsis-survivors (23 ± 13 mg/dL, $p<0.05$) and non-sepsis controls (36 ± 9 mg/dL, $p<0.01$). A similar trend was observed for ApoA-I levels, which also differed significantly between sepsis-expired (46 ± 25 mg/mL), sepsis-survivors (61 ± 26 mg/mL, $p<0.05$), and non-sepsis controls (89 ± 18 mg/mL, $p<0.01$), as shown in **Fig. 2-1B**. As ApoA-I levels are an indirect measure of both HDL function and the number of circulating HDL particles, we hypothesize that a decrease in ApoA-I levels confers a temporary loss in the anti-inflammatory, anti-oxidant and anti-thrombotic functions of HDL, and that this may contribute to the vascular dysfunction observed in sepsis.

2.4.2 Low HDL Levels Correlate with a Poor Prognosis

Given the drastic alterations in HDL-C and ApoA-I observed in septic patients, we next sought to explore the relationship between HDL-C and survival among septic patients. Interestingly, we found that patients entering the ICU with HDL-C levels <10

mg/dL had about a 2-fold increase in mortality compared to those with HDL-C >10 mg/dL (**Fig. 2-1C**), suggesting that decreased HDL-C may be a predictive factor for sepsis-related mortality. The levels of ApoA-I also correlated with survival (**Fig. 2-1D**). Interestingly, among the patients with low HDL-C levels < 10 mg/dL, the ApoA-I and HDL-C levels remained low until death, while they gradually increased in the patients who had recovered (**Fig. 2-1E and F**), indicating that restoring HDL-C and ApoA-I levels may have a protective effect in sepsis. Taken together, these data support the notion that HDL-infusion therapy may increase a patient's chances of survival by restoration of the depleted endogenous HDL and its essential functions.

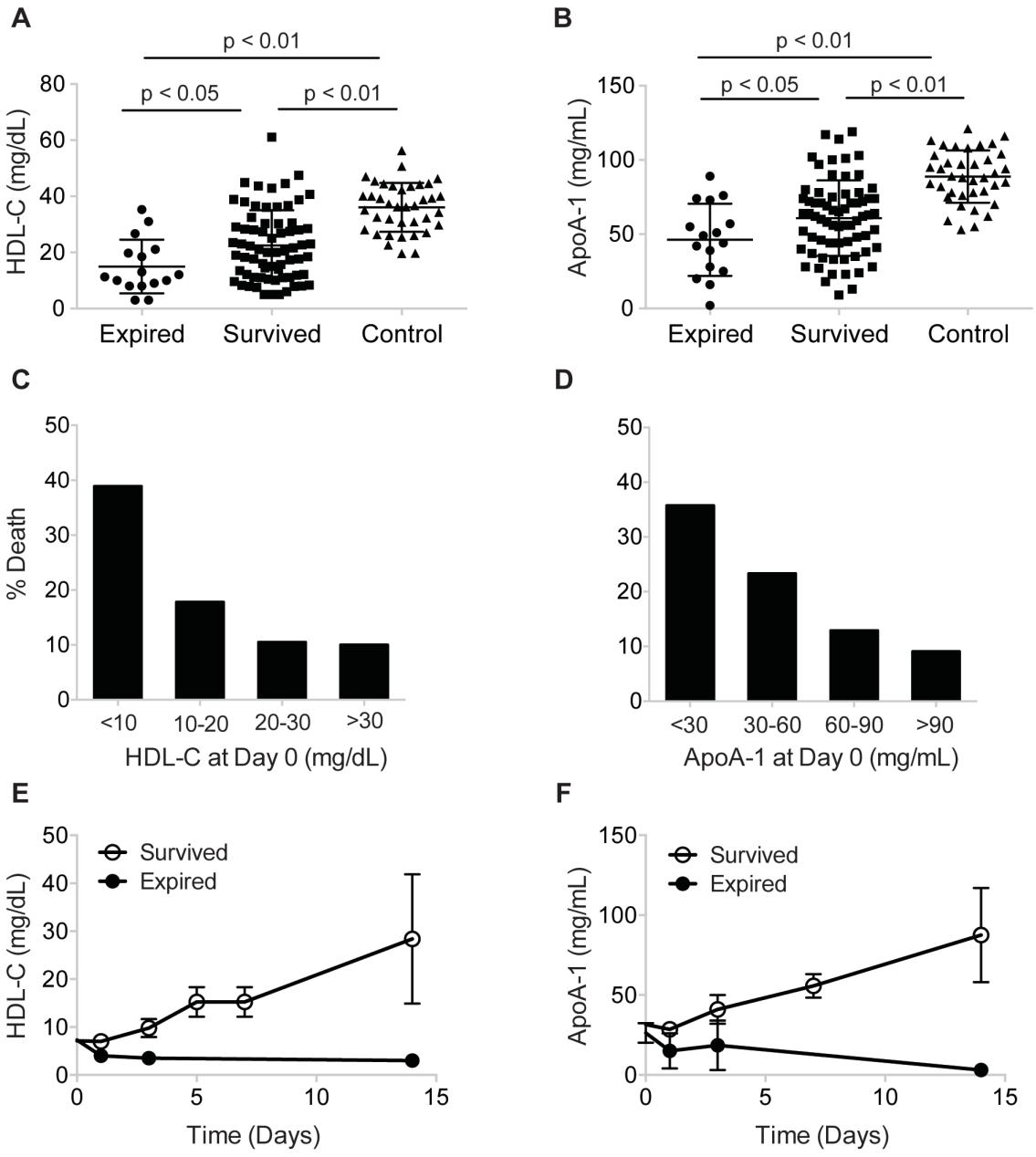


Figure 2-1 Septic patients have lower HDL levels, which is associated with poor survival*. At time of intake (Day 0), there is a significant difference between plasma concentrations of HDL-C (**A**) and ApoA-1 (**B**) in expired sepsis patients versus non-sepsis controls. Patients entering the ICU with HDL-C levels <10 mg/dL had a higher incidence of death than those with HDL-C levels >10 mg/dL (**C**); those with ApoA-1 levels <30 mg/mL also had a higher incidence of death than those with ApoA-1 >30 mg/mL (**D**); HDL-C (**E**) and ApoA-1 (**F**) levels over 14 days in septic patients with HDL-C <10 mg/dL at day 0; statistical significance determined by one-way ANOVA with Tukey's multiple comparison test.*

2.4.3 ETC-642 Preparation Results in Pure, Homogeneous Peptide-Lipid Nanoparticles

Based on the strong clinical correlation between increased HDL-C and ApoA-I levels and higher survival, we decided to test the ability of synthetic HDL (sHDL) infusion to improve murine survival in CLP model. To do this, we used ETC-642, a sHDL product developed by Esperion Therapeutics (Ann Arbor, MI) and tested in single- and multiple-dose Phase I clinical trials for the treatment of acute coronary syndrome. Previously established clinical manufacturing, animal and human safety of ETC-642 greatly increases our ability to rapidly test protective ability of sHDL in septic patients. ETC-642 sHDL was made by a co-lyophilization technique (**Fig. 2-2A**) using the 22 amino acid apolipoprotein A-I mimetic peptide (22A), 1,2-dipalmitoyl-*sn*-glycero-3-phosphocholine (DPPC) and sphingomyelin (SM) [19, 83, 106]. As seen in Fig. 2-2, we were able to successfully produce highly homogeneous sHDL nanoparticles as seen by TEM (**Fig. 2-2B**), purity >99% as evidenced by GPC (**Fig. 2-2C**), with a size range of 10.4 ± 3.3 nm with with low polydispersity (PDI = 0.11) measured by DLS (**Fig. 2-2D**). The levels of residual endotoxin in ETC-642 was determined to be belowe limit of detection (<0.03 EU/mL) by limulus amebocyte lysate assay. Notably, the sHDL appeared to be stable for over a year when stored frozen and retained their homogeneous size and purity after storage.

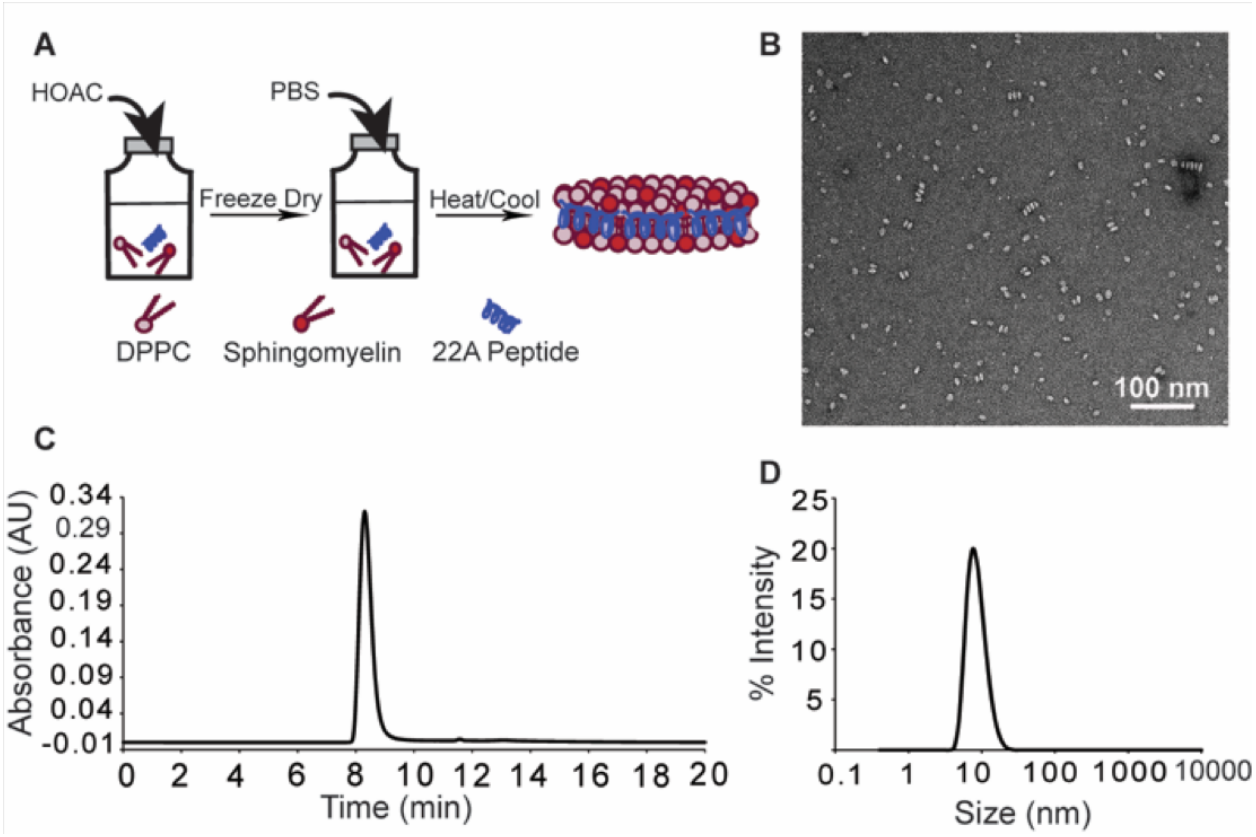


Figure 2-2 sHDL preparation and characterization*. Schematic of sHDL preparation procedure (**A**); Transmission electron microscopy (TEM) image shows nanosized, discoidal sHDL particles (**B**); gel permeation chromatography (GPC) profile of sHDL indicates >99% purity (**C**); Size distribution of sHDL particles is 10.43 ± 3.28 nm with a PDI of 0.112 as determined by dynamic light scattering (DLS) (**D**).*

2.4.4 sHDL Restores HDL Levels and Protects Against CLP-Induced Animal Death

We next set up to test our central hypothesis that infusion of sHDL could restore HDL-C levels and HDL function and improve survival in septic mice. B6 mice subjected to CLP (21g, 2/3 ligation) were administered sHDL (7.5 mg/kg) or saline 2 h post-CLP and monitored for survival over 7 days. As expected, HDL-C levels in mice treated with sHDL were significantly elevated (59.2 ± 5.3 mg/dL) over saline-treated controls (26.5 ± 7.1 mg/dL, $p<0.05$) 18 h post-CLP (**Fig. 2-3A**), showing the ability of sHDL to efflux cholesterol *in vivo* and restore endogenous levels of HDL-C. Remarkably, sHDL (n =

21) was also able to improve the 7-day survival rate nearly 2-fold ($p<0.01$) over PBS-treated controls (n = 19), as seen in **Fig. 2-3B**. The potential mechanisms of sepsis protection by sHDL include combination of direct physical binding of LPS/LTA, inhibilition of inflammaroty signaling, diminishing vascular dysfunction and possible other and we set out to explore each of these possibilities.

2.4.5 sHDL Attenuates CLP-Induced Organ Injury and Suppresses Inflammatory Cytokine Production

To better understand the extent of sHDL-mediated protection in sepsis, we monitored several physiological factors common to the disease, including drop in body temperature, increase in organ damage and elevated plasma cytokine levels 18 h post-CLP. Most notably, sHDL therapy was able to restore normal body temperature 16 hours post-treatment to 36.6 ± 1.5 °C (n = 8) compared to PBS-treated mice (n = 7), whose body temperature lingered at 28.7 ± 0.7 °C ($p <0.01$), as shown in **Fig. 2-3C**. Additionally, we assessed organ injury of the liver (ALT), lungs (lung wet/dry ratio), and kidneys (BUN), as seen in **Fig. 2-3 D-F**, respectively, and found that sHDL therapy significantly protected kidney function ($p<0.05$), as indicated by reduction in BUN levels for sHDL-treated (36.62 ± 2.82 mg/dL, n=16) vs PBS-treated controls (52.63 ± 4.51 mg/dL, n=15). Cytokine levels in the plasma were measured, and although sHDL was unable to reduce circulating TNF-α levels (**Fig. 2-3G**), it was indeed effective in attenuating both plasma IL-6 (0.964 ± 0.296 ng/ml for sHDL group versus 9.364 ± 3.637 ng/ml for PBS group, $p<0.01$) and plasma IL-10 levels (0.432 ± 0.235 ng/ml for sHDL group versus 1.182 ± 0.450 ng/ml for PBS group, $p<0.05$), as shown in **Fig. 2-3H and 2-3I**, respectively.

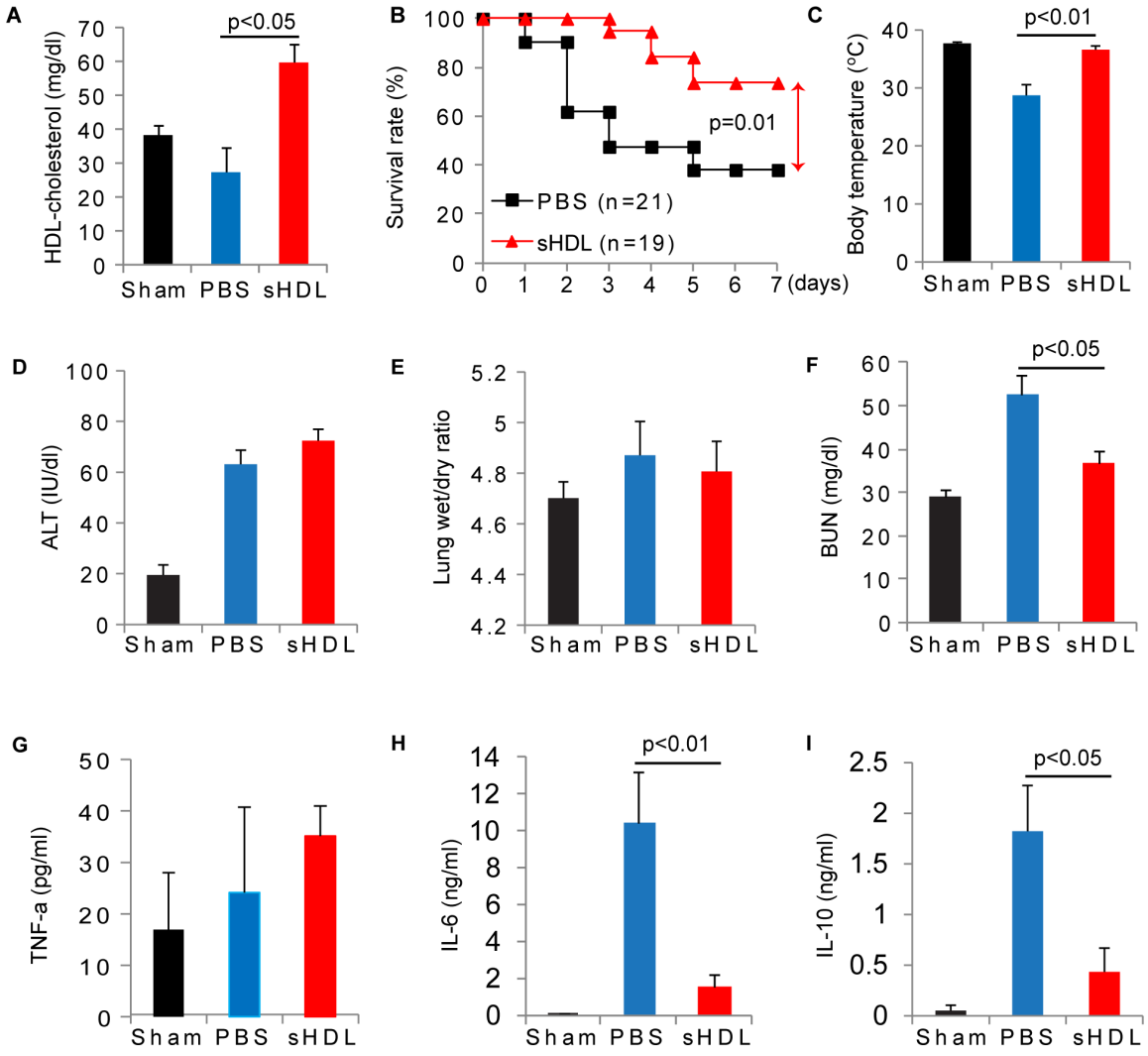


Figure 2-3 sHDL protects CLP-induced animal death and attenuates CLP-induced organ injury and inflammatory cytokine production. *B6 mice were subjected to CLP (21G needle, 2/3 ligation). 2h post CLP, mice were treated with 100 µl of PBS or sHDL containing 7.5 mg protein/kg body weight (i.v.). Plasma and lung were collected 18 h post CLP and HDL was prepared by sequential ultracentrifugation (1.5 ml plasma from 5 mice were used to make one HDL preparation); HDL-cholesterol concentrations (**A**); 7d Survival (**B**); Body temperature (**C**). Organ injury was detected by quantifying plasma ALT (**D**), lung wet/dry ratio (**E**), and plasma BUN (**F**). Plasma cytokines TNF-α (**G**), IL-6 (**H**) and IL-10 (**I**) were quantified with ELISA kits.*

2.4.6 Modeling of sHDL Binding to Endotoxins

Although our *in vivo* results suggest sHDL is effective in protecting against sepsis, lack of a clear mechanism warranted additional *in vitro* studies. While the ability of both liposomes and HDL to bind and neutralize LPS is known [152, 153], we questioned whether sHDL had a higher affinity for LPS binding, and whether this also holds true for LTA, a component of *gram positive* bacteria. The energetics of LPS and LTA binding were estimated computationally through CG MD simulation using both the lipid-only and self-assembled ETC-642 nano-sized particles (**Fig. 2-4 A-D and 2-4 E-F**, respectively). As shown in **Fig. 2-4 F-H**, the ETC-642 peptides are arranged in parallel around the edge of lipid bilayer, similar to the parallel alignment of ApoA-I proteins in the double-belt model of native HDL. The calculated PMF energies show that ETC-642 assembled particles efficiently bind both LTA and LPS with binding free energies of around 30 kcal/mol and 80 kcal/mol, respectively. We also show that assembled ETC-642 nanoparticles have higher affinity to LTA and LPS relative to lipid alone by 4.4 kcal/mol (**Fig. 2-4I)** and 17.7 kcal/mol (**Fig. 2-4J**), respectively, indicating that the ApoA-I peptide may play a key role in the ability of ETC-642 particle to neutralize LTA/LPS. We also directly measured the binding enthalpies of LPS to ETC-642 and phospholipids by isothermal titration calorimetry to be -39.94 and -23.63 kcal/mol, indicating stronger binding sHDL nanoparticle rather than to it's lipid component (**Table 2-2**).

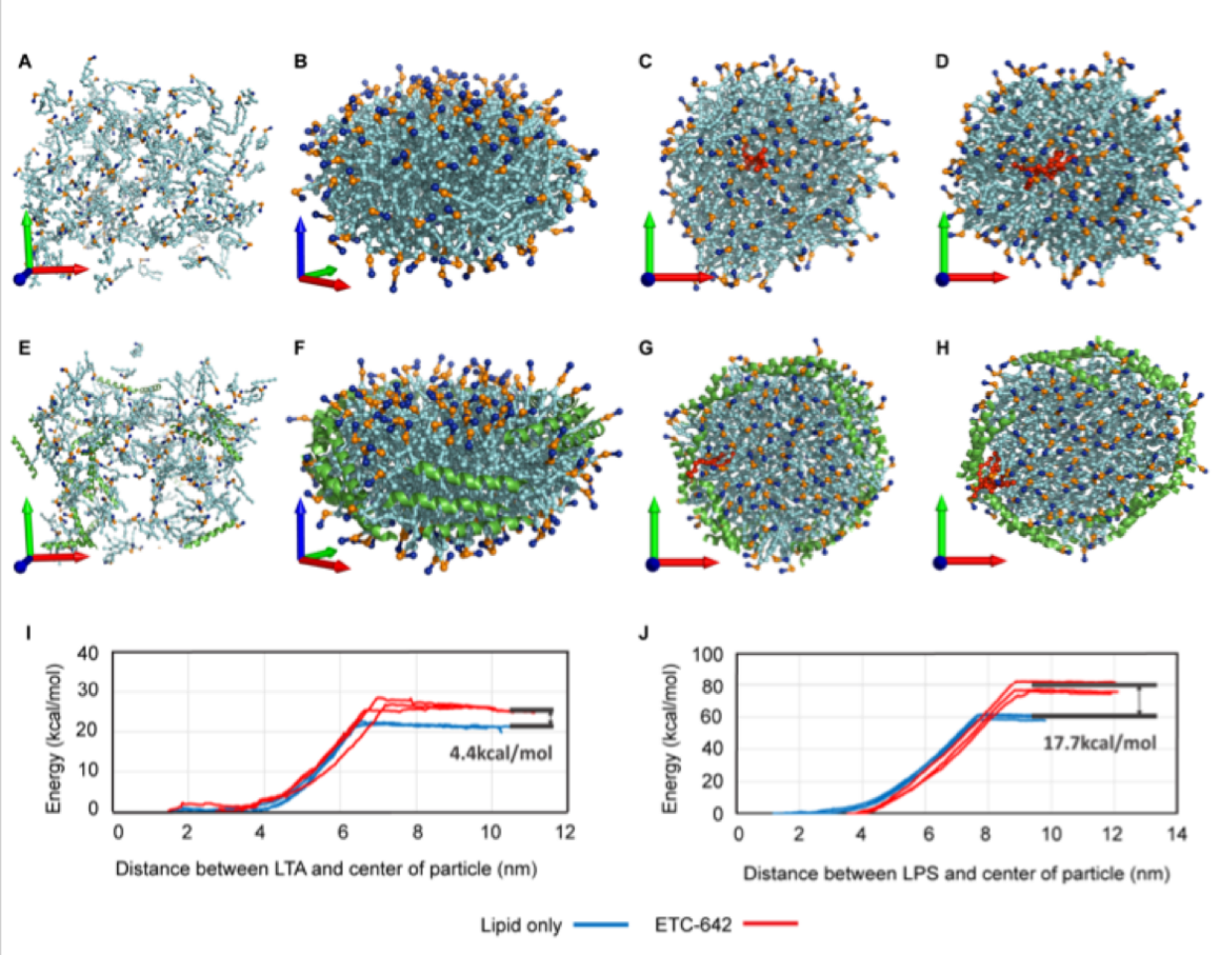


Figure 2-4 Modeling of sHDL binding to endotoxins. *The initial state of the lipid-only particle (**A**), all lipid (colored in cyan) are randomly distributed. The positively charged choline head and the negatively charged phosphoric acid group are colored in blue and gold, respectively. The X, Y, and Z axes of the coordination system are showed by red, green, and blue arrows, respectively. The final state of lipid-only particle (**B**), its self-assembly to a discoid nanodisc in 3 μs simulation. The hydrophilic surface of the Nanodisc is aligned with XY plane. LTA (**C**) and LPS (**D**) are showed in stick-ball style and colored in red and can insert into the lipid-only particle. The initial state of ETC-642 particle (**E**) , 22A peptides are showed in cartoon style and colored in green. ETC-642 particle also forms a nanodisc (**F**) with all peptides arranged around the lipid. LTA (**G**) and LPS (**H**) can also insert into the ETC-642 particle, however, they favorably localize near the 22A peptides. PMF calculated binding free energy of (**I**) LTA and (**J**) LPS binding with lipid-only (blue) or ETC-642 particle (red) show ETC-642 particles have more favorable binding energy for both LPS and LTA over lipid-only particle.*

2.4.7 sHDL Suppresses LPS/LTA-Induced NF-κB Activation

Next, we were interested in investigating the molecular pathways involved in the effect of ETC-642 on inflammatory signaling. To do this, we utilized stably transfected HEK-Blue cells expressing either human TLR-4 or TLR-2 (**Fig. 2-5A**). Cells were challenged with the corresponding receptor ligands (LPS for TLR-4 and LTA for TLR-2) in the presence/absence of sHDL at varying concentrations. In both cases, we observed a dose-dependent decrease in NF-κB activation with increasing sHDL concentrations, with maximal sHDL treatments inhibiting activation by roughly 95% (**Fig. 2-5B**) and 85% (**Fig. 2-5D**) for LPS/TLR-4 and LTA/TLR-2 models, respectively.

While the LPS binding capability of HDL is known [152, 153], others suggest that HDL may also exert a multitude of anti-inflammatory properties via cellular signaling pathways [83, 154, 155]. To assess whether the observed inhibition was solely due to endotoxin binding/neutralization, we performed a series of experiments in which we pre-treated TLR-4/TLR-2 expressing HEK-Blue cells with sHDL (60 μg/mL) for 6 hours, and then challenged with the corresponding ligands in the absence of sHDL. Although the extent of NF-κB inhibition was less than that of cells challenged in the presence of sHDL, pretreatment with sHDL was still able to reduce NF-κB activation by >30% in the LPS/TLR-4 model (**Fig. 2-5C,** $p<0.01$) and >25% in the LTA/TLR-2 cell model (**Fig. 2-5E,** $p<0.01$). This suggests that physical binding of LPS/LTA by sHDL is not the only mechanism by which sHDL exerts protection in sepsis/inflammation.

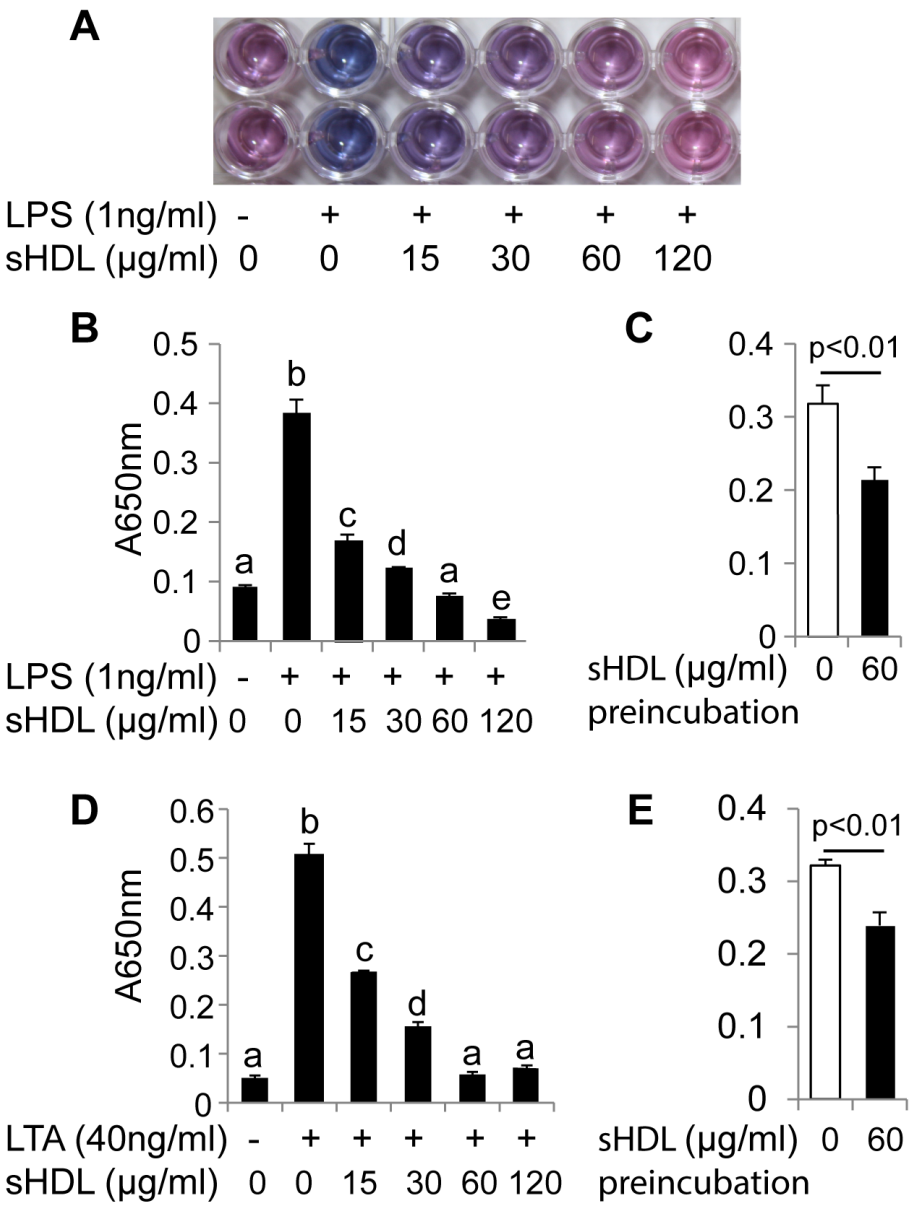


Figure 2-5 sHDL suppresses LPS/LTA/TNF-α-induced NF-κB activation. *HEK-Blue cells expressing TLR4, TLR2 or TNF-α receptors were cultured to 70% confluency and treated with LPS at 1ng/ml (**A** and **B**) or LTA (**D**) in the presence of sHDL ETC642 for 16 hours. Alternatively, cells were pre-treated with sHDL ETC642 at 60 µg/ml for 6 h and stimulated with the corresponding ligands (**C** and **E**). Then, 100µl of the culture supernatant was mixed with 100µl HEK-Blue™ Detection and the activation of NF-κB reporter was quantified by measuring absorption at 650nm. Data was analyzed by one-way ANOVA (**B and D**) or student's t-test (**C and E**).*

2.4.8 sHDL Suppresses LPS and LTA-Induced Cytokine Production in Macrophages

While it is evident that sHDL confers protection against TLR-4/TLR-2-induced NF-κB activation in HEK cells, we wanted to confirm that inhibition was also applicable in macrophages, the major immune cells involved in the onset and progression of sepsis. Here, we used the presence of cytokines TNF-α and IL-6 in the supernatant as our endpoint. In RAW 264.7 cells challenged with LPS (2 ng/mL), co-incubation with sHDL resulted in greater than 2-fold reduction in both TNF-α (**Fig. 2-6A**) and IL-6 (**Fig. 2-6B**) production over PBS-treated controls ($p<0.01$). In cells challenged with LTA (40 ng/mL), incubation in the presence of sHDL (120 μg/mL) reduced TNF-α production by more than 50% ($p<0.05$), as seen in **Fig. 2-6C**.

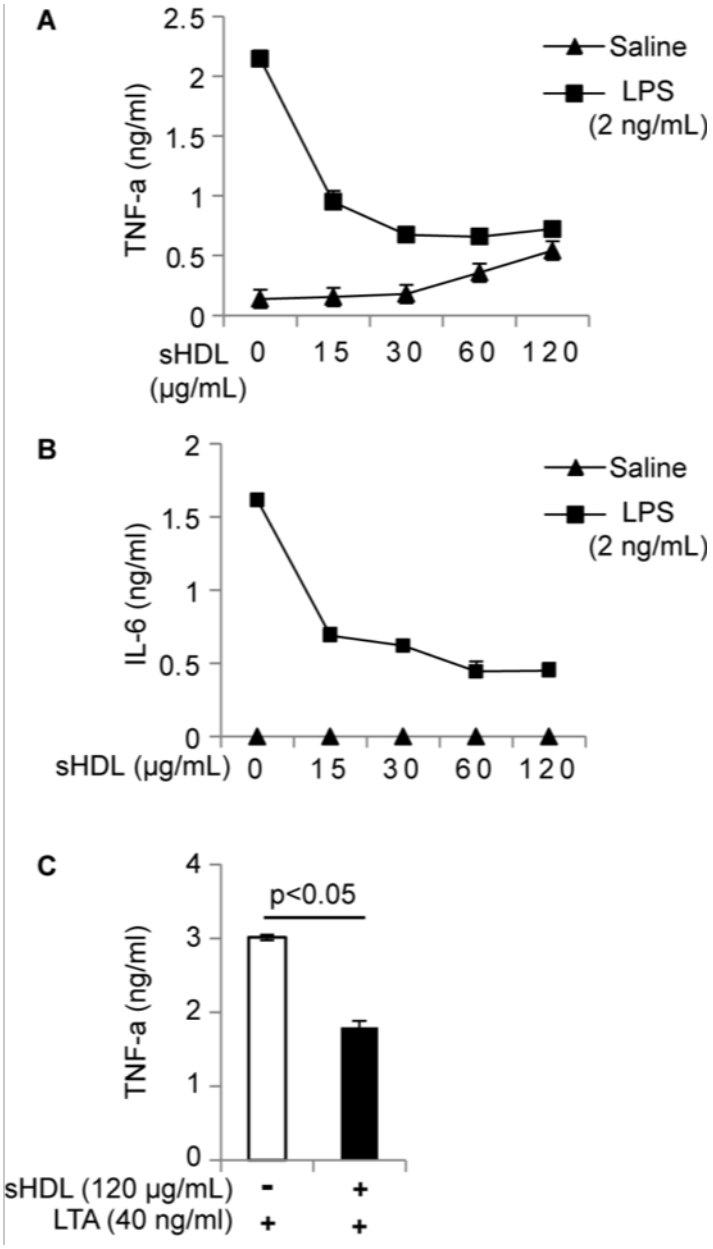


Figure 2-6 sHDL suppresses LPS and LTA-induced cytokine production in macrophages. *Raw 264.7 cells were cultured to 70% confluency and treated with LPS (**A** and **B**) or LTA (**C**) in the presence of sHDL ETC-642 for 16 hours. The concentrations of TNF-α and IL-6 in the supernatant were measured by ELISA.*

2.4.9 sHDL Suppresses LPS-Induced Endothelial Cell Activation

In addition to macrophages, sepsis also manifests as a disorder of the endothelium [155-158]. As mentioned earlier, we hypothesize that the drop in HDL-C and ApoA-I observed in septic patients is a major contributor to the vascular dysfunction. Thus, the next step in our research was to assess sHDL protection against endothelial activation *in vitro*. Characteristic inflammatory markers in endothelial cells include expression of cell adhesion molecules, reduction in eNOS expression, and the induction in pro-inflammatory cytokine release. Here, we used HUVECs activated with LPS (1 μg/mL) as our cell model, and examined the ability of sHDL to reduce cell adhesion molecule mRNA expression (VCAM-1, ICAM-1, and E-selectin), increase endothelial nitric oxide synthase (eNOS) mRNA levels, and decrease the production of pro-inflammatory cytokines IL-6 and IL-8. As expected, ICAM-1 (**Fig. 2-7 A**), VCAM-1 (**Fig. 2-7 B**), and E-selectin (**Fig. 2-7 C**) mRNA expression levels were reduced >10-fold in HUVECs challenged with LPS in the presence of sHDL compared to PBS ($p<0.01$). Additionally, sHDL at concentrations of 30 and 60 μg/mL were also able in increase eNOS mRNA expression by 1.8 and 2.4-fold, respectively (**Fig. 2-7D**, $p<0.05$). There was no significant change in eNOS expression for cells treated with sHDL at 15 and 120 μg/mL compared to PBS-treated controls. Additionally, sHDL at all concentrations (15-120 μg/mL) was able to suppress production of IL-6 (**Fig. 2-7 E**) and IL-8 (**Fig. 2-7 F**) by >4-fold and >50-fold over PBS controls, respectively ($p<0.01$).

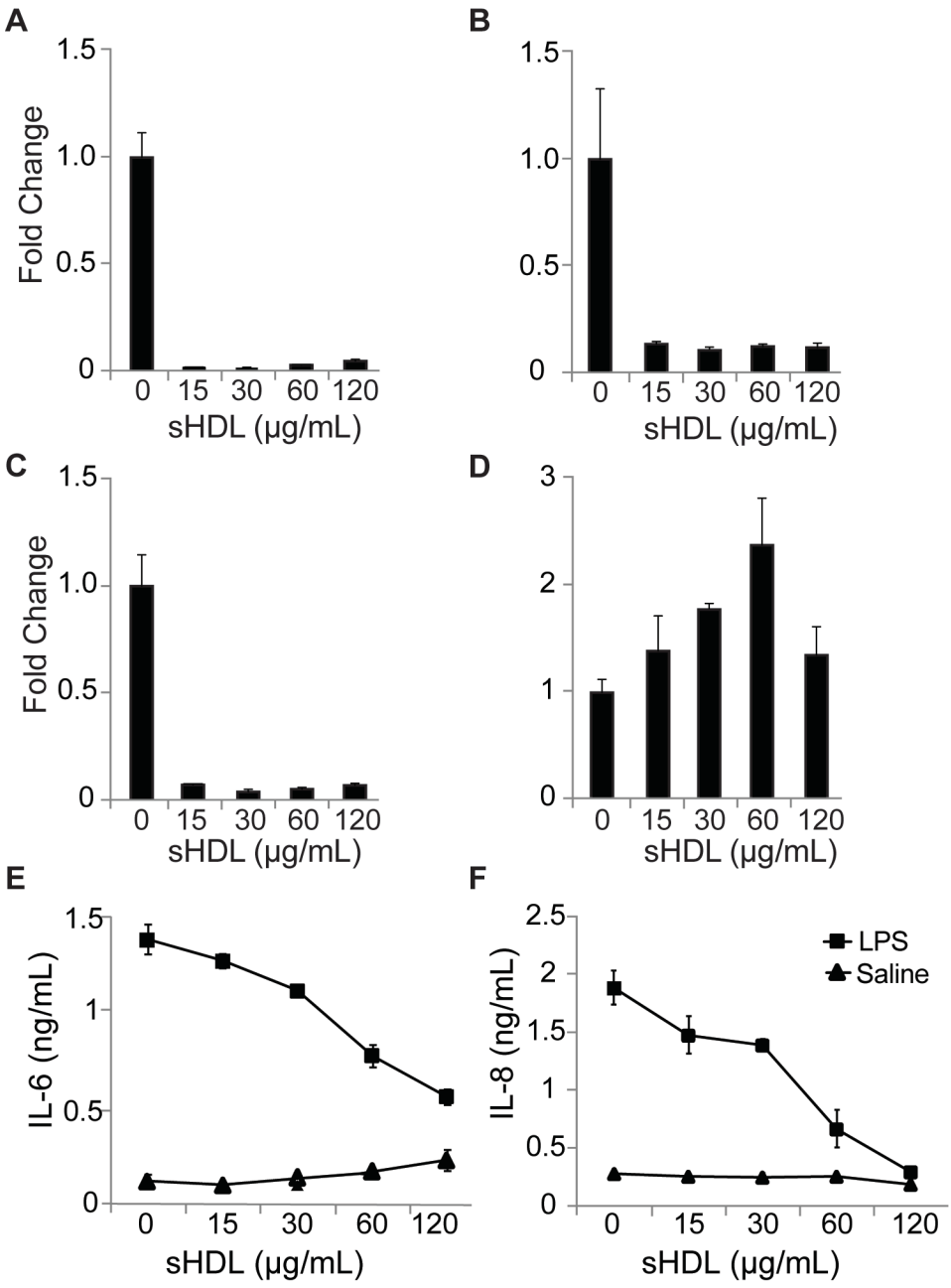


Figure 2-7 sHDL inhibits LPS/TNF-α-induced endothelial cell activation and inflammatory cytokine production. *Human umbilical vein endothelial cells (HUVEC) were treated with LPS in the presence of sHDL at the concentrations indicated in the figure. Fold change in gene expression of VCAM-1 (**A**), ICAM-1 (**B**), E-selectin (**C**), and eNOS (**D**) were determined by RT-qPCR and normalizing to endogenous GAPDH expression. Concentrations of cytokines IL-6 (**E**) and IL-8 (**F**) in the supernatant were measured by ELISA.*

2.4.10 sHDL Promotes Efflux of Membrane Cholesterol which Down-Regulates Caveoli TLR Levels and Suppresses TLR-4 Signaling in Macrophages

Although we clearly show that ETC-642 can bind and neutralize LPS/LTS, HDL is known to possess other anti-inflammatory properties independent of endotoxin binding. This is evident through our findings that TLR4/NF-kB signaling is still significantly reduced in cells that are treated with sHDL and LPS *separately* (**Fig. 2-5 C,E**). TLR4 is located in lipid rafts, which are microdomains rich in cholesterol. We speculated that sHDL reduces lipid raft cholesterol levels which suppresses TLR4/NF-kB signaling. To test this, we first examined the cholesterol efflux capacity of ETC-642 at different doses from [^{3}H]-cholesterol-loaded RAW 267.4 macrophages. Indeed, we found that ETC-642 can take up cholesterol from cellular pools in a dose-dependent manner (**Fig. 2-8 A**). We then quantified total cellular cholesterol in macrophages after treatment with ETC-642 or vehicle. Our results clearly show that those cells receiving sHDL treatment had >2-fold lower total cholesterol levels than those receiving PBS vehicle ($p<0.01$, **Fig 2-8 B**). Finally, we examined whether sHDL suppresses TLR4 lipid raft localization. To do this, RAW 264.7 macrophages were pretreated with/without sHDL (60 μg/mL) for 6 hours. Following incubation, sHDL was removed and cells were stimulated for 10 minutes with/without LPS. TLR4 and SR-B1 were blotted for in each subcellular fraction. In cells receiving sHDL treatment, TLR4 in the lipid rafts was drastically reduced compared to cells receiving vehicle (**Fig. 2-8 C**). To confirm these findings, we also tested the cholesterol efflux activity of ETC-642 using [^{3}H]-cholesterol loaded RAW264.7 macrophages and found that our sHDL could efflux cholesterol in a dose-dependent manner, with roughly 30% total [^{3}H]-cholesterol efflux to sHDL after 18 hours

of incubation. The efflux activity of 22A peptide was also tested but had significantly less activity compared to in-tact sHDL particles (**Fig. 2-8 D**), further supporting the notion that the entire sHDL particle, rather than individual peptide or lipid components alone, is necessary to elicit the entire array of HDL protection.

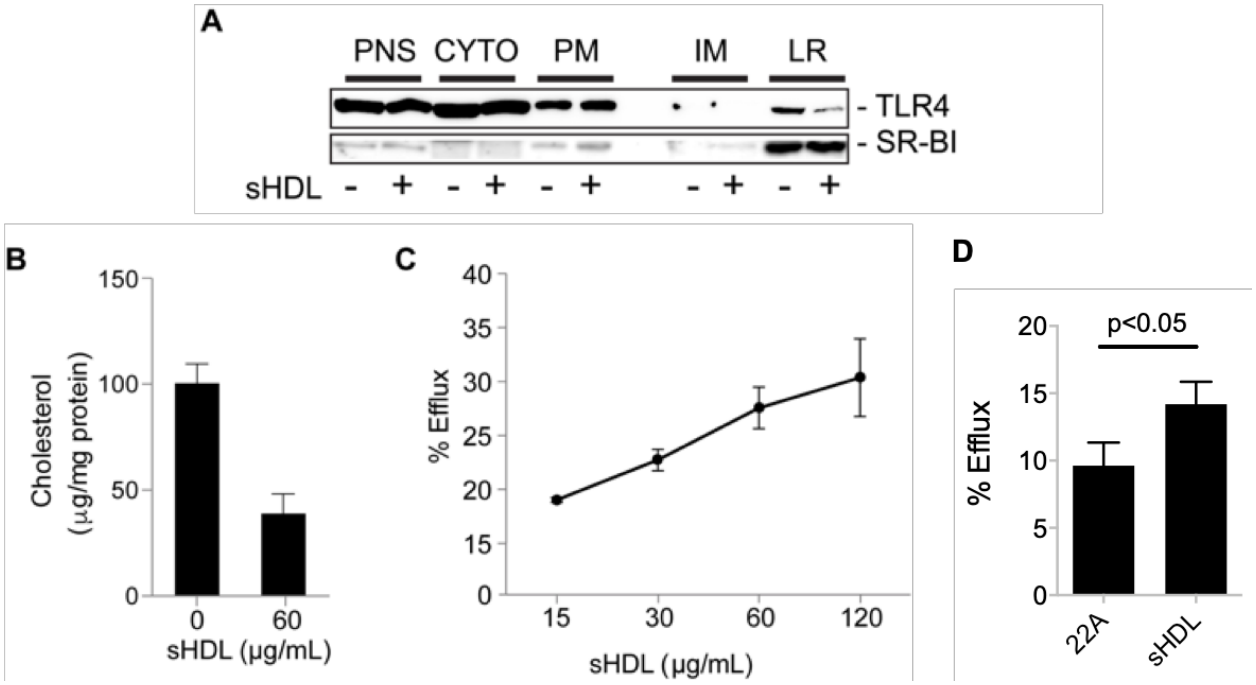


Figure 2-8 sHDL suppresses TLR4 lipid raft targeting*. For (**A**) and (**B**), RAW 264.7 cells were cultured to 70% confluency and pre-treated with sHDL at 60 µg/mL for 12 h, stimulated with LPS at 2 ng/ml (k12) for 10 min. (**A**) The cells were harvested and the subcellular fractions were isolated with Opti-Prep method and TLR4 or SR-BI in each fraction was analyzed by Western blot. Post-nuclear supernatant (PNS), cytosol (CYT), intracellular membrane (IM), plasma membrane (PM) and lipid raft (LR) fractions. (**B**) Cells were harvested and total cellular cholesterol was extracted and quantified using Wako Diagnostics total cholesterol reagent kit using the FPLC method. (**C-D**) RAW 264.7 cells were loaded with [^{3}H]-cholesterol for 24 hours followed by incubation with sHDL for 18 h at 0, 15, 30, 60, or 120 µg/mL (**C**) or 6h incubation with sHDL or 22A peptide at 15 µg/mL (**D**) . Percent cholesterol efflux was determined by dividing radioactive counts in media by the sum of counts in media and cellular fraction. Average blank values were subtracted to yield net cholesterol efflux due to sHDL; data are expressed as mean +/- SD.*

2.5 Discussion

In this study, we showed that septic patients have a significant decrease in HDL levels. ETC-642—a new generation of sHDL—significantly increased HDL levels and improved the 7-day survival in CLP-treated mice. We also provided evidence supporting our hypothesis that sHDL protects against sepsis through multiple protective mechanisms, not solely by neutralizing endotoxins (both LPS and LTA), but also by suppressing inflammatory signaling in both macrophages and endothelial cells, i.e. cytokine production and cell adhesion molecule expression. Together, our findings in the clinic*, in vitro* and *in vivo* reveal that a second generation of a fully-synthetic and endotoxin-free sHDL, ETC-642, can be an effective and clinically translatable therapy for sepsis.

Consistent with previous findings by Chien *et al.* in 2003, HDL-C levels are markedly reduced in septic patients, and patients with HDL-C less than 10 mg/dL (or 20 mg/dL as described by [57]) had nearly double the incidence of mortality than those with higher HDL-C levels. It was also evident that, in survivors, HDL-C levels slowly increased over 14 days while non-survivors exhibited no increase (**Fig. 2-1**). In 2014, Al-Zaidawi reported similar data, where patients with HDL-C less than 15 mg/dL had a significantly increased risk of developing sepsis, and those who eventually died from sepsis all had HDL-C <5 mg/dL in the 1-2 days preceding death [159]. More recently, Trinder, et. al. identified that carriers of a gain-of-function genetic variant in the cholesterol ester transfer protein (CETP) gene, rs1800777, exhibit an exacerbated drop in HDL-C under septic conditions when compared to non-carriers and consequently, lower overall survival rates. [160] The allele and accompanying drop in HDL-C was also

determined to increase sepsis-associated acute kidney injury and compromised renal function. [161, 162] Thus, increasing circulating HDL in sepsis patients presenting low HDL-C remains an attractive therapeutic strategy.

Despite overwhelming evidence, the exploitation of HDL for use as a sepsis therapy has been somewhat abandoned in the past 10 years. Numerous earlier efforts were made to test the feasibility of “first generation” rHDL/sHDL as a sepsis therapy. Findings in endotoxemia animal models were encouraging and showed that rHDL and sHDL treatment can improve survival in LPS-challenged animals [72, 141-143, 155, 163-165]. Using rHDL made of human ApoA1, Quezado et al. reported that administration of rHDL suppressed inflammatory cytokine production in gram-negative bacterial infection model, but failed to improve survival, likely due to toxicity and impurity of the rHDL product [166]. Studies using the ApoA-I-mimetic peptide 4F showed that peptide treatment could increase HDL-cholesterol levels and improve 2- and 4-day survival in CLP-treated rats [154, 167].

Despite these findings, studies using first generation rHDL/sHDL suffer from a lack of clinical translatability. While effective, the use of naked ApoA-1 mimetic peptides, such as 4F, is limited by the short circulation time of the free peptide, requiring high or repeated-dosing over a short period of time to achieve clinical efficacy. This may explain the need for high doses of rHDL to show efficacy, ranging anywhere from 45-500 mg/kg in various animal models [72, 163, 164, 168-171], whereas highly pure “second generation” sHDL, in this case ETC-642, is effective in many aspects as doses as little as 7.5 mg/kg in mice. In toxicology evaluations high doses of rHDL and sHDL resulted in off-target toxicity such as elevation of liver enzymes due to mobilization and delivery

to the liver large amount of cholesterol [94, 97, 98]. On the other hand, purified human ApoA-I contains inherent variability, which is impossible to avoid, and, in addition to the costly and challenging purification, remains developmentally limited by the ability to obtain mass quantities of human plasma to meet clinical yield. Nevertheless, experiments using first generation rHDL/sHDL show encouraging results, however, their effect in a clinically relevant sepsis animal model remains less clear [166, 172].

In addition to biological assays, we investigated the protective mechanism of HDL in sepsis by employing a computer-based approach using coarse-grained (CG) model to simulate the binding of ETC-642 with LTA/LPS molecules. The calculated ΔH between ETC-642/LPS binding and Lipids/LPS binding (-17.7 kcal/mol, as shown in Fig. 4) is consistent with the calorimetry experimental data from ITC (-16.31 kcal/mol, as shown in **Table 2-2**), suggesting that the PMF energy calculated using our CG model can provide an accurate prediction of the experimental values. Furthermore, according to the PMF calculation based on the computational models, the lower binding free energy of LTA/LPS with ETC-642 compared with lipid-only particle reveals a possible protective mechanism of the ETC-642 (22A) peptide against sepsis. That is, ETC-642 is potent in the capture and neutralization of free LPS/LTA in plasma.

Developed by Esperion Therapeutics in the early 2000's, ETC-642 presents an advantageous opportunity for the rapid translation of this therapeutics as an acute sepsis treatment. Unlike other investigational therapies, ETC-642 has already shown promise in manufacturing scalability, and more notably, exhibited a wide therapeutic window with low toxicity in several single- and multiple-dose clinical trials, showing safety at doses ranging from 1 – 30 mg/kg in humans [95, 96]. Its manufacturing is well-

established and toxicology complete and, hence, could be rapidly translated to the clinic for evaluation as a sepsis treatment. Additionally, the use of synthetic peptides and lipids circumvents toxicity-related concerns associated with rHDLs made from human plasma-purified apoA-1 due to residual endotoxin and other host-related impurities. Moreover, generating peptide-based sHDL eliminates the demand for massive quantities of human plasma required to produce rHDL in large-scale. Overall, the synthetic-based approach of sHDL development allows for greater control and flexibility over the production process and results in a cheaper, purer, and user-defined end product.

Several sepsis therapies have reached clinical trial over the past 20 years, yet for one reason or another they have all failed. One problem with such treatments is the lack of patient selection. Simply put, the rapid onset and progression of sepsis presents a challenge when deciding which patients would benefit from which therapy, and one therapy may be both helpful and detrimental in patients, depending on the severity of their condition. Unlike such examples, sHDL holds the advantage of patient selection. As previously discussed, low HDL-C levels have been consistently correlated with poor outcomes in septic patients. That being said, sHDL therapy would be intended for use in patients with low HDL-C, and the dose determined by patient HDL-C levels at the time of hospital intake. The ability to discriminate between those patients who would and would not benefit from such treatment is a major advance in the sepsis field, aiding in clinical trial design while also minimizing adverse patient outcomes.

One issue with past therapeutic approaches is that they only targeted one element of an incredibly complex and dynamic disease. Such examples include TNF

receptor agonists, LPS and TNF-neutralizing antibodies, among others [173]. Given the multifaceted nature of the disease, sHDL offers a wider range of protection through its multiple mechanisms of action. While we and others have documented the inherent ability of HDL to neutralize and detoxify endotoxin [72, 152, 153], in the current study we also show that HDL exerts other anti-inflammatory properties, i.e. inhibition of endothelial cell activation and lipid raft modulation, which remains consistent with other recent reports showing anti-inflammatory properties of HDL in models of cardiovascular disease [83, 174, 175]. Given the cardiovascular protection that HDL infers, and that sepsis manifests largely as a disorder of the endothelium, it is worth considering whether sHDL can prevent or reverse endothelial dysfunction in septicemia.

While our findings utilizing ETC-642 as a sepsis therapy are encouraging, there is even greater potential in the optimization of second-generation sHDL for sepsis-specific purposes. As previously mentioned, ETC-642 was developed for the treatment of cardiovascular disease, optimized primarily for ability to efflux cholesterol. However, we have previously shown that the phospholipid makeup of sHDL can potently affect its overall behavior, i.e. cytokine inhibition, efflux capacity and others [133]. With that in mind, there is great potential for the reformulation of sHDL composition to reflect optimal performance in sepsis. Additionally, our study employed a one-time bolus administration of ETC-642 at a low dose, leaving a large window of opportunity to improve clinical outcome by exploring alternative dosing regimens. Overall, our findings reveal that second-generation sHDL particles are a promising avenue toward the treatment of sepsis. While future work is needed to build upon this platform and maximize the potential benefit, we have for the first time demonstrated efficacy against sepsis using a

clinically translatable therapeutic with considerable tailorability and broadly applicable applications in inflammatory disease models

2.6 Supplemental Information

Table 2-1 Demographic and clinical characteristics of the patient population.

	Control (no-sepsis) patients		Sepsis patients	
Subjects (Samples)	39 (85)		85 (215)	
Age (years ± SEM)	64.8±2.6		60.5±1.8	
Gender	24M/15F		44 M/41 F	
Race, % Caucasian	92		91.7	
Cause of sepsis or ICU admission	Respiratory	15 (38.5%)	Pneumonia	41 (48%)
	Metabolic	8 (20.5)	Urinary tract infection	13 (15%)
	Cardiac	6 (15.4%)	Primary bacteremia	5 (5.8%)
	Neurological	4 (10.2%)	Biliary tract/peritoneal	5 (5.8%)
	GI bleed	3 (7.7%)	Other	21 (24.7%)
	Other	3 (7.7%)		
Survivors	38 (97%)		69 (81%)	
Non-survivors	1 (3%)		16 (19 %)	
Length of hospital stay (days)	18.3		21.6 15.8 (non-survivors)	

Table 2-2 ITC experiments data for different particle-LPS mixtures*. The ∆H between ETC642-LPS and Lipids-LPS mixtures in 37°C is -16.31 kcal/mol.*

Sample	Temperature (°C)	Binding Enthalpy DH (kcal/mol)	Binding Energy K (1/M)
ETC-642	37	-39.94	1.25×10^5
Lipids	37	-23.63	1.02×10^4
22A Peptide	37	-0.70	N/A

Chapter 3: Synergetic effect of rHDL and LXR ligand co-administration on induction of cholesterol efflux and reduction of atherosclerosis.

3.1 Abstract

Reconstituted high-density lipoproteins (rHDL) are potent regulators of reverse cholesterol transport and rHDL infusions in cardiovascular disease patients induce rapid mobilization of cholesterol from the periphery, resulting in overall reduction in atheroma volume. Because the efficacy of rHDL relies heavily upon its ability to efflux cholesterol, we propose that a combination therapy of rHDL and a liver X receptor (LXR) agonist could maximize the therapeutic benefit of rHDL by upregulating key cholesterol transporters, ABCA1 and ABCG1. In this study, we show that expression of ABCA1/G1 mRNA *in vitro* is reduced in macrophages after treatment with rHDL, and this expression is upregulated by addition of the LXR agonists, T0901317 (T1317) and GW3695. We also show that in combination, rHDL and T1317 exhibit greater overall cholesterol efflux from J774A.1 foam cells *in vitro*. This effect was mimicked *in vivo*, whereby ApoE$^{-/-}$ mice treated with rHDL + T1317 combination therapy had a significant reduction in atheroma burden at the end of 6 weeks compared to PBS treated controls, while neither rHDL nor T1317 alone had a significant effect. Together, we show that rHDL paired with an LXR agonist can induce a synergetic effect and maximize the capacity of rHDL to efflux cholesterol and reduce the burden of atherosclerosis.

3.2 Introduction

Reconsituted high-density lipoprotein (rHDL) therapeutics are both an intriguing and controversial class of therapeutics being developed for treatment of acute coronary syndrome (ACS) [176]. Designed to mimic the athero-protective function of endogenous pre-β HDL particles, rHDL are composed of apolipoprotein A-I (ApoA-I) or ApoA-I mimetic peptides complexed with phospholipids to form 8-10 nm nanodiscs [106]. They are shown to be safe and well tolerated in humans, and their ability to rapidly mobilize cholesterol and reduce atheroma burden in patients has been proven [94-98]. However, despite success in early phase clinical trials, Phase 2 trials resulted in a lack of plaque burden reduction and toxicity at high doses [94, 98] and no reduction of cardiovascular events rates (CSL-112). The extrapolation between clinical results of various rHDL products is somewhat difficult, as their protein and phospholipid composition varies, resulting in significant differences in doses required to elicit cholesterol efflux in patients as well as variable pharmacokinetics and toxicity [100-103] . While there are no approved HDL infusion therapies on the market yet, and a 17,400-patient Phase 3 trial is currently ongoing for CSL-112 to show possible reduction of major adverse cardiovascular events (MACE) in subjects with ACS [104, 105].

HDL's ability to reduce atherosclerosis can be largely explained by its role in driving reverse cholesterol transport by acting as a cholesterol acceptor and shuttling excess cholesterol from the periphery back to the liver for excretion [5]. Its ability to do so is also largely dependent on the function of ATP-binding cassette transporters A1 and G1 (ABCA1 and ABCG1, respectively) located on the plasma membrane of foam cell macrophages. Interestingly, it was observed that one of these transporters, ABCA1,

is down-regulated both *in vitro* [177] and *in vivo* upon administration of both native HDL and rHDL, CER-001, contributing to a lack of dose-response in a mouse model of accelerated atherosclerosis [178]. Moreover, others have reported decreased ABCA1 protein expression present in human carotid artery plaques [179]. In this context, it is likely that following the first administration of rHDL, cholesterol transporters levels in plaque foam cells are reduced, thus, making subsequent doses of rHDL unable to reach their maximum cholesterol efflux and atheroma reduction potential. This was one of the explanations for the lack of clinical efficacy of high doses of CER-001 rHDL.

Both ABCA1 and ABCG1 are regulated at the transcriptional level by liver X receptor (LXR), and several orally active small molecule LXR agonists have been developed to induce ABCA1/G1 expression and decrease cellular cholesterol accumulation in cardiovascular disease, including T0901317 (Tularik), GW3965 (GSK), and LXR 623 (Wyeth) [180, 181]. However, clinical development of this drug class is hindered by the large doses required to achieve therapeutic benefit and, consequentially, significant off-target toxicity [180, 182]. In addition, increasing ABCA1/G1 expression by LXR agonist relies on the presence of endogenous HDL to serve as acceptor to facilitate cholesterol efflux from atheroma foam cells and transport it to the liver for elimination. However, many ACS patients exhibit low circulating levels of HDL or possess “dysfunctional” HDL, unable to efflux and offload cholesterol for excretion [183-185]. For this reason, the addition of a functional, cholesterol-free rHDL may maximize the efficacy of this class of drugs while lowering the overall effective dose.

In this study, we propose to investigate the potential synergetic effect of co-administering rHDL and LXR agonist on atherosclerosis reduction. We hypothesized that a potential synergy between two drugs stems from the abilities of 1) LXR agonists to increase expression of key cholesterol transports ABCA1 and ABCG1 in foam cells, 2) rHDL to act as a functional cholesterol acceptor, taking up excess cholesterol via interactions with ABCA1/G1 and 3) LXR agonist to overcome rHDL-induced reduction of ABCA1/G1 expression. By targeting these key components of the RCT pathway, we could synergistically enhance their therapeutic benefit over rHDL and LXR agonist therapies alone. Furthermore, a synergetic effect could potentially lead to reduction in dose of rHDL and LXR agonist required for therapeutic efficacy, leading to subsequent reduction in unwanted side effects and a renewed interest in clinical development of these two promising drug classes.

3.3 Materials and Methods

3.3.1 Reagents

22A peptide (PVLDLFRELLNELLEALKQKLK) was synthesized by Genscript (Piscataway, NJ) and purity was determined to be >95% by HPLC. Egg sphingomyelin (SM), 1,2-dipalmitoyl-*sn*-glycero-3-phosphocholine (DPPC), and 1-palmitoyl-2-oleoyl-*sn*-glycero-3-phosphocholine (POPC) were purchased from Avanti Polar Lipids (Alabaster, AL) and Nippon Oil and Fat (Osaka, Japan). T0901317 (T1317), GW3695, and LXR623 were purchased from Cayman Chemical (Ann Arbor, MI). T1317, GW3695 and LXR623 were dissolved in DMSO as a stock solution at 10 mg/mL. Anti-ABCA1 (ab18180) mouse monoclonal antibody and secondary antibody goat-anti-mouse IgG H+L (HRP)

(ab205719) were purchased from Abcam (Cambridge, UK). Anti-GAPDH (D16H11) XP® rabbit monoclonal antibody (#5174) and HRP-conjugated goat anti-rabbit secondary antibody (#7074) were purchased from Cell Signaling Technology (Danvers, MA). For animal studies, the stock T1317 solution was diluted with PBS to a final concentration at 0.15 mg/ml and administered at 1.5 mg/kg via intraperitoneal (i.p.) injection immediately. The final DMSO concentration in cell culture did not exceed 0.1% throughout the study. All other materials were obtained from commercial sources.

3.3.2 rHDL Preparation

Discoidal ETC-642 rHDL was made by co-lyophilization followed by thermal cycling as described previously [133]. Briefly, 22A peptide and phospholipids were combined and dissolved in glacial acetic acid at a 22A:SM:DPPC ratio of 1:1:1 by weight. The resulting solution was frozen in liquid nitrogen and freeze-dried overnight to remove the acid. Once dried, the lyophilized powder was reconstituted in 1X phosphate buffered saline (PBS) to the desired final peptide concentration and vortexed to completely dissolve, forming a cloudy white suspension. The resulting solution was subjected to 3 heat/cool cycles, each cycle consisting of 5 minutes heating at 55 °C and 5 minutes cooling at room temperature (above and below the transition temperature of the lipids, respectively). By the end of 3 cycles the solution had turned from cloudy to clear, indicating formation of rHDL nanoparticles. The pH of the rHDL solution was adjusted to 7.4 using NaOH and 0.2 μm sterile-filtered.

ApoA-I containing rHDLs were prepared by a thin-film method. Briefly, lipids (SM or POPC) were dissolved in chloroform followed by removal of the solvent under a stream of nitrogen gas and overnight incubation under vacuum at room temperature. The

resulting lipid film was hydrated by a solution of ApoA-I to achieve the desired weight ratio of ApoA-I:lipids (1:1.5 ApoA-I:POPC for “CSL-112 like”, and 1:2.7 ApoA-I:SM for “CER-001 like”) . The resulting mixture was vortexed, followed by brief (<30 sec) bath sonication in order to fully disperse the lipid film. The solution then underwent 3 heat/cool cycles, as described above, to form a clear, homogeneous solution of rHDL and sterilized by 0.22 μm filtration.

3.3.3 rHDL Characterization

Quality of rHDL particles was assessed using the following analytical techniques. Size distribution was determined by dynamic light scattering (DLS) on a Malvern Zetasizer Nano ZSP (Westborough, MA), and particle purity was determined by gel permeation chromatography (GPC) with UV detection at 220 using a Tosoh TSK gel G3000SWxl column (Tosoh Bioscience, King of Prussia, PA) on a Waters HPLC, as previously described [133].

3.3.4 Cell Culture

J774A.1 macrophages were purchased from ATCC (Manassas, VA) and maintained in Dulbecco’s Modified Eagle’s Medium (DMEM) containing 10% fetal bovine serum (FBS) and 100 U/mL penicillin/streptomycin. Prior to treatment, cells were switched to DMEM containing 1% FBS overnight. Cells were then treated with rHDL (1, 10, or 100 μg/mL 22A peptide), T1317 (1μM), GW3965 (1μM), LXR623 (1μM), PBS or a combination of rHDL and LXR agonist for 24 h. At the end of treatment, cells were washed with PBS before proceeding to downstream applications.

3.3.5 Western Blot

Cells were treated with rHDL (100 μg/mL), T1317 (1μM), PBS, or rHDL + T1317 for 24 h. After treatment cells were washed twice with ice cold PBS and lysed in radioimmune precipitation assay (RIPA) buffer containing cOmplete™ mini, EDTA-free protease inhibitor cocktail (Sigma). Protein lysates (30 μg/lane) were separated by 7.5% SDS-polyacrylimide gel and transferred to 0.45 μm PVDF membrane using a Bio-Rad semi-dry transfer system. ABCA1 expression was determined by Western Blotting using antibodies for ABCA1 (1:1000) and GAPDH (1:1000). Signal was detected using horseradish peroxidase-conguated secondary antibodies (Cell Signaling Technologies) and ECL (Amersham Biosciences).

3.3.6 Cholesterol Efflux

Cholesterol efflux studies were performed, as described previously [186, 187]. Murine J774.1 macrophages (ATCC, Manassas, VA) were seeded in 48-well plates for 24 h. Cells were labeled with 1 μCi/ml [1,2-^{3}H]-cholesterol (Perkin Elmer, USA) in DMEM (Life Technology. Inc) containing 0.5 % fatty acid-free bovine serum albumin (BSA) and 5 μg/mL ACAT inhibitor Sandoz 58-035 (Sigma) for 24 h. Then cells were washed and treated with PBS, rHDL, T1317, or rHDL + T1317 compound for 24 h. Media was collected and cells were then incubated with DMEM/0.5 % BSA containing 50 μg/mL commercial HDL or 10 μg/mL ApoA-I as acceptors for 6 h. Medium was collected and filtered to remove detached cells and efflux was quantified by liquid scintillation and expressed as a percentage of total cell [^{3}H]-cholesterol content.

3.3.7 Quantitative Real-Time PCR

At indicated time points post-rHDL treatment, cells were washed twice with cold PBS and scraped and collected in lysis buffer. Total RNA was purified with the GeneJET RNA Purification Kit (Thermo Scientific), followed by cDNA synthesis with the SuperScript III First-Strand Synthesis System kit (Invitrogen). qPCR was carried out using Power SYBR Green Master Mix (Applied Biosystems) and primers for mouse *Abca1*, *Abcg1, Fasn, and Srebp1* (**Table 3-2**). Relative abundance of mRNA was normalized to the geometric average of housekeeping controls *18sRNA* and *Ppia*.

3.3.8 In vivo Macrophage Study

Male C57BL/6J mice, 7-9-week-old, were purchased from Jackson Laboratories (Bar Harbor, ME) and were housed at 22 ± 1°C in a 12:12-h light-dark cycle. All animal work was performed in accordance with the guidelines set by the University of Michigan Animal Care and Use Committee. Macrophages were elicited by injecting mice i.p. with 2 mL of 3% thioglycolate medium (BD Biosciences) 48 h prior to dosing. Animals were then randomly assigned (n=5/group) to receive vehicle (PBS/DMSO), rHDL (50 mg/kg ETC-642), T1317 (5 mg/kg), or a combination of rHDL and T1317 (50 mg/kg and 5 mg/kg, respectively) by i.p. injection. 24 h post-dose mice were sacrificed, and peritoneal macrophages were collected by peritoneal lavage with DMEM. Cells were resuspended in red blood cell lysis buffer to remove any red blood cells and washed twice in cold PBS prior to downstream RNA isolation and RT-PCR to measure expression of ABCA1.

3.3.9 Atherosclerosis Regression Study

C57BL/6J and ApoE$^{-/-}$ mice were purchased from Jackson Laboratories (Bar Harbor, ME) and were housed at 22 ± 1°C in a 12:12-h light-dark cycle. All animal work was performed in accordance with the guidelines set by the University of Michigan Animal Care and Use Committee. Atherosclerosis was established by placing 7-9-week-old male ApoE$^{-/-}$ mice on a high-fat/high-cholesterol diet (HFHC, 21% fat, 34% sucrose, and 0.2% cholesterol, Harlan, T.D. 88137) for 6 weeks prior to dosing, and were maintained on the HFHC diet for the duration of the study. After 6 weeks, mice were randomly assigned (n=8/group) to receive either vehicle (PBS/DMSO), rHDL (30 mg/kg), T1317 (1.5 mg/kg) or rHDL + T1317 (30 mg/kg rHDL and 1.5 mg/kg T1317) 3 times per week for 6 weeks by I.P. injection. 48 h following the final dose, mice were sacrificed and perfused with 10% normal buffered formalin to fix tissues. Aorta roots were microdissected, embedded in OCT, and frozen in liquid nitrogen for analysis of lesion area. The atherosclerotic lesions in the aortic sinus were analyzed in 3 different regions, each separated by 80 μm. Lesions were visualized by staining with Oil Red O and lesion area quantified using ImageJ software.

3.3.10 Statistical Analysis

All experiments were performed in triplicate and data are presented as means ± S.E.M. Statistical significance between multiple groups was assessed by two-way ANOVA and p values < 0.05 were considered significant.

3.4 Results

3.4.1 rHDL affects ABCA1 and ABCG1 gene expression in vitro

Previous studies have shown that HDL can alter gene expression of ABCA1 transporters both *in vitro* and *in vivo [177, 178, 188]*. As we are seeking to increase expression of these transporters in the current study, it was important for us to first understand the effects of our cholesterol acceptor, rHDL, on ABCA1 and ABCG1 expression *in vitro*. As rHDL composition is known to significantly affect its cholesterol efflux capacity [133, 189] and possibly ABCA1/ABCG1 expression, we prepared rHDL mimicking three clinically tested products, i.e. CER-001, CSL-111 and ETC-642 to obtain clinically relevant data. The rHDL formulations varied in both lipid and protein/peptide composition: CER-001 (ApoA-I:SM, 1:2.7 w/w), CSL-112 (ApoA-I:POPC, 1:1.5 w/w), and ETC-642 (22A:DPPC:SM, 1:1:1 w/w/w). Using J774A.1 macrophages treated for 24 h with rHDL, we show that increasing concentrations of rHDL decreased mRNA expression of both ABCA1 and ABCG1 relative to PBS (**Fig. 3-1**). We also show that rHDL composition affects the magnitude of reduction for ABCA1 expression, with 100 μg/mL treatment reducing ABCA1 expression >85% for CER-001 “like” rHDL, >60% for ETC-642, >45% for CSL-112 “like” rHDL (**Fig. 3-1A**). A similar trend was also observed for ABCG1 expression (**Fig. 3-1B**).

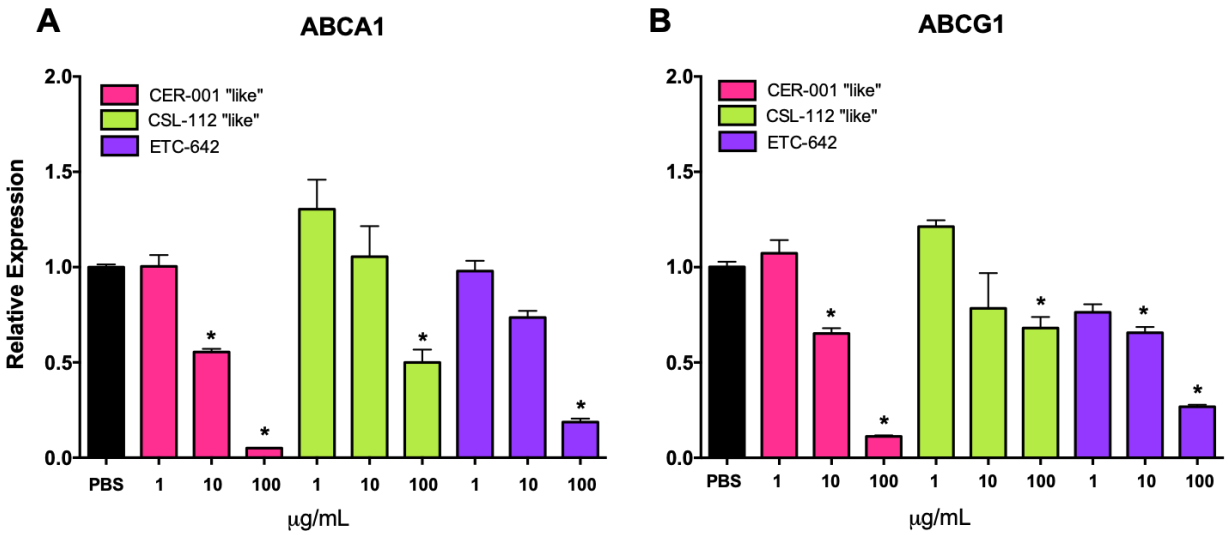


Figure 3-1 sHDL reduces ABCA1 and ABCG1 expression in vitro. *J774A.1 murine macrophages treated for 24 h with clinically-mimicking rHDLs CER-001 (ApoA-I-SM 1:2.7 w/w), CSL-112 (ApoA-I-POPC 1:1.5 w/w), or ETC-642 (22A-DPPC-SM 1:1:1 w/w) exhibit decreased levels of ABCA1 (**A**) and ABCG1 (**B**) mRNA relative to PBS treated controls, as measured by RT-qPCR. sHDL concentration is expressed in terms of peptide or protein. Data represented as mean ± SEM. *p<0.05.*

In attempt to identify the main component of rHDL responsible for driving the downregulation of ABCA1 and ABCG1 mRNA, we incubated J774A.1 macrophages for 24 h with either free 22A peptide, ApoA-I protein, or lipid emulsions of SM, DPPC, or POPC. As seen in Figure 2A-B, neither 22A peptide nor ApoA-I protein induced significant changes in ABCA1 or ABCG1, indicating that the lipid composition of rHDL may have a greater influence on gene expression. As such, we noticed significant reductions in macrophages treated with lipids alone, with slightly stronger responses elicited for SM and DPPC as compared to POPC (**Fig. 3-2 C-D**). However, reduction in ABCA1 and ABCG1 mRNA were higher overall for rHDL particles, rather than any individual component alone.

Building upon this logic, we then looked at how whole rHDL particles prepared from either 22A peptide or ApoA-I and lipids SM, DPPC, or POPC influenced ABCA1 and ABCG1 mRNA expression in the same *in vitro* system. In this case, rHDL was prepared similarly for both 22A and ApoA-I based formulations, holding the peptide/protein to lipid ratio at 1:2 by weight for all formulations. Similar to the results seen for our clinically mimicking rHDLs, both ApoA-I and 22A-based rHDL at 100 μg/mL were able to reduce relative expression of ABCA1 and ABCG1, with no obvious differences between 22A vs. ApoA-I or SM vs. DPPC vs. POPC under the tested conditions (**Fig. 3-2 E-F**).

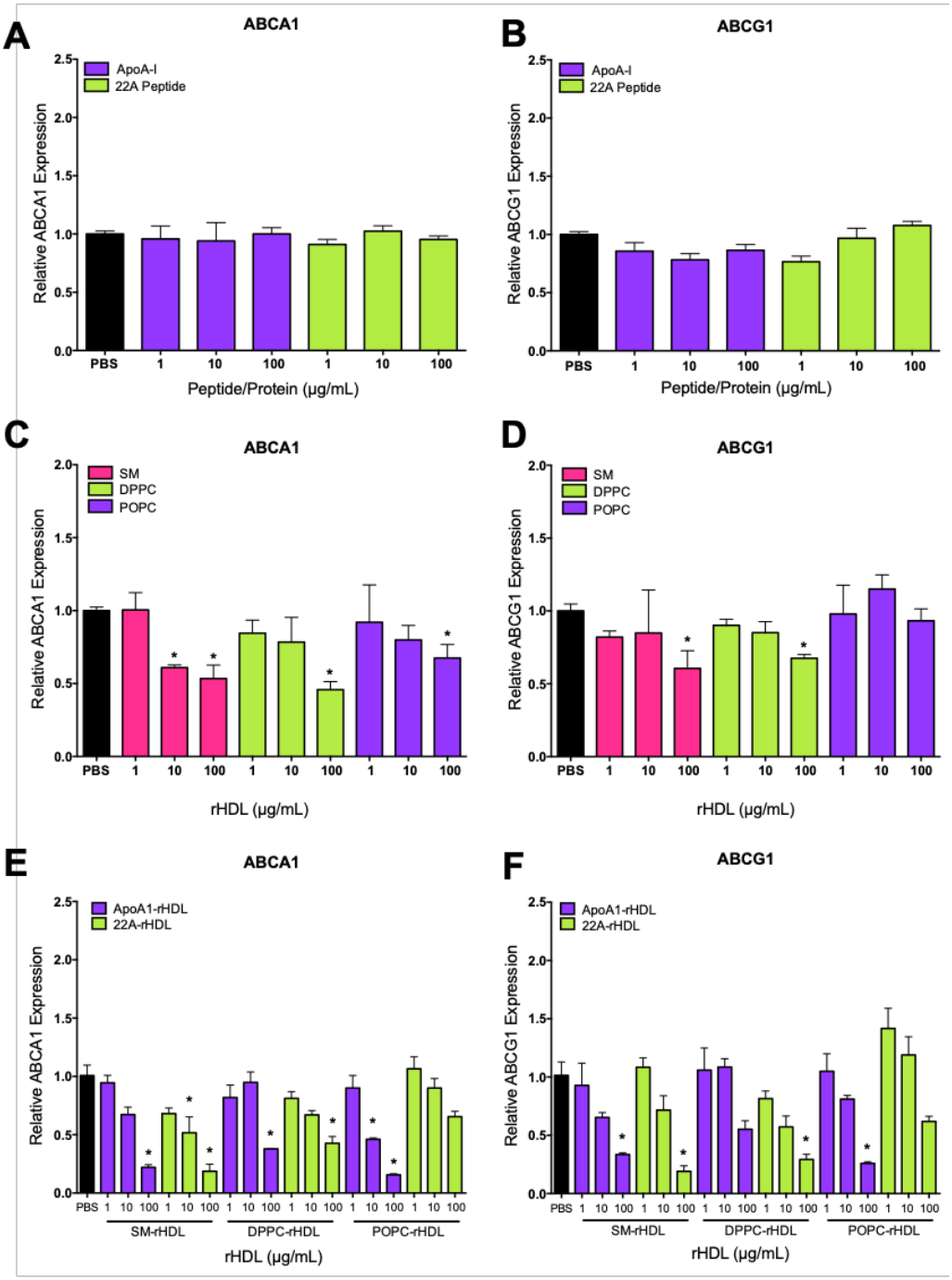


Figure 3-2 Effect of sHDL individual components on ABCA1 and ABCG1 expression in vitro. *ABCA1 and ABCG1 expression in J774A.1 murine macrophages treated for 24 hr with 22A peptide or ApoA-I protein (**A-B**) or lipid emulsions of SM, DPPC, or POPC (**C-D**). Effect of peptide/protein and lipid composition on whole-particle induced ABCA1 and ABCG1 expression probed by incubating J774A.1 cells for 24 hr with rHDL prepared from either 22A peptide or ApoA-I protein complexed with SM, DPPC, or POPC lipids (all at 1:2 protein:lipid ratio by weight) (**E-F**). Expression values were determined relative to PBS treated controls. Data represented as mean ± SEM. *p<0.05*

3.4.2 rHDL-LXR agonist co-administration synergistically increases ABCA1 and ABCG1 expression and increases cholesterol efflux

Given our hypothesis that co-administration of rHDL and an LXR agonist could act in synergy to increase cholesterol transporter expression and maximize cholesterol efflux, we decided to screen three well-characterized LXR agonists (T1317, GW3965, and LXR623) *in vitro* for their ability to upregulate ABCA1 and ABCG1 expression in the presence of rHDL. We chose ETC-642, a peptide-based rHDL, as our model rHDL at a concentration of 100 μg/mL, as this concentration exhibited maximal inhibition of ABCA1 and ABCG1 expression in the earlier experiments. J774A.1 macrophages were treated for 24 h with PBS, ETC-642 (100 μg/mL) T1317 (1 μM) , GW3965 (1 μM), LXR623 (1 μM), or a combination of ETC-642 and LXR agonist at 100 μg/mL and 1 μM, respectively. As seen in **Figure 3-3A**, the combination of rHDL and LXR agonist increased ABCA1 mRNA expression >6-fold for rHDL + T1317 and >10-fold for rHDL + GW3965 compared to PBS-treated controls ($p<0.001$). This trend also held true for ABCG1 expression (**Fig. 3-3B**), and the combination of rHDL and LXR agonist produced >3-fold increase in mRNA expression for rHDL + T1317 and >6-fold increase for rHDL + GW3965 ($p<0.001$). Notably, the combination of rHDL and LXR agonist induced greater upregulation of ABCA1 and ABCG1 expression over treatment with LXR agonist alone, suggesting a synergy between rHDL and LXR agonist.

Of course, increasing mRNA expression is only valuable to our hypothesis if we are also producing increases in ABCA1 protein expression. To test this, we treated J774A.1 macrophages for 24 h with PBS, rHDL (100 μg/mL), T1317 (1 μM), or a combination of rHDL and T1317 (100 μg/mL and 1 μM, respectively) and performed

Western Blot to detect ABCA1 protein. Aligning with our previous data, treatment with rHDL alone completely diminished ABCA1 protein levels, while the addition of T1317 restored protein levels to that similar to PBS and free T1317-treated controls (**Fig. 3-3C**). The addition of T1317 also led to an increase in total cholesterol efflux over rHDL alone (26.43 $\pm$ 0.62% vs. 22.46 $\pm$ 2.48%, respectively), while the presence of T1317 alone (0.29 $\pm$ 0.38%) had little measurable efflux (**Fig. 3-3D**).

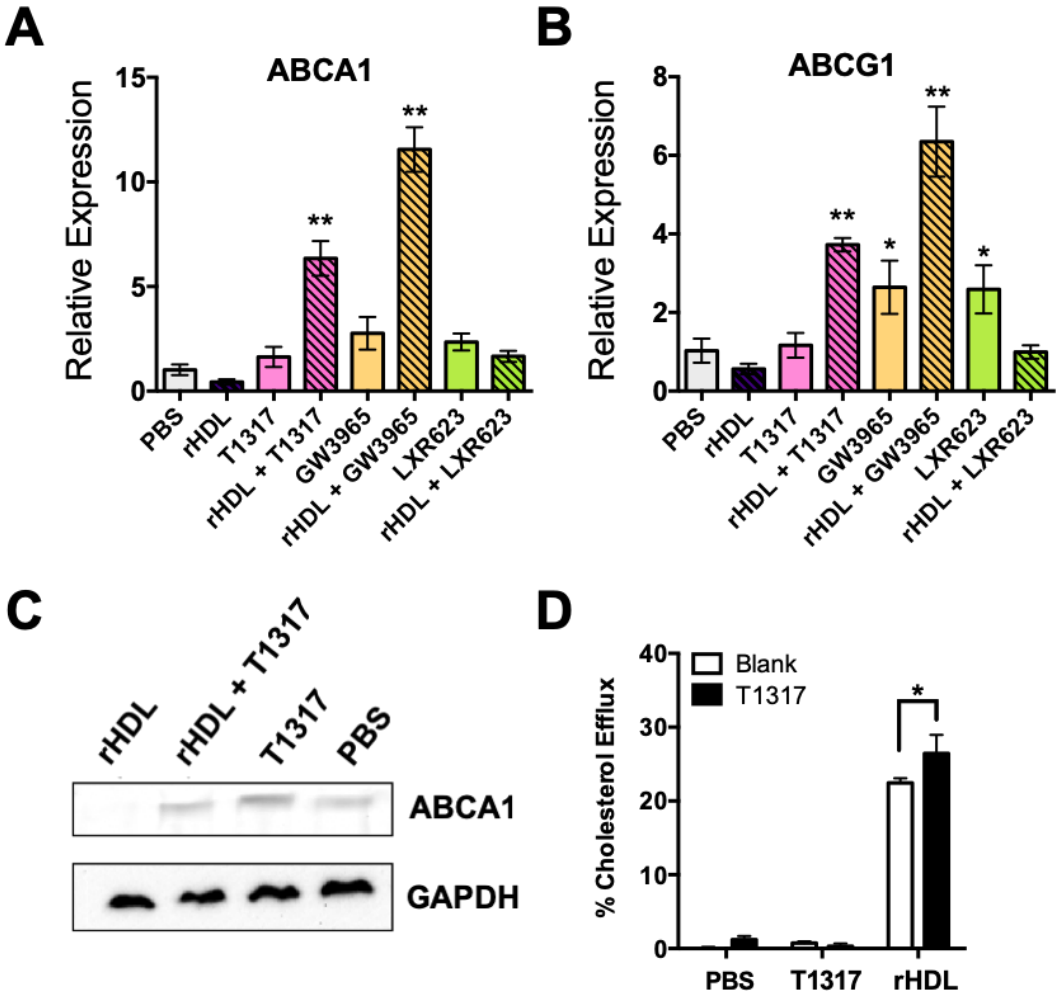


Figure 3-3 Effect of LXR agonist on ABCA1 and ABCG1 expression and cholesterol efflux in vitro. *Levels of ABCA1 and ABCG1 mRNA in J774A.1 murine macrophages (**A-B**) treated with different combinations of rHDL (100 µg/mL), T1317 (1 µM), GW3965 (1 µM), or LXR623 (1 µM) for 24 hours. ABCA1 protein levels in J774A.1 macrophages were determined by Western Blot following 24h incubation rHDL (100 µg/mL 22A) in the presence/absence of T1317 (1 µM) (**C**). [^{3}H]-cholesterol efflux to sHDL acceptor (50 µg/mL) in J774A.1 cells incubated with or without T1317 (1 µM) for 24 hr (**D**). Data are expressed as mean ± SEM. *p<0.05, **p<0.001.*

3.4.3 rHDL/T1317 combination therapy reduces atherosclerosis in vivo

While our findings *in vitro* suggest that rHDL-LXR agonist combination therapy can upregulate ABCA1 and ABCG1 at the mRNA and protein level as well as increase total cholesterol efflux when compared to either drug alone, we wanted to confirm whether these findings confer a greater anti-atherosclerosis effect *in vivo*. To do this, we first explored the ability of rHDL-LXR agonist co-administration to induce ABCA1 expression in macrophages following a single-dose acute model. Macrophages were elicited by i.p. injection of 3% thioglycolate media in male C57BL/6J mice 48 h prior to dosing. Mice then received a single i.p. injection of either PBS, rHDL (50 mg/kg), T1317 (5 mg/kg), or rHDL + T1317 (50 mg/kg and 5 mg/kg, respectively). 24 h later, macrophages were collected via peritoneal lavage and assayed for ABCA1 expression via RT-PCR. Indeed, we found that rHDL-T1317 combination increased ABCA1 mRNA expression >2-fold relative to either rHDL or PBS alone ($p<0.01$) (**Fig 3-4**).

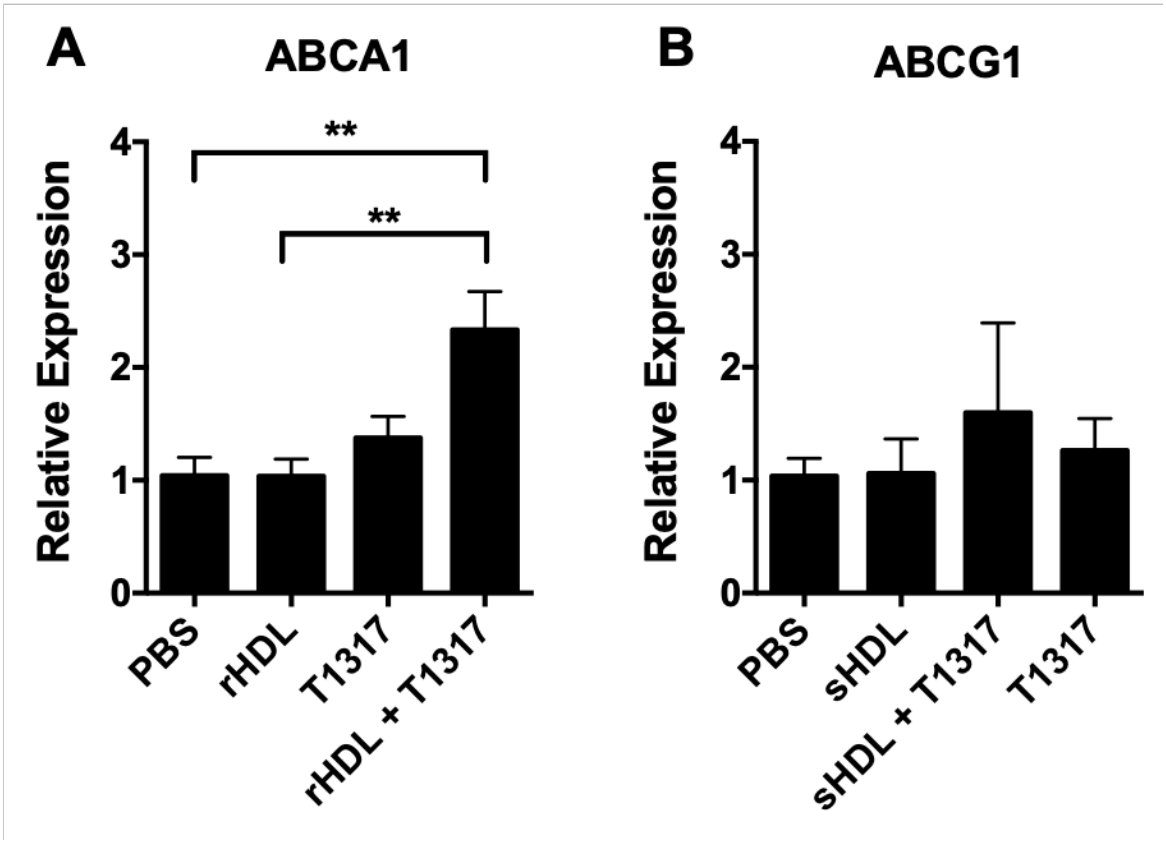


Figure 3-4 sHDL/T0 co-administration effect on ABCA1/ABCG1 expression in vivo. *Macrophages were elicited I.P. in C57BL/6J mice with 3% thioglycolate broth for 48 hr prior to administration of PBS, rHDL (50 mg/kg), T1317 (5 mg/kg), or rHDL+T1317 (50 mg/kg and 5 mg/kg, respectively). Macrophages were collected 24 hr post-dose and ABCA1 (**A**) and ABCG1 (**B**) expression were calculated relative to PBS control. **p<0.01.*

Building on these findings, we next tested the effect of rHDL-LXR agonist co-administration in a mouse model of atherosclerosis. Male ApoE$^{-/-}$ mice were fed a HF/HC diet for seven weeks prior to the start of dosing in order to establish atherosclerosis. Then, mice were randomized to receive either PBS, rHDL (30 mg/kg), T1317 (1.5 mg/kg), or rHDL + T1317 combination therapy (30 mg/kg and 1.5 mg/kg, respectively) via i.p. injection 3x/week for 6 weeks while maintained on the HF/HC diet. At the end of 6 weeks, mice receiving rHDL + T1317 combination therapy had a marked reduction in total plaque area compared to PBS controls (24.16 ± 1.93 % vs. 31.59 ±

1.93%, respectively), as assessed by Oil Red O staining at the aortic root (**Fig 3-5**). There were no significant changes in plaque volume for either rHDL (28.30 ± 1.78%) or free T1317 (28.30 ± 1.39%) only groups compared to PBS-treated controls, supporting our hypothesis that rHDL-T1317 combination therapy could act in synergy to maximize the anti-atherosclerosis effect over either drug individually. There were no measurable differences in aorta or liver ABCA1 or ABCG1 mRNA expression between any of the groups (**Fig. 3-7**).

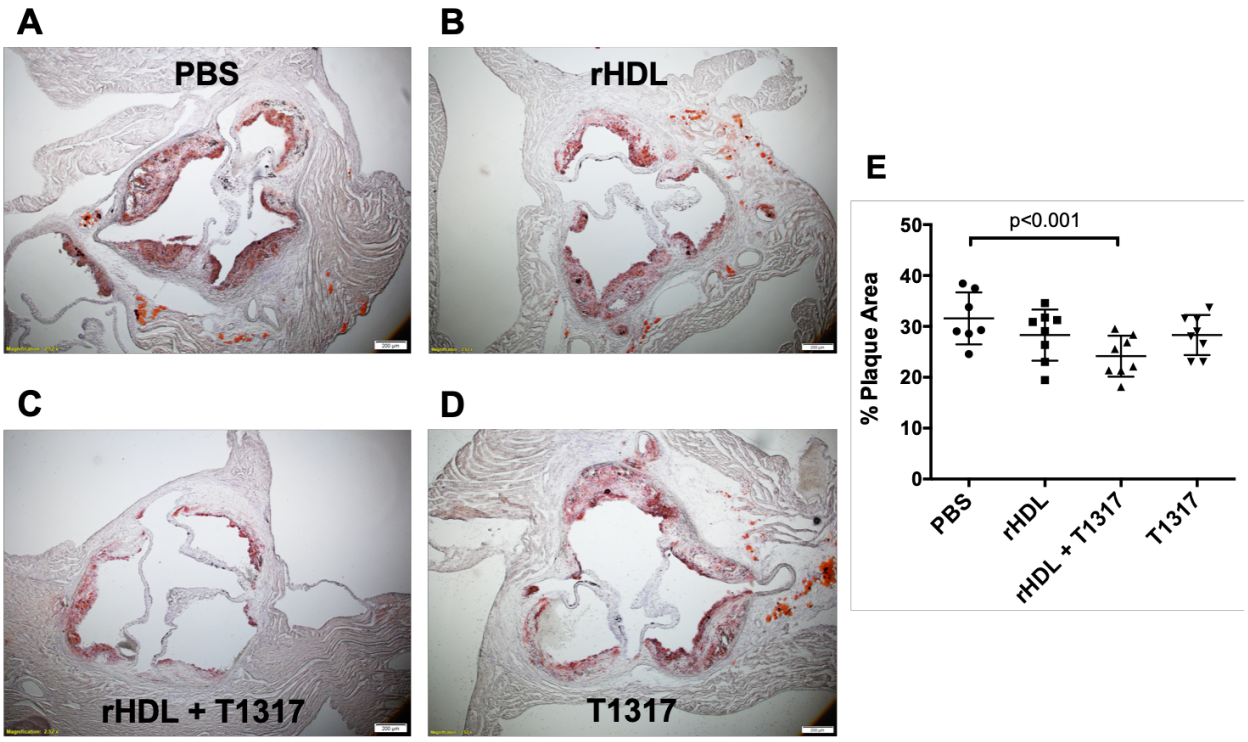


Figure 3-5 sHDL-T1317 anti-atherosclerosis effect in ApoE$^{-/-}$ mice. *ApoE $^{-/-}$ mice were fed a high fat/high cholesterol diet to induce atherosclerosis prior to treatement. At week 7, animals were dosed by I.P. injection 3 times weekly for a duration of 6 weeks with PBS, rHDL (30 mg/kg), rHDL+T1317 (30 mg/kg rHDL and 1.5 mg/kg T1317), or T1317 (1.5 mg/kg). At the end of treatment mice were sacrificed and aortas were fixed and sectioned for plaque area visualization by Oil Red O staining (**A-D**). Plaque area was quantified using ImageJ (**E**).*

In addition to ABCA1 and ABCG1, LXR also regulates transcription of the cholesterol biogenesis genes, fatty acid synthase (Fasn) and sterol-response-element binding protein 1 (Srebp1). Thus, LXR agonist drugs, including T1317, are known to have toxic side effects by way of inducing lipogenesis in the liver activity in the plasma. We therefore assessed liver toxicity by looking at gene transcript levels of Srebp1 and Fasn in the liver, as well as liver transaminase activity (alanine aminotransferase, ALT, and aspartate aminotransferase, AST) in the plasma of ApoE$^{-/-}$ mice post- treatment (**Fig. 3-6**). We found no significant differences in ALT or AST activity nor witnessed changes in Fasn expression between any of treatment groups. Surprisingly, mice receiving rHDL-T1317 combination therapy had reduced expression of Srebp1 compared to free T1317-treated mice ($p<0.05$). There were no significant differences in plasma lipids (total cholesterol, HDL-C, LDL-C, triglycerides) between any of the treatment groups (**Table 3-1**).

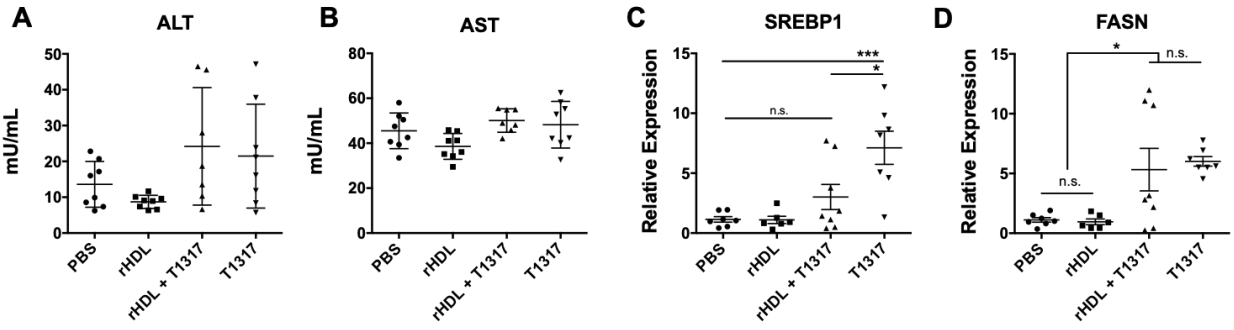


Figure 3-6 Liver safety biomarkers following anti-atherosclerosis therapy. *Liver safety biomarkers in ApoE$^{-/-}$ mice following 6 weeks of anti-atherosclerosis therapy with PBS, rHDL (30 mg/kg), rHDL + T1317 (30 mg/kg + 1.5 mg/kg, respectively), or T1317 (1.5 mg/kg) were measured. Activity of liver enzymes alanine aminotransferase (ALT) and aspartate aminotransferase (AST) were determined in the plasma (**A-B**), and gene expression of sterol response element binding protein 1 (SREBP1) and fatty acid synthase (FASN) were determined in liver lysates (**C-D**). *p<0.05, ***p<0.001*

3.5 Discussion

ABCA1 and ABCG1 transporters are critical regulators of cellular cholesterol, and loss of function or absence of ABCA1 in both human (Tangier Disease) and mice leads to HDL deficiency and increased risk of atherosclerosis [190-194]. Under normal conditions, ABCA1 interacts with poorly-lipidated ApoA-I protein at the cell surface to efflux cholesterol and phospholipids, while ABCG1 has a preference for more mature HDL particles [195, 196]. However, in advanced atherosclerotic this process is disrupted and cholesterol-overloaded macrophages, known as foam cells, accumulate and propagate inflammation within the plaques, ultimately leading to plaque rupture and in many cases, death [15]. Given the importance of both ABCA1 and HDL in in this context, therapies to increase ABCA1 expression (i.e. LXR agonists) or raise HDL levels (i.e. HDL infusions, fibrates, CETP inhibitors) have gained increasing attention. Yet, there are still no approved LXR agonists on the market, and HDL-raising therapies have yet to achieve significant clinical end points. Rather than targeting one component or the other, we here show that a combination therapy stimulating ABCA1/ABCG1 expression (LXR agonist) and providing an acceptor for effluxed cholesterol (HDL infusion) can maximize the anti-atherosclerosis effect over targeting either component alone.

While we knew we could upregulate ABCA1 expression using an LXR agonist, we also knew that HDL has been reported to downregulate its expression [177, 178]. Indeed, ABCA1 expression is sensitive to cholesterol levels within the cell. Denis et. al. showed that upon free-cholesterol loading in human skin fibroblasts, there was a significant rise in both ABCA1 mRNA and protein, and that this trend was reversed upon

induction of cholesterol efflux with HDL [188]. Thus, it makes sense that our *in vitro* studies show dose-dependent down regulation of ABCA1/ABCG1 in the presence of clinically-mimicking HDL therapies. Furthermore, it may explain why our HDL particles induced a more potent downregulation than protein/peptide or lipid alone, as the HDL particles are more potent inducers of cholesterol efflux and ApoA-I protein/peptide has been shown to stabilize ABCA1 protein [197]. Additionally, we saw differences in degree of ABCA1/ABCG1 between the different rHDL formulations, with CER-001 having the greatest effect, ETC-642 having slightly less, and CSL-112 having the least reduction of the three. This may also be attributed to the cholesterol efflux capacity of these rHDLs, as SM-containing rHDL has been shown to induce greater cholesterol efflux from foam cells than POPC-based rHDLs due to its higher cholesterol binding affinity [133, 198-200]. Although our studies were conducted in healthy J774 macrophages, Guo et. al. reported similar effects of HDL on ABCA1/ABCG1 expression in J774 foam cells [201]. This may, in part, explain why HDL-raising therapies have yet to hit a milestone, especially since ABCA1 expression and cholesterol efflux is known to be impaired both in atherosclerotic plaques *in vivo* and in the presence of oxidized LDL and unsaturated fatty acids *in vitro* [202, 203].

Knowing that rHDL products are potent inducers of cholesterol efflux, but that ABCA1/ABCG1 levels are reduced in this process, we looked to LXR agonists to combat this issue. LXR agonists have gained increasing attention as therapeutics due to their ability to upregulate both ABCA1 and ABCG1 and lessen the burden of atherosclerosis. However, their use has been limited due to toxicity, including induction of hepatic lipogenesis via activation of FASN and SREBP-1c genes leading to increased

serum and hepatic triglycerides [204]. Moreover, their poor pharmaceutical properties necessitate frequent (i.e. daily oral gavage) and long-term dosing regimens to achieve clinical endpoints that are often outweighed by the overarching toxicity [205-207]. Attempts to solve this issue have emerged in the form of drug-delivery systems to lower systemic exposure. Approaches include targeted antibody-drug conjugates [208], poly(lactic-co-glycolic acid) (PLGA) and other modified nanoparticles [209, 210], and even ApoA-I-containing PLGA nanoparticles to target atherosclerotic plaques [211]. While these approaches have varied in success, they only work to target ABCA1 expression levels but do not provide an acceptor for the effluxed cholesterol. We previously showed that encapsulation of T1317 in rHDL nanoparticles promotes atherosclerosis regression and avoids systemic toxicity observed with free T1317 administration [201]. Hence, we sought to explore the potential synergy between the rHDL drug carrier and LXR agonist in separate, leading to the current study.

The central hypothesis of our study was that the co-administration of rHDL and LXR agonist could target two critical components of the RCT pathway that act in synergy to enhance overall plaque reduction in atherosclerosis and potentially reduce the doses of both drugs needed to see these benefits. We see clearly *in vitro* that the combination of rHDL and LXR agonists, particularly T1317 and GW3965, can upregulate ABCA1/ABCG1 mRNA and protein and enhance overall cholesterol efflux. Moreover, we observed a similar increase in ABCA1 expression in peritoneal macrophages after a one-time dosing regimen in healthy mice, indicating that our hypothesis may hold true in a long-term dosing study in diseased mice. Indeed, we witnessed a reduction in overall plaque area in mice treated with both rHDL and T1317

compared to non-treated mice, and this effect was not seen for animals treated with rHDL or T1317 only. We did not observe any differences in ABCA1 or ABCG1 expression in the aortas or livers between any group (**Fig 7**), but this is likely due to the timing of necropsy being 48 h following the final dose, and mRNA transcript levels had likely re-normalized. In this study, we were able to achieve our clinical endpoint using a 1.5 mg/kg dose of T1317 that was administered only 3 times/week for 6-weeks. In comparison, studies administering free T1317 by oral gavage required daily dosing in the range of 10-50 mg/kg to see significant reduction in atherosclerosis, but at the cost of unwanted toxicity [205, 212-214]. We also used a relatively moderate dose of rHDL, 30 mg/kg, but the synergy between rHDL and LXR agonist may confer us the flexibility to further decrease rHDL dose and avoid potential elevation in liver transaminase activity seen after administration of high doses of rHDL [98]. And although both rHDL-T1317 combination therapy and T1317 only group induced hepatic FASN expression, the rHDL-T1317 combination group had significantly lower SREBP1c expression than the free drug group, indicative of a mild reduction in hepatic toxicity.

In conclusion, we show that rHDL and LXR agonists can act in synergy to: 1) upregulate ABCA1 and ABCG1 cholesterol efflux transporters, and 2) enhance cholesterol efflux by providing an acceptor for the effluxed cholesterol. This synergy leads to an increase in anti-atherosclerosis efficacy when both drugs are administered together as opposed to individually. Moreover, >10-fold lower doses of LXR agonist could be used when combined with rHDL, lowering its systemic toxicity while still achieving plaque reduction. Thus, co-administration and the resulting synergy between

rHDL and LXR agonists could be of great potential interest to the pharmaceutical industry and revive interest in development of these two classes of drugs.

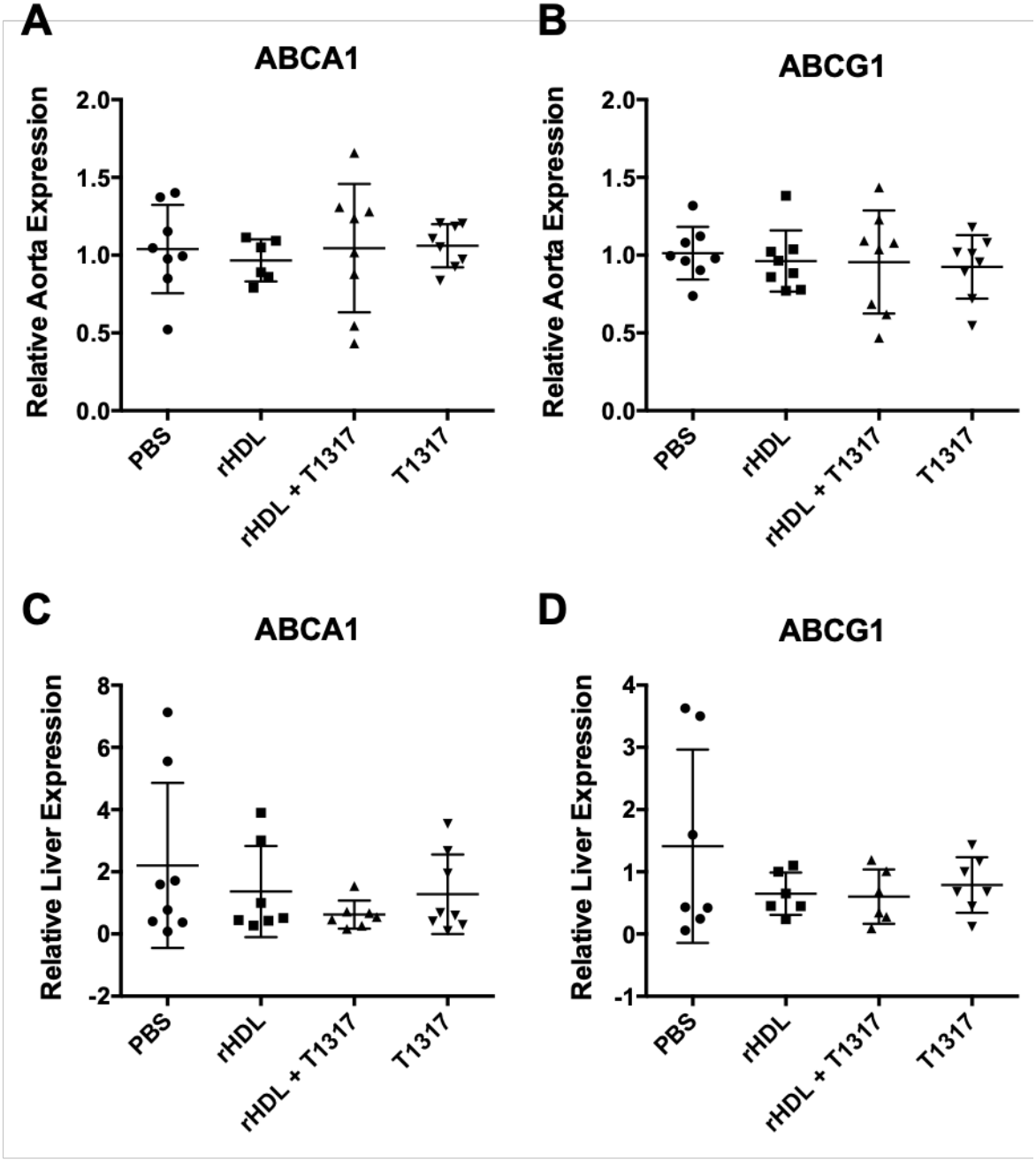


Figure 3-7 ABCA1 and ABCG1 expression in ApoE$^{-/-}$ mice after anti-atherosclerosis therapy. *ABCA1 and ABCG1 expression in ApoE$^{-/-}$ mice following 6 weeks of anti-atherosclerosis therapy with PBS, rHDL (30 mg/kg), rHDL+T1317 (30 mg/kg + 1.5 mg/kg, respectively), or T1317 (1.5 mg/kg) were measured in the aortas (**A-B**) and livers (**C-D**) 48 hr after administration of the final treatment dose.*

Table 3-1 Plasma lipid markers. *Total cholesterol (TC), HDL-cholesterol (HDL-C), LDL-cholesterol (LDL-C), and triglycerides (TG) were measured in plasma collected from ApoE$^{-/-}$ fed a high fat/high cholesterol diet for 6 weeks followed by treatment with PBS, rHDL (30 mg/kg), rHDL+T1317 (30 mg/kg + 1.5 mg/kg, respectively), or T1317 (1.5 mg/kg) for 6 weeks. Blood was collected 48 hr following the administration of the final dose. Data are expressed as mean ± SEM.*

Parameter	PBS	rHDL	rHDL + T1317	T1317
N	8	8	5	6
TC (mg/dL)	1650 ± 54.9	1474 ± 64.3	1417 ± 116.1	1660 ± 131.7
HDL-C (mg/dL)	19.6 ± 1.3	22.0 ± 1.7	23.8 ± 0.8	21.83 ± 2.3
LDL-C (mg/dL)	629.4 ± 38.4	541.8 ± 27.0	488.0 ± 58.7	508.7 ± 89.2
TG (mg/dL)	228.4 ± 22.9	260.6 ± 33.3	326.4 ± 44.7	294.3 ± 32.4

Table 3-2 Primer sequences used for RT-PCR assays.

Gene	Forward	Reverse
mAbca1	gggagtcccagaaaaggaag	tgtggttggttcatccagaa
mAbcg1	gtaccatgacatcgctggtg	agccgtagatggacaggatg
mFasn	ctgaagagcctggaagatcg	gtcacacacctgggagaggt
mSrebp1	ggagccatggattgcacatt	gcttccagagaggaggccag
m18sRNA	ggaagggcaccaccaggagt	tgcagccccggacatctaag
mPpia	gtctccttcgagctgtttgc	gatgccaggacctgtatgct

Chapter 4: Synthetic high-density lipoproteins containing sphingosine-1-phosphate for modulation of endothelial function

4.1 Abstract

Vascular dysfunction is an underlying manifestation of several deadly inflammatory diseases, including cardiovascular disease and sepsis. Yet, there have been no specific therapies designed to treat these disorders from this perspective. Sphingosine-1-phosphate (S1P) is a potent anti-inflammatory signaling lipid carried in the body by circulating high-density lipoproteins (HDL) and albumin. S1P regulates endothelial barrier function by activation of endothelial nitric oxide synthase (eNOS) and subsequent production and release of nitric oxide (NO) by endothelial cells. However this effect is only elicited when S1P is delivered to endothelium by HDL rather than by albumin. Thus, the development of S1P targeted therapies is hindered by its carrier-specific necessity. Here, we developed and optimized an S1P delivery platform via synthetic HDL nanodiscs made from apolipoprotein A-I (ApoA-I) mimetic peptide, 22A, and phospholipids. We optimized sHDL composition to prepare pure, homogenous sHDL particles of 8-10 nm diameter and facilitate S1P incorporation. Our optimized S1P-sHDL formulation consisted of 22A ApoA-I peptide and 1,2-dipalmitoyl-*sn*-glycero-3-phosphocholine (DPPC) at a 1:2 w/w ratio and contained S1P at 0.00063, 0.0063, and 0.063 % (w/w) loading. These S1P loading corresponded to physiological S1P

concentrations of 0.05, 0.5, and 5 μM, respectively. In vitro, S1P-sHDL induced a potent and dose-dependent release of nitric oxide from primary human endothelial cells which was directed in part by phosphorylation of endothelial nitric oxide synthase (eNOS) at Ser1177. We also observed a significant increase in transendothelial electric resistance. Furthermore, S1P-sHDL was able to dampen endothelial activation after inflammatory insult, as seen by decreased expression of adhesion molecules VCAM-1 and E-Selectin and inhibition of IL-6 and IL-8 pro-inflammatory cytokine production. Given these promising data *in vitro*, S1P-sHDL presents a viable strategy for the endothelial-targeted delivery of S1P in an HDL-directed manner, warranting further evaluation *in vivo* for the treatment of endothelial dysfunction.

4.2 Introduction

Vascular dysfunction, in particular endothelial dysfunction, is a hallmark of an many disorders, including atherosclerosis, hypertension, sepsis, and lupus [215, 216]. Cardiovascular disease continues to be the deadliest and most costly disease to treat claiming nearly 630,000 lives each year with estimated treatment expendatures of $550 billion annually [217, 218]. Similary, sepsis continues to be the leading cause of hospital-related deaths in the U.S. with no approved therapies to date [52, 219]. It is estimated that over 215,00 patients in the U.S. alone die each year from sepsis with the healthcare cost of disease treatment exceeding $17 billion annually [52-54]. Endothelial dysfunction is broadly characterized by dysregulated vascular tone, endothelial barrier leakage, and activation of endothelial cells inducing cytokine production and cell adhesion molecule expression [220]. It is typically a result of acute inflammatory insult,

as the case in sepsis, but can also occur over time with continual exposure to low level inflammation as seen with lupus and cardiovascular disease [16]. Hence, targeting endothelial dysfunction itself presents a unique opportunity to overcome the current challenges in intervention.

Sphingosine-1-phosphate (S1P) is a sphingolipid present in human blood at roughly 200 nM concentrations, with > 55% bound to high-density lipoprotein (HDL) and remaining fraction bound to serum albumin [31]. When carried by HDL, S1P has been shown to signal through G-protein coupled receptors and promote endothelial growth, survival, and tube formation. S1P plays an important role in maintaining vasculature health by controlling the expression of cell adhesion molecules expressed on the surfaces of endothelial cells that would otherwise promote platelet aggregation, monocyte recruitment to the vessel wall, and vascular leakage [20]. In both acute and chronic disease, high-density lipoprotein HDL-associated S1P levels are decreased in patients [33, 34]. Thus, S1P has served great interest as a therapy for vascular-related disorders.

S1P is poorly water soluble, hence special formulation strategies have been employed including for S1P delivery including polymer nanoparticles, hydrogels, albumin, and even design of soluble molecular analogs. However, much of S1P beneficial effects in the vasculature are shown to be specific to HDL-associated S1P. HDL is a small, 8-10 nm protein-lipid nanoparticle consisted primarily from apolipoprotein A-I (ApoA-I) wrapped around a phospholipid core [106]. Endogenous HDL is known for its protective functions in the cardiovascular system, namely through its ability modulate cholesterol homeostasis in the body [9]. Additionally, HDL

possesses its own anti-inflammatory and anti-thrombotic effects which promote endothelial barrier function [221], much of which are attributed to the presence of S1P [33]. Hence, formulating S1P within an HDL-like particle could overcome the aforementioned barriers in therapeutic development, and skew its pharmacological response toward that of HDL-associated S1P.

In this study, we propose the use of synthetic HDL (sHDL) as a delivery vehicle for S1P. sHDL products, made from purified ApoA-I protein or mimetic peptides and phospholipids, have been developed for direct infusion in patients to stabilize vulnerable atheromas following an acute coronary event [105]. In clinical trials, they were shown safe and well-tolerated in patients [94, 96, 101, 103, 115]. Sterile manufacturing has been established and formal toxicology studies have already been completed for sHDL nanoparticles, posing them for rapid clinical translation [222]. In addition. sHDL infusions have even been shown to restore endothelial function in hypertensive men [108]. One product, CSL-112, is currently enrolling subjects for a 17,400 subject Phase III trial to demonstrate the reduction of major cardiovascular events in patients with acute coronary syndrome [104, 223]. Along with its endothelial-directed effects, proven safety, and established manufacturing, sHDL presents an attractive and rapidly translatable strategy for directed S1P therapy and will be investigated as such in the following study.

4.3 Materials and Methods

4.3.1 Reagents

22A peptide (PVLDLFRELLNELLEALKQKLK) was synthesized by Genscript (Piscataway, NJ) and purity was determined to be >95% by HPLC. 1,2-dimyristoyl-*sn*-glycero-3-phosphocholine (DMPC), 1,2-dipalmitoyl-*sn*-glycero-3-phosphocholine (DPPC), and 1-palmitoyl-2-oleoyl-*sn*-glycero-3-phosphocholine (POPC) were purchased from Avanti Polar Lipids (Alabaster, AL) and Nippon Oil and Fat (Osaka, Japan). Sphingosine-1-phosphate (S1P) was purchased from Cayman Chemical (Ann Arbor, MI). Human serum albumin-conjugated S1P (HSA-S1P) was purchased from Avanti Polar Lipids. Primary antibodies for eNOS (Rabbit polyclonal #9572), phospho-eNOS-Ser1177 (Rabbit polyclonal #9571) and GAPDH (D16H11 XP® rabbit monoclonal #5174) were sourced from Cell Signaling Technology (Danvers, MA). Secondary anti-rabbit IgG, HRP linked antibody (#7074) was also purchased from Cell Signaling Technology. All other reagents were procured from commercial sources.

4.3.2 Cell Culture

Human umbilical vein endothelial cells (HUVEC) C2519A Clonetics™ were purchased from Lonza (Walkersville, MD) and maintained in gelatin coated flasks containing EGM-2 media (Lonza). HUVECs were used between passage 3-5. RAW 264.7 macrophages were purchased from ATCC (Manassas, VA) and maintained in Dulbecco's Modified Eagle Medium containing 10% fetal bovine serum and 100 U/mL penicillin/100 μg/ mL streptomycin. All cells were maintained at 37 °C and 5% CO_2.

4.3.3 S1P-sHDL preparation

All sHDL formulations were made using the lyophilization method described previously [133]. Briefly, 22A peptide and lipids (POPC, DMPC, or DPPC) were dissolved in glacial acetic acid and combined at a 1:2 peptide:lipid weight ratio. S1P was dissolved in methanol containing 10% acetic acid and added directly to vials containing 22A and lipids. Samples were then frozen in liquid nitrogen and lyophilized for at least 24 h to remove solvents. The freeze-dried powders were hydrated with PBS (pH 7.4) and cycled between room temperature and 50 °C (5 min each x 3 cycles) to form sHDL particles. pH was adjusted to 7.4 using NaOH and the final solutions were sterile filtered using a 0.22 μm syringe filter.

4.3.4 S1P-sHDL Characterization

Size distribution was determined by dynamic light scattering (DLS) on a Malvern Zetasizer Nano ZSP (Westborough, MA), and particle purity was determined by gel permeation chromatography (GPC) with UV detection at 220 using a Tosoh TSK gel G3000SWxl column (Tosoh Bioscience**,** King of Prussia, PA) on a Waters HPLC, as previously described [133]. The morphology of sHDL was assessed by transmission electron microscopy (TEM). sHDL samples were loaded on a carbon film-coated 400 mesh copper grid from Electron Microscopy Sciences (Hatfield, PA) that were negatively stained with 1% (w/v) uranyl formate and dried before TEM observation. All specimen were imaged with 100kV Morgagni TEM equipped with a Gatan Orius CCD.

4.3.5 Cell Viability Assay

sHDLs were screened for cell toxicity in both human endothelial cells (HUVECs) and in murine macrophages (RAW 264.7 cells). Briefly, cells were seeded into 96-well

plates and allowed to adhere overnight. The following day, different sHDL formulations were added to cells at concentrations of 0, 0.625, 0.125, 0.5, and 1 mg/mL sHDL (based on peptide concentration). After 24 h incubation with sHDL, cell viability was measured using the MTS-based CellTiter 96® AQ_{ueous} One Solution Cell Proliferation Assay (Promega) per manufacturer instruction. PBS-treated cells were set as 100% viability.

4.3.6 Nitric Oxide Release Assay

HUVEC cells (passage 5) were plated into 12-well plates at 10^6 cells per well and incubated for 48 hours at 37°C and 5% CO_2. Cells were washed and incubated with fresh media containing sHDL, S1P-sHDL, 22A peptide, or PBS for 15 minutes. After 15 minutes, the media was collected and assayed for Nitric Oxide (NO) using ozone chemiluminescence with Sievers 280i Nitric Oxide Analyzer (NOA) (GE Analytical Instruments, Boulder, CO, USA) with liquid setup.

4.3.7 TEER Measurements

Transendothelial electrical resistance (TEER) was measured in HUVEC cells 24 h after incubation with sHDL or S1P-sHDL. Briefly, HUVECs were seeded into fibronectin-coated 24-well 3 μm polycarbonate inserts (BD Falcon) at 2.5 x 10^4 cells/well. Cells were allowed to form a confluent monolayer (~ 3 days, as monitored by TEER) before adding sHDL, S1P-sHDL, or PBS for 24 h. TEER was measured at baseline (0 h) and after treatment (24 h) using the Millicell® ERS-2 voltohmmeter (MilliporeSigma).

4.3.8 Western Blot

HUVECs (passage 5) were grown to ~80% confluency in gelatin-coated T-25 flasks. sHDL (1 mg/mL), S1P-sHDL (1 mg/mL sHDL containing either 0.01 or 0.05 μM S1P), or PBS were added to cells and incubated at 37 °C and 5% CO_2 for 30 minutes. Cells were then washed with ice cold PBS and radioimmune precipitation assay (RIPA) buffer containing cOmplete™ mini, EDTA-free protease inhibitor cocktail (Sigma) and PhosSTOP™ phosphatase inhibitor cocktail (Roche). Protein lysates (30 μg/lane) were separated by gel electrophoresis using 7.5% Tris-Glycine gels (Mini-protean TGX, BioRad, Richmond, CA) and transferred to methanol activated 0.45 μm PVDF membranes. Membranes were blocked with 5% BSA and expression of eNOS and phospho-eNOS-Ser1177 were determined using antibodies for eNOS (1:1000), p-eNOS-S1177 (1:1000), and GAPDH (1:1000). Bands were visualized using HRP-labeled secondary antibody and ECL reagent.

4.3.9 Quantitative Real Time PCR

HUVECs were seeded into 6-well plates and incubated at 37 °C and 5% CO_2 overnight. The following day cells were pre-treated with PBS, sHDL (0.2 mg/mL), S1P-sHDL (0.2 mg/mL sHDL and 0.5 μM S1P), or HSA-S1P (0.5 μM S1P) for 18 h. Next, 1 μg/mL LPS (+) or an equal volume of PBS (-) was added and cells were allowed to incubate an additional 6 h. Cells were washed twice with cold PBS and scraped and collected in lysis buffer. Total RNA was purified with the GeneJET RNA Purification Kit (Thermo Scientific), followed by cDNA synthesis with the SuperScript III First-Strand Synthesis System kit (Invitrogen). mRNA expression levels were determined using Taqman assays for E-Selectin (Hs00174057_m1), VCAM-1 (Hs01003372_m1), S1PR

(Hs01922614_s1), and eNOS (Hs01574659_m1) and normalized to 18S rRNA (Hs03928990_g1). Expression levels relative to PBS-treated/PBS-challenged controls were determined using the ddCt method.

4.3.10 Cytokine Release Assay

HUVECs were seeded into 96 well plates and allowed to adhere overnight. The following day, cells were pre-treated with PBS, sHDL (0.2 mg/mL), S1P-sHDL (0.2 mg/mL sHDL and 0.5 μM S1P), or HSA-S1P (0.5 μM S1P) for 18 h. Next, 1 μg/mL LPS (+) or an equal volume of PBS (-) was added and cells were allowed to incubate an additional 6 h. Supernatants were collected and levels of IL-6 and IL-8 were measured by ELISA (eBioscience).

4.3.11 Statistics

All experiments were performed in triplicate and data are presented as means ± S.E.M. Statistical significance between groups was assessed by one-way ANOVA with Tukey's post-hoc correction for multiple comparisons. P values < 0.05 were considered significant.

4.4 Results

4.4.1 S1P-sHDL characterization

We first screened sHDL formulations made from 22A peptide and different lipids for their ability to incorporate S1P while forming homogeneous particle sizes in the range of 8-10 nm to mimic endogenous HDL. We chose to use the phospholipids POPC, DMPC, and DPPC, as they vary in degree of saturation and carbon chain length which are known to affect sHDL particle size and drug loading efficiency [224, 225].

Peptide to lipid ratio was held constant at 1:2 peptide:lipid by weight, and S1P was incorporated at either 0.05 (S1P-sHDL #1), 0.5 (S1P-sHDL #2), or 5 μM (S1P-sHDL #3), representing S1P concentrations spanning below and above physiological plasma levels. These S1P concetrations corresponded to the theoretical drug loading levels of 0.00063, 0.0063, and 0.063 weight %. As evident by DLS, both DMPC and DPPC-based sHDL had average particle sizes within our target range, with DMPC-sHDL ranging from 9.2 - 10 nm for all formulations and DPPC-sHDL ranging from 9.9 – 10.7 nm (**Fig 4-1 B,C**). POPC-sHDL, on the other hand, had slightly larger particle sizes, ranging from 14.3 – 15.9 nm (**Fig 4-1 A,G**). Upon further examination by GPC, we saw that POPC-sHDL was only ~90% pure (**Table 4-1**), with the presence of larger particles eluting around 5.5 min for all POPC formulations (**Fig 4-1 D**), which were also visible by TEM (**Fig. 4-1G**). Both DMPC and DPPC-sHDL formed particles with >99% purity for all S1P loading levels (**Fig 4-1E,F**), and their overall morphology was homogeneous as seen by TEM (**Fig. 4-1 H-I**). Based on both size and purity, we proceeded to *in vitro* testing with both DMPC and DPPC formulations and excluded POPC-sHDL.

4.4.2 S1P-sHDL effect on cell viability

Much of the benefit of HDL and HDL-associated S1P occurs at the endothelial and macrophage level, promoting vessel integrity and preventing inflammation [20]. Thus, we then tested the cell toxicity of our sHDL and S1P-sHDL in both human endothelial cells (HUVEC) and murine macrophages (RAW 264.7) in order to further narrow down our final formulation. In HUVECs, neither DMPC nor DPPC-based sHDLs induced significant cytotoxicity for any tested concentration, and the same held true for the respective S1P-sHDLs (**Fig 4-2A**). In macrophages, however, DMPC-based sHDLs

(with and without S1P) elicited strong cytotoxicity at concentrations of 0.125 mg/mL and above (**Fig 4-2B**). Given the significant cell death seen with DMPC-sHDL, we eliminated these formulations and moved forward with DPPC-sHDL for further functional characterization. For this reason, all references to S1P-sHDL moving forward will refer to DPPC-based sHDL.

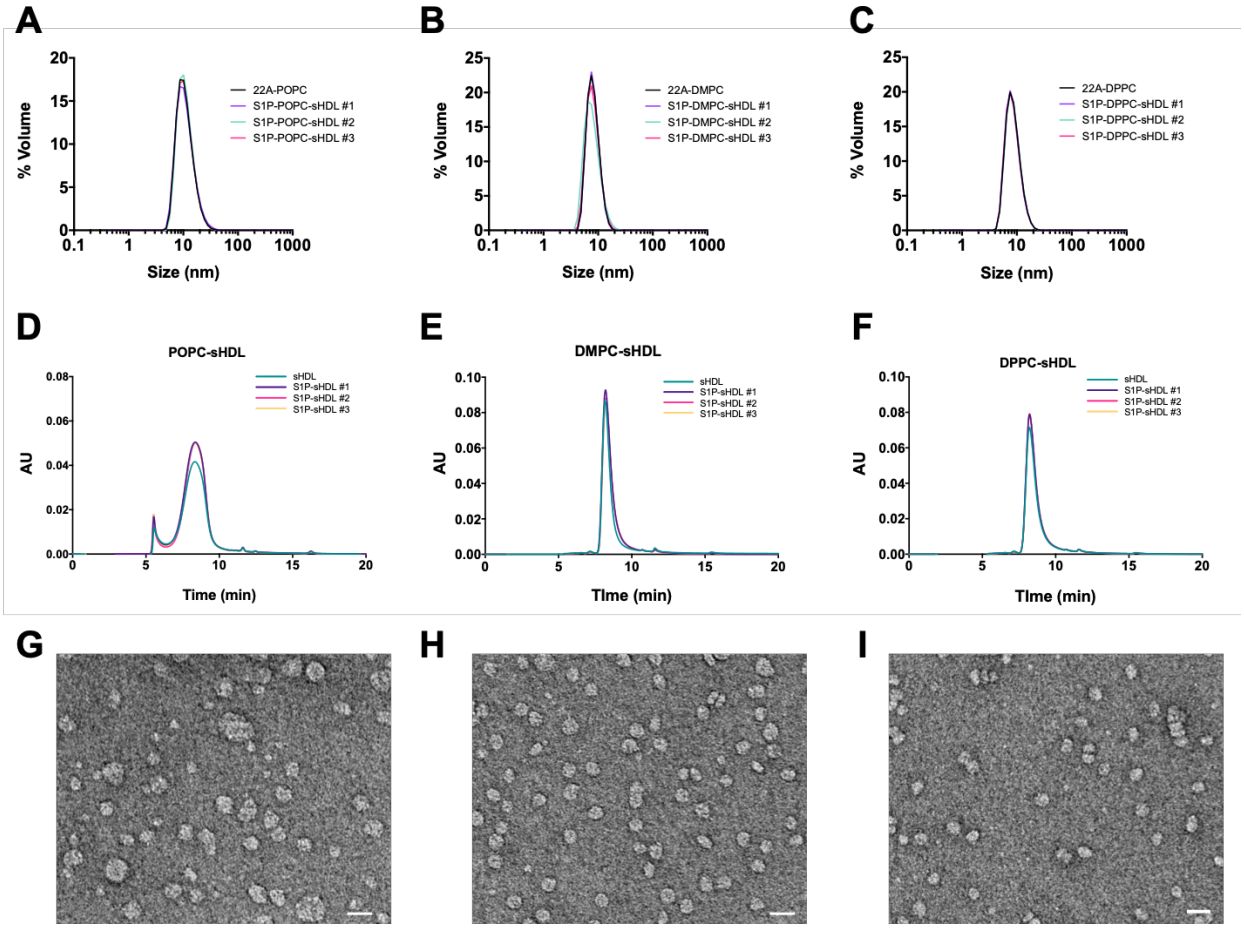


Figure 4-1 Characterization of sHDL containing S1P. *sHDL was prepared with 22A peptide complexed with either POPC (**A,D**), DMPC (**B,E**), or DPPC (**C,F**) lipids at a 1:2 peptide:lipid weight ratio, containing 0, 0.05 (S1P-sHDL #1), 0.5 (S1P-sHDL #2), or 5 (S1P-sHDL #3) μM of sphingosine-1-phosphate. Dynamic light scattering was used to measure particle size (**A-C**) and gel permeation chromatography with detection at 220 nm was used to measure particle purity (**D-F**). Particles were imaged by TEM for further analysis of size and morphology (**G-I**).*

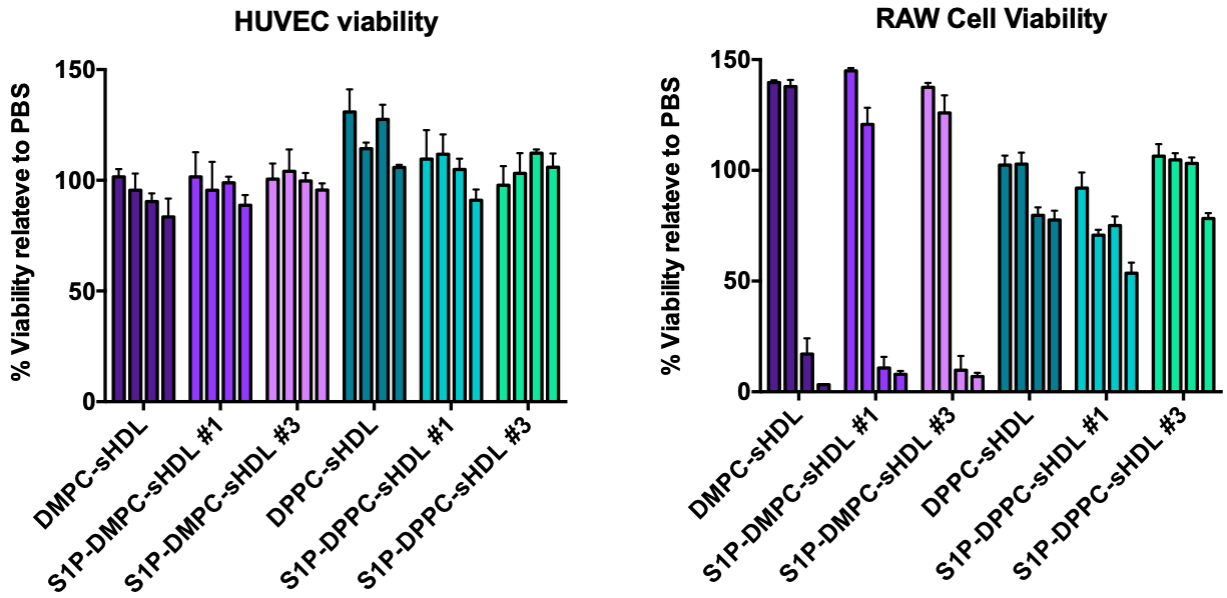


Figure 4-2 sHDL toxicity screening in endothelial cells and macrophages. *Primary human endothelial cells (HUVEC) or RAW 264 murine macrophages were incubated for 24 h in the presence of sHDL made from DMPC (purple bars) or DPPC (green bars) lipids containing 0, 0.05 (S1P-sHDL #1), 0.5 (S1P-sHDL #2), or 5 (S1P-sHDL #3) μM of sphingosine-1-phosphate. Cell viability was measured by MTS reagent and PBS-treated controls were set to 100%. Data is reported as mean ± SEM.*

Table 4-1 Summary and comparison of size and purity of S1P-containing sHDL made from different phospholipids. *sHDL was prepared with 22A peptide complexed with either POPC, DMPC, or DPPC lipids at a 1:2 peptide:lipid weight ratio, containing 0 (Blank), 0.05 (S1P #1), 0.5 (S1P #2), or 5 (S1P #3) μM of sphingosine-1-phosphate. Dynamic light scattering was used to measure particle size and gel permeation chromatography with detection at 220 nm was used to measure particle purity. Data represented at mean ± SEM.*

Sample	Blank			S1P #1			S1P #2			S1P #3		
	Size (nm)	PDI	% Purity	Size (nm)	PDI	% Purity	Size (nm)	PDI	% Purity	Size (nm)	PDI	% Purity
POPC-sHDL	14.4 ± 0.1	0.13	>90	15.9 ± 0.1	0.19	>90	14.3 ± 0.1	0.13	>90	14.7 ± 0.1	0.14	>90
DMPC-sHDL	9.3 ± 0.1	0.04	>99	9.2 ± 0.1	0.03	>99	10.0 ± 0.2	0.14	>99	9.5 ± 0.1	0.06	>99
DPPC-sHDL	10.2 ± 0.2	0.15	>99	10.2 ± 0.2	0.16	>99	9.9 ± 0.2	0.1	>99	10.7 ± 0.2	0.22	>99

4.4.3 S1P-sHDL induces NO release via eNOS activation

After narrowing down the lipid composition of our sHDL to DPPC, we next decided to test the functionality of S1P incorporation at the endothelial level. One of the most prominent actions of HDL-associated S1P *in vivo* is the activation of endothelial nitric oxide synthase (eNOS) and subsequent production of nitric oxide (NO). To test our S1P-sHDL, we incubated HUVECs with PBS, sHDL at 0.01, 0.1, and 1 mg/mL, or S1P-sHDL at 0.01. 0.1, and 1 mg/mL (sHDL) corresponding to 0.05, 0.5, and 5 μM S1P, respectively. Indeed, we saw that sHDL alone could increase NO production modestly over PBS controls, however the addition of S1P drastically increased NO production over both PBS and sHDL-only groups, with the highest dose of S1P-sHDL showing nearly 5-fold increase in NO production over PBS controls and 2-fold increase over sHDL only controls (**Fig 4-3 A**). Since the first experiment varied both sHDL and S1P concentrations simultaneously, we sought to look at the effect of S1P alone by holding the sHDL concentration constant at 1 mg/mL and varying S1P from 0 (sHDL), 0.05 (S1P-sHDL #1), 0.5 (S1P-sHDL #2), and 5 μM S1P (S1P-sHDL #3). As seen in Figure 2B, the addition of sHDL alone produced a 2-fold increase in NO release (0.27 ± 0.02 μM vs 0.13 ± 0.01 μM for PBS), as expected. Furthermore, the addition of S1P induced a dose-dependent increase in NO production: 0.35 ± 0.03, 0.44 ± 0.01, and 0.59 ± 0.01 μM for sHDL containing 0.05, 0.5, and 5 nmol/mL S1P, respectively (**Fig 4-3 B**). These results are reflected by an increase in TEER values for HUVECs treated with S1P-sHDL, with the most significant effect observed for S1P-sHDL #2 (**Fig 4-3 C**).

To verify that this effect was due in part to activation of eNOS, we collected cell lysates after 30-minute treatment with sHDL or S1P-sHDL and performed Western

Blotting for phospho-eNOS-Ser1177 (the active form of eNOS) and total eNOS (**Fig 4-3 D**). Indeed, we saw that S1P-sHDL increased the total ratio of phospho-eNOS/total eNOS compared to sHDL or PBS controls, indicating that the increase in NO release observed could be partially explained by S1P-induced eNOS phosphorylation. From here, we narrowed down our final S1P-sHDL formulation to S1P-sHDL #2 (0.5 μM S1P), as this both induced significant NO production, eNOS phosphorylation, and increased TEER in endothelial cells compared to S1P-sHDLs #1 and #3.

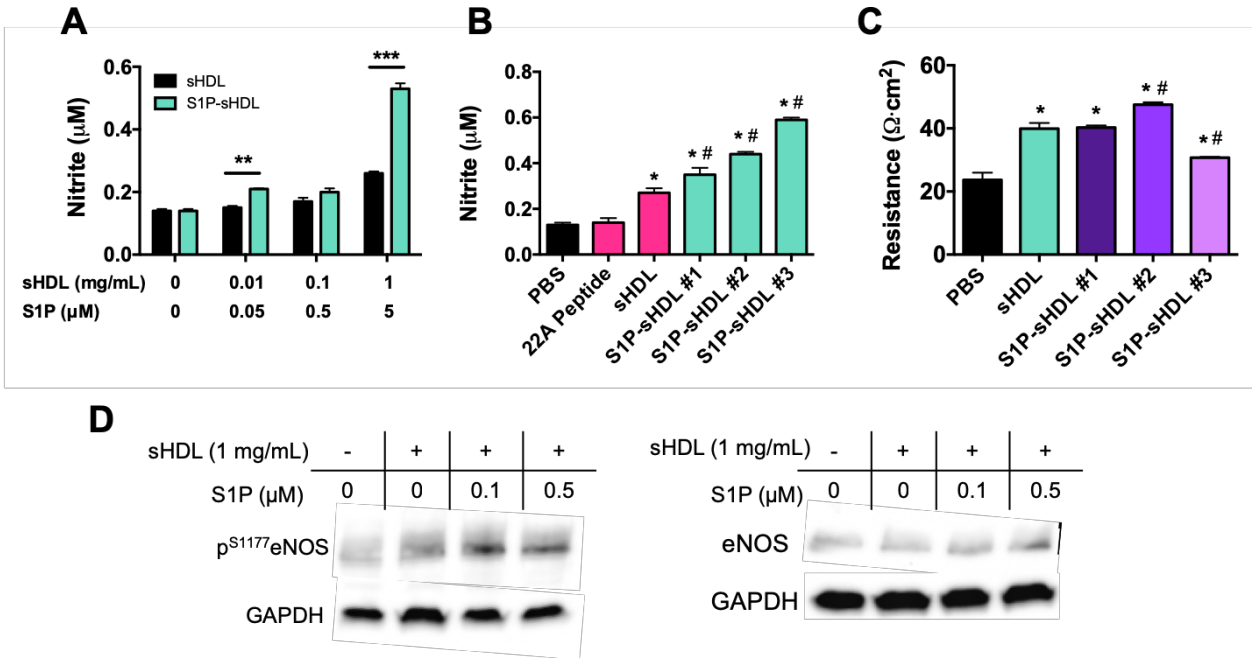


Figure 4-3 sHDL containing S1P promotes endothelial cell integrity through NO release via eNOS. *Primary human endothelial cells (HUVEC) were incubated for 15 min with sHDL containing 0 (sHDL), 0.05 (S1P-sHDL #1), 0.5 (S1P-sHDL #2), or 5 (S1P-sHDL #3) μM. Nitric oxide release was quantified by ozone chemiluminescence measurement of nitrite in the media (**A,B**). Transendothelial electric resistance (TEER) was monitored over 48 h in HUVECs treated with sHDL or S1P-sHDL (**C**). eNOS activation in HUVECs treated with sHDL or S1P-sHDL was measured by Western blot for eNOS and phospho-eNOS-Ser1177 and normalized to GAPDH housekeeping control (D). Data are reported as mean ± SEM. *p<0.05 vs. PBS control; **p<0.01; ***p<0.001; #p<0.05 vs sHDL.*

4.4.4 S1P-sHDL reduces endothelial activation and pro-inflammatory cytokine production

Another known property of endogenous HDL is its ability to reduce inflammation and prevent endothelial activation and dysfunction. While we have previously shown that sHDL alone is capable of reducing cytokine production after inflammatory assault in macrophages [133], we sought to explore whether the addition of S1P could further protect endothelial cells against the same inflammatory stimulus. Since S1P's protective function in endothelial cells is known to be HDL-specific, we used HSA-S1P as a control, since albumin is the second most abundant carrier of S1P in plasma and should not elicit such effects. Indeed, we saw that pre-treatment of HUVEC cells with sHDL (0.2 mg/mL) and S1P-sHDL (0.2 mg/mL sHDL and 0.1 μM S1P) prior to LPS challenge reduced mRNA expression of E-Selectin by ~50% for sHDL and ~75% for S1P-sHDL as well as VCAM-1 by ~40% for sHDL and 60% for S1P-sHDL (**Fig 4-4 A,B**). HSA-S1P had no significant effect on VCAM-1 expression but did slightly reduce levels of E-Selectin (~30%) when compared to PBS controls. We also measured levels of S1P receptor 1 (S1P1R) and eNOS to verify that our experimental conditions and/or treatments did not alter expression of these genes, as they are key pathways for S1P signaling. We saw no changes in S1P1R or eNOS expression (**Fig 4-4 C,D**) as expected.

Finally, we looked at the ability of S1P-sHDL to prevent pro-inflammatory cytokine production in HUVECs challenged with LPS. Briefly, HUVECs were pre-treated with sHDL, S1P-sHDL or controls for 18 h, followed by a 6 h challenge with LPS in the presence of treatment. Cytokine levels in the supernatant were measured, and while

HSA-S1P had no effect, both sHDL (142.7 ± 8.7 pg/mL) and S1P-sHDL (132.9 ± 7.2 pg/mL) exhibited drastic reductions in IL-6 compared to PBS controls (325.1 ± 39.6 pg/mL) (**Fig. 4-4 E**). Similarly, both sHDL and S1P-sHDL reduced levels of IL-8 in the media relative to PBS controls, with values of 35.3 ± 7.2, 47.0 ± 3.4, and 264.7 ± 22.4 ng/mL, respectively ($p<0.01$) (**Fig. 4-4 F**). Taken together, our data suggests that sHDL is an effective carrier for S1P, retaining all of the endothelial protective effects of S1P *in vitro*.

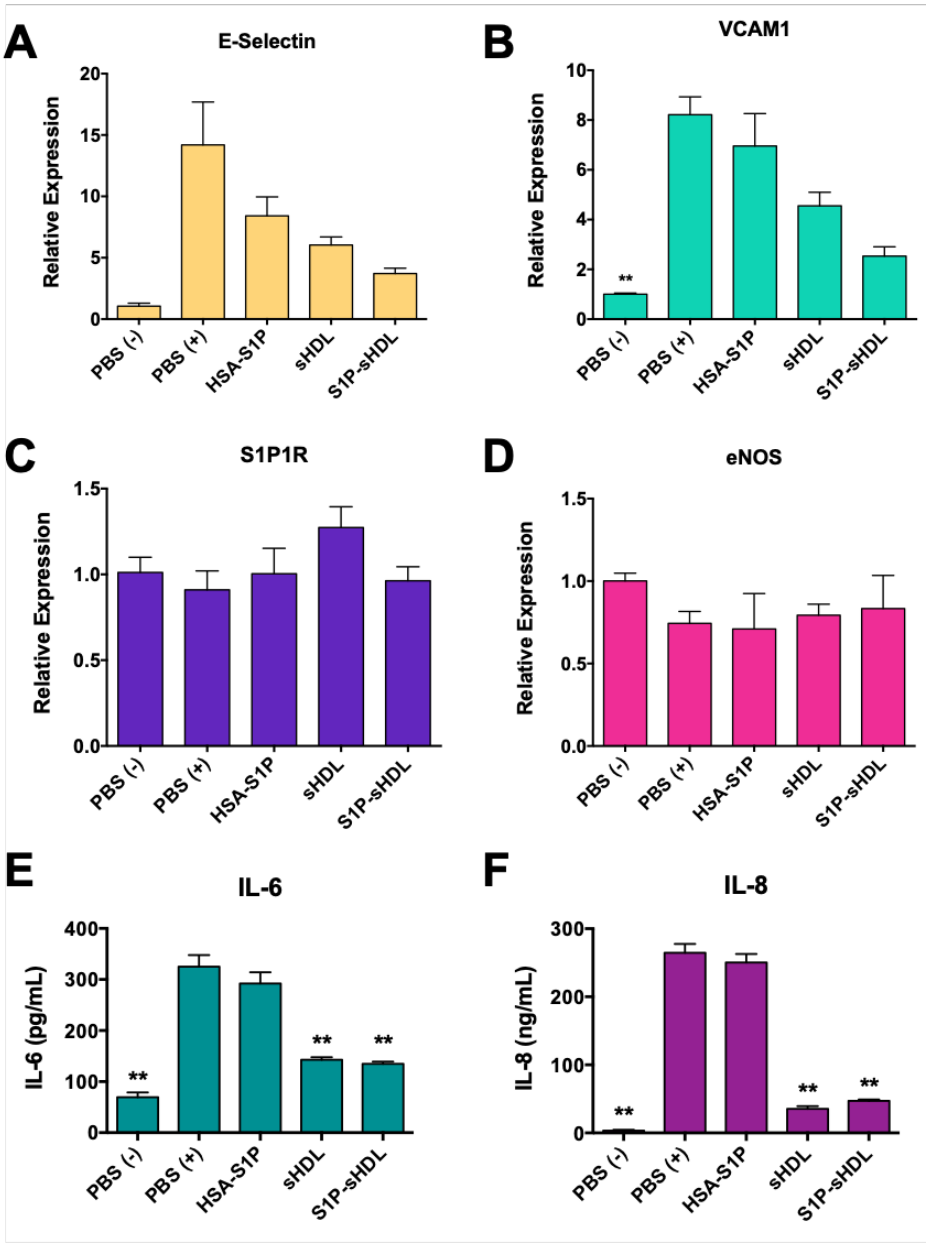


Figure 4-4 sHDL containing S1P inhibits endothelial cell activation induced by LPS. *Primary human endothelial cells (HUVEC) were pretreated with PBS, sHDL (0.2 mg/mL), S1P-sHDL (0.2 mg/mL sHDL and 0.1 μM S1P), or HSA-S1P (0.1 μM S1P) for 18 h, then challenged with (+) or without (-) LPS (1 μg/mL) for 6 h. mRNA levels in lysates were determined by RT-PCR and normalized to PBS (-) using the ddCt method (**A-D**). Cytokine levels in the supernatants were measure by ELISA (**E,F**). Data are represented as mean ± SEM. **p<0.01 vs PBS (+).*

4.5 Discussion

Given its ability to regulate and maintain vascular endothelial integrity, S1P's therapeutic potential has gained increasing attention. Yet, it has been shown that S1P-elicited effects in the vasculature are carrier-dependent, and that HDL-associated S1P signaling requires engagement of both HDL signaling events via scavenger receptor B-1 (SR-B1) as well as S1P signaling events (via S1P receptors) [226]. Endogenous HDL-S1P [38, 44] and isolated HDL enriched with S1P [227] have both been shown to restore and protect endothelial function *in vitro* and *in vivo*. In this study, we sought to formulate S1P in synthetic HDL nanoparticles to mimic endogenous presentation of S1P and promote endothelial function. Using the clinically tested mimetic peptide 22A, we screened 3 different lipid formulations for their abilities to form homogeneous sHDL particles, effectively incorporate S1P and activate S1P pathways *in vitro*. Our final formulation consisted of 22A peptide and DPPC containing 0.5 μM S1P (0.0063% loading). We show that our S1P-sHDL particles are capable of inducing NO production in a dose-dependent fashion, and that this effect is due to phosphorylation and activation of eNOS. Moreover, S1P-sHDL increased TEER values in endothelial monolayers to a greater extent than PBS or sHDL treated controls, consistent with previous reports [226].

Although others have previously reported that S1P-HDL particles can promote endothelial function and restore dysfunctional vasculature [226, 228] [38], we are the first to develop fully-synthetic, pharmaceutical grade HDL nanoparticle system for delivery of S1P. Other methods utilizing plasma-isolated HDL enriched with S1P or using plasma-purified ApoA-I protein to form S1P-HDL suffer from complicated

manufacturing processes, including endotoxin contamination and the use of detergents. Our delivery platform utilizes short mimetic peptides with established manufacturing processes that retain full bioactivity and are easier and cheaper to produce than full-length protein [99, 222]. Additionally, sHDL made from 22A peptide was tested in human clinical trials and was shown to be safe and well-tolerated over a wide dosing range [95, 96] and could be rapidly translated for other indications.

Other methods of S1P delivery include polymer and hydrogel-based formulations, made from materials such as poly(ethylene glycol) [229] and poly(lactic-co-glycolic-acid) [230, 231]. This is the case for many tissue-scaffold and ischemia-related applications, where a high local concentration of S1P is desired to promote angiogenesis and vascularization of tissue transplants [229, 230, 232, 233]. Often albumin is incorporated in the formulation as an S1P-stabilizing agent [231], since S1P itself is insoluble in water, although albumin-mediated S1P signaling has been shown to differ from that of HDL [226, 234]. Thus, while polymeric delivery systems have proven successful in promoting vascularization and suppressing immune response during graft transplants, the effects seen are not specific to HDL-presented S1P and would likely have varied outcomes in global models of endothelial dysfunction, which require a more specific and HDL-tailored response.

S1P is also known to regulate immune cell trafficking and lymphocyte egress from the lymph nodes, playing a critical role in immunomodulation, although this effect is not faciliatated by HDL [235, 236]. Thus, the development of therapeutics targeting S1P receptors has been of significant clinical interest [237]. One such drug, FTY720 (known as Fingolimod or Gilenya), is an FDA approved for the treatment of relapsing multiple

sclerosis (MS) [236]. Others have also shown that it is effective in reducing atherosclerosis in rodents although shown to interfere with normal macrophage and lymphocyte function [238, 239]. While oral S1P receptor modulators may serve great potential in immunomodulating settings, their functions as complete S1P analogs are generally limited by the receptors they target. For example, unlike native S1P, FTY720 is not specific for $S1P_2$ receptors and thus does not possess the ability to regulate basal vascular tone or cell adhesion molecule expression, which require both HDL (via SR-B1) and S1P (via $S1P_1$) signaling events [240]. Additionally, FTY720 also induces internalization and degradation of $S1P_1$ receptors which, in our setting, are essential for mediating S1P-HDL signaling events such as inhibition of cell adhesion molecule expression [240].

In conclusion, we have presented for the first time a pharmaceutical grade delivery strategy for S1P that harnesses not only the cardioprotective actions of S1P, but also that of the sHDL carrier itself. In vitro, we see potent induction of eNOS generated NO release from primary human endothelial cells which led to an increase in endothelial barrier integrity, as assessed by TEER. Furthermore, our particles were capable of suppressing endothelial activation by inhibiting LPS-induced expression of cell adhesion molecules and downstream cytokine production. Compared to previous attempts, including reconstituted S1P-HDL, polymer-based S1P delivery, and small molecule analogs, our platform benefits from established manufacturing processes, proven clinical safety in humans, and most importantly a tailored induction of S1P signaling events specific to HDL. Given our promising *in vitro* data, sHDL-mediated S1P

delivery presents a unique and rapidly translatable approach to treating a variety of vascular disorders and warrants future *in vivo* evaluation.

Chapter 5: Conclusions and Perspective

The work presented in this thesis expands the utility of traditional sHDL and rHDL therapies beyond facilitation of reverse cholesterol transport. Given the prevalence of vascular dysfunction underlying and leading to more serious conditions, and the innate ability of HDL to modulate several aspects of the inflammatory and endothelial activation cascades, the development of sHDL as a multi-factorial treatment for endothelial health holds great potential.

In the context of sepsis, sHDL could be a ground-breaking therapeutic effort. In Chapter 2 we show that HDL levels in septic patients were highly correlated with their chances of survival. Additionally, we show that a one-time, low-dose infusion of sHDL can markedly improve survival in CLP-challenged mice, and that this observation is due to the abilities of sHDL to bind endotoxin, inhibit TLR-4 signaling in macrophages, and prevent activation of the endothelium. While intriguing, our efforts thus far have focused on a single composition of sHDL. Yet, studies by our lab and others have shown that phospholipid composition of sHDL can greatly affect its circulation half-life, anti-inflammatory properties, and cholesterol efflux capacity, yielding great potential for the reformulation of sHDL composition to reflect optimal performance in sepsis. Additionally, the efficacy of sHDL in sepsis was tested after a one-time low-dose infusion of sHDL, leaving a large window of opportunity to improve clinical outcome by exploring alternative dosing regimens. Thus, future work to optimize sHDL composition and

dosing regimen is warranted in order to maximize the therapeutic potential of sHDL therapy for sepsis.

In Chapter 3, we focused on enhancing sHDL's therapeutic benefit in atherosclerosis by exploring the synergy between sHDL and LXR agonist combination therapy. While previous reports have alluded that HDL and/or cholesterol efflux causes a down-regulation of ABCA1/G1 cholesterol transporters, we are the first to show a strong and dose-dependent down-regulation of these transporters after treatment with clinically tested sHDL products. We also see that this effect is correlated with the cholesterol efflux capacity of sHDL. This study is important because sHDL efficacy is highly dependent on its ability to interact with ABCA1/G1 transporters to remove excess cholesterol from the body, and transporter down-regulation may account for the lack of sHDL efficacy in clinical trials. To overcome this, we combined sHDL with a low-dose LXR agonist which reversed ABCA1/G1 down-regulation and enhanced the atheroma-reducing efficacy over sHDL therapy alone. Moreover, synergy between the two drugs may allow for efficacy at lower doses, circumventing many of the unwanted side-effects of both drugs and renewing pharmaceutical interest in both classes of drugs. And, while we focused mainly on cholesterol efflux for this study, both sHDL and LXR agonists are known to have anti-inflammatory effects in the vasculature, and studies evaluating plaque composition (i.e. macrophage content, endothelial activation markers) will be valuable in assessing the global impact of combination therapy on the vasculature. Finally, while we observed synergy between sHDL and LXR agonist under the given conditions, it is necessary to evaluate these effects under a range of dosing conditions

to fully understand the synergetic effect between these two drug classes and could potentially lead to further reductions in dose and subsequent side-effects.

Finally, we show that sHDL's endothelial protective properties can be enhanced by the addition of S1P. Given its potent anti-inflammatory and endothelial protective propertied, S1P has long been sought after as a therapeutic target. However, due to its poor pharmaceutical properties and pleiotropic effects *in vivo*, advanced drug delivery strategies are needed to harness the endothelial-specific benefits of S1P. sHDL presented an ideal strategy for delivering S1P due to its vascular-targeting properties and its ability to carry hydrophobic substances in the lipid-bilayer core. Chapter 4 shows that S1P can be incorporated into sHDL particles over several concentration ranges. Importantly, we show that these S1P-sHDL particles can elicit the desired endothelial protective effects *in vitro*, most notably by increasing NO production in endothelial cells in a dose-dependent manner. While our *in vitro* results are promising, these findings still need to be evaluated *in vivo*. Future studies in murine models of endothelial dysfunction will be telling of the potential of S1P-sHDL for therapeutic applications. Additional experiments to assess the stability of S1P in sHDL particles are also necessary in order to fully-optimize these formulations from a pharmaceutical perspective. While the work presented in Chapter 4 is largely preliminary, it presents a unique and rapidly translatable approach to both S1P delivery and enhancement of traditional sHDL therapies.

The major limitations to the work presented here are the extrapolations of findings from animal models to human disease. In particular, this has been a great challenge in the sepsis field, reflected by the lack of approved therapies due to the

disconnect between findings in animals and outcomes in humans. Aside from inherent species differences, rodent models of sepsis are limited in scope due to the complexity of the human pathology. Several animal models of sepsis have been employed in the literature, including endotoxemia models, bacterial inoculum models, and surgical models such as cecal-ligation and puncture (CLP, used in our work). Endotoxemia models benefit from simplicity and high reproducibility but suffer from a lack of recapitulation of the full human condition as they only trigger TLR-4-dependent responses [241]. While bacterial inoculum models involve host response to pathogens, they too suffer drawbacks as they do not represent the diversity of infectious agents and are induced with high-load bacterial challenges typically not seen in human cases of sepsis [242]. On the other hand, CLP is regarded as the “gold-standard” for animal sepsis models as it recreates the dynamic human response, including the hemodynamic and metabolic changes as well as polymicrobial infection [243]. However, reproducibility is more difficult to control in CLP models as surgical procedures introduce variability and the severity of sepsis is highly dependent on the protocol (i.e. length of ligation, number and gauge of punctures) [242, 244].

Similar difficulties are also been reported for atherosclerosis animal models, as rodents are particularly resistant to CVD and require genetic and diet modifications to induce disease. Additionally, mouse cholesterol metabolism differs from humans in that mice lack cholesterol ester transfer protein (CETP) and have high levels of endogenous HDL and low levels of LDL, whereas LDL is the major circulating lipoprotein in humans [245]. To overcome these challenges, several mouse models of atherosclerosis have been employed in the literature, the most widely used being mice on an $ApoE^{-/-}$ or

LDLR$^{-/-}$ background fed a high-fat-high-cholesterol diet for several weeks to induce lesion formation [246]. Mouse models benefit from lower costs and higher turnover, as they are cheaper and easier to generate and maintain in high numbers than their larger animal counterparts (i.e. rabbits, pigs), especially given the lengthy model establishment and experimental timeframe [246, 247]. Although major differences exist between species, many of the mechanistic pathologies are conserved between murine and human atherosclerosis making the mouse model a suitable starting point to screen pharmacological efficacy of therapeutics prior to moving to larger animal models.

Together, the work from this thesis casts a new light on the applications of sHDL infusion therapies in the context of vascular disease. Not only do we provide strategies to overcome existing barriers in sHDL therapy for cardiovascular disease via combination with LXR agonists, but we also explore the utility of sHDL to treat vascular dysfunction in a more general sense, by delivery of S1P or by exploiting its anti-inflammatory effects in sepsis models. This research is important for several reasons, but notably for its emphasis on exploiting the multi-factorial properties of sHDL, whereas much of the clinical development of sHDL therapies to date have focused solely on the cholesterol lowering properties. We hope that by shedding light on the other beneficial aspects of sHDL in the vasculature, we can renew interest in their clinical development and expand the potential therapeutic applications to treat vascular dysfunction in a more comprehensive fashion.

Bibliography

1. von Eckardstein, A., J.-R. Nofer, and G. Assmann, *High Density Lipoproteins and Arteriosclerosis: Role of Cholesterol Efflux and Reverse Cholesterol Transport.* Arteriosclerosis, Thrombosis, and Vascular Biology, 2001. **21**(1): p. 13-27.

2. Ohashi, R., et al., *Reverse cholesterol transport and cholesterol efflux in atherosclerosis.* QJM, 2005. **98**(12): p. 845-856.

3. Vickers, K.C. and A.T. Remaley, *HDL and cholesterol: life after the divorce?* Journal of Lipid Research, 2014. **55**(1): p. 4-12.

4. Lewis, G.F. and D.J. Rader, *New Insights Into the Regulation of HDL Metabolism and Reverse Cholesterol Transport.* Circulation Research, 2005. **96**(12): p. 1221-1232.

5. Remaley, A.T., M. Amar, and D. Sviridov, *HDL-replacement therapy: mechanism of action, types of agents and potential clinical indications.* Expert Review of Cardiovascular Therapy, 2008. **6**(9): p. 1203-1215.

6. Nofer, J.-R., et al., *HDL and arteriosclerosis: beyond reverse cholesterol transport.* Atherosclerosis, 2002. **161**(1): p. 1-16.

7. Barter, P.J., et al., *Antiinflammatory Properties of HDL.* Circulation Research, 2004. **95**(8): p. 764-772.

8. Zannis, V., et al., *HDL Biogenesis, Remodeling, and Catabolism*, in *High Density Lipoproteins*, A. von Eckardstein and D. Kardassis, Editors. 2015, Springer International Publishing. p. 53-111.

9. Lund-Katz, S. and M. Phillips, *High Density Lipoprotein Structure–Function and Role in Reverse Cholesterol Transport*, in *Cholesterol Binding and Cholesterol Transport Proteins:*, J.R. Harris, Editor. 2010, Springer Netherlands. p. 183-227.

10. Favari, E., et al., *Cholesterol Efflux and Reverse Cholesterol Transport*, in *High Density Lipoproteins*, A. von Eckardstein and D. Kardassis, Editors. 2015, Springer International Publishing. p. 181-206.

11. Kontush, A., M. Lhomme, and M.J. Chapman, *Unraveling the complexities of the HDL lipidome.* Journal of Lipid Research, 2013. **54**(11): p. 2950-2963.

12. Kontush, A., et al., *Structure of HDL: Particle Subclasses and Molecular Components*, in *High Density Lipoproteins*, A. von Eckardstein and D. Kardassis, Editors. 2015, Springer International Publishing. p. 3-51.

13. Kontush, A. and M.J. Chapman, *High-Density Lipoproteins : Structure, Metabolism, Function and Therapeutics*. 2011, Hoboken, NJ, USA: John Wiley & Sons.

14. Lüscher, T.F., et al., *High-Density Lipoprotein: Vascular Protective Effects, Dysfunction, and Potential as Therapeutic Target.* Circulation Research, 2014. **114**(1): p. 171-182.

15. Lusis, A.J., *Atherosclerosis.* Nature, 2000. **407**(6801): p. 233-241.

16. Hansson, G.K., A.-K.L. Robertson, and C. Söderberg-Nauclér, *Inflammation and atherosclerosis.* Annual Review of Pathology: Mechanisms of Disease, 2006. **1**(1): p. 297-329.

17. Morin, E.E., et al., *HDL in sepsis - risk factor and therapeutic approach.* Frontiers in Pharmacology, 2015. **6**.

18. Morin, E.E., X.-A. Li, and A. Schwendeman, *HDL in Endocrine Carcinomas: Biomarker, Drug Carrier, and Potential Therapeutic.* Frontiers in Endocrinology, 2018. **9**(715).

19. Li, D., et al., *Apolipoprotein mimetic peptides for stimulating cholesterol efflux*, in *Apolipoprotein Mimetics in the Management of Human Disease*. 2015, Springer. p. 29-42.

20. Argraves, K.M. and W.S. Argraves, *HDL serves as a S1P signaling platform mediating a multitude of cardiovascular effects.* Journal of Lipid Research, 2007. **48**(11): p. 2325-2333.

21. De Nardo, D., et al., *High-density lipoprotein mediates anti-inflammatory reprogramming of macrophages via the transcriptional regulator ATF3.* Nat Immunol, 2014. **15**(2): p. 152-160.

22. Harris, H.W., J.A. Johnson, and S.J. Wigmore, *Endogenous lipoproteins impact the response to endotoxin in humans.* Critical Care Medicine, 2002. **30**(1): p. 23-31.

23. Mineo, C., et al., *Endothelial and Antithrombotic Actions of HDL.* Circulation Research, 2006. **98**(11): p. 1352-1364.

24. Riwanto, M. and U. Landmesser, *High density lipoproteins and endothelial functions: mechanistic insights and alterations in cardiovascular disease.* Journal of Lipid Research, 2013. **54**(12): p. 3227-3243.

25. Gordon, B.R., *Poor outcomes associated with low lipid and lipoprotein levels *.* Critical Care Medicine, 2004. **32**(3): p. 878-879 10.1097/01.CCM.0000117318.84442.9F.

26. Catapano, A.L., et al., *HDL in innate and adaptive immunity.* Cardiovascular Research, 2014. **103**(3): p. 372-383.

27. Westerterp, M., et al., *ATP-Binding Cassette Transporters, Atherosclerosis, and Inflammation.* Circulation Research, 2014. **114**(1): p. 157-170.

28. Brandenburg, K., et al., *Biophysical characterization of the interaction of high-density lipoprotein (HDL) with endotoxins.* European Journal of Biochemistry, 2002. **269**(23): p. 5972-5981.

29. Mineo, C. and P.W. Shaul, *Regulation of signal transduction by HDL.* Journal of Lipid Research, 2013. **54**(9): p. 2315-2324.

30. Yuhanna, I.S., et al., *High-density lipoprotein binding to scavenger receptor-BI activates endothelial nitric oxide synthase.* Nat Med, 2001. **7**(7): p. 853-857.

31. Lucke, S. and B. Levkau, *Endothelial Functions of Sphingosine-1-phosphate.* Cellular Physiology and Biochemistry, 2010. **26**(1): p. 87-96.

32. Nofer, J.-R. and G. Assmann, *Atheroprotective Effects of High-Density Lipoprotein-Associated Lysosphingolipids.* Trends in Cardiovascular Medicine, 2005. **15**(7): p. 265-271.

33. Sattler, K. and B. Levkau, *Sphingosine-1-phosphate as a mediator of high-density lipoprotein effects in cardiovascular protection.* Cardiovascular Research, 2009. **82**(2): p. 201-211.

34. Sattler, K.E., et al., *Sphingosine 1-phosphate levels in plasma and HDL are altered in coronary artery disease.* Basic Research in Cardiology, 2010. **105**(6): p. 821-832.

35. Candipan, R.C., et al., *Regression or Progression: Dependency on Vascular Nitric Oxide.* Arteriosclerosis, Thrombosis, and Vascular Biology, 1996. **16**(1): p. 44-50.

36. Potì, F., M. Simoni, and J.-R. Nofer, *Atheroprotective role of high-density lipoprotein (HDL)-associated sphingosine-1-phosphate (S1P).* Cardiovascular Research, 2014. **103**(3): p. 395-404.

37. Nofer, J.-R., *High-density lipoprotein, sphingosine 1-phosphate, and atherosclerosis.* Journal of Clinical Lipidology, 2008. **2**(1): p. 4-11.

38. Nofer, J.-R., et al., *HDL induces NO-dependent vasorelaxation via the lysophospholipid receptor S1P3.* The Journal of Clinical Investigation, 2004. **113**(4): p. 569-581.

39. Aviram, M., et al., *Paraoxonase inhibits high-density lipoprotein oxidation and preserves its functions. A possible peroxidative role for paraoxonase.* The Journal of Clinical Investigation, 1998. **101**(8): p. 1581-1590.

40. Maceyka, M. and S. Spiegel, *Sphingolipid metabolites in inflammatory disease.* Nature, 2014. **510**(7503): p. 58-67.

41. Spiegel, S. and S. Milstien, *Sphingosine-1-phosphate: an enigmatic signalling lipid.* Nat Rev Mol Cell Biol, 2003. **4**(5): p. 397-407.

42. Kerage, D., D.N. Brindley, and D.G. Hemmings, *Review: Novel insights into the regulation of vascular tone by sphingosine 1-phosphate.* Placenta, 2014. **35, Supplement**(0): p. S86-S92.

43. Mineo, C., et al., *High Density Lipoprotein-induced Endothelial Nitric-oxide Synthase Activation Is Mediated by Akt and MAP Kinases.* Journal of Biological Chemistry, 2003. **278**(11): p. 9142-9149.

44. Nofer, J.-R., et al., *Suppression of Endothelial Cell Apoptosis by High Density Lipoproteins (HDL) and HDL-associated Lysosphingolipids.* Journal of Biological Chemistry, 2001. **276**(37): p. 34480-34485.

45. Keul, P., et al., *The Sphingosine-1-Phosphate Analogue FTY720 Reduces Atherosclerosis in Apolipoprotein E–Deficient Mice.* Arteriosclerosis, Thrombosis, and Vascular Biology, 2007. **27**(3): p. 607-613.

46. Shimamura, K., et al., *Expression of adhesion molecules by sphingosine 1-phosphate and histamine in endothelial cells.* European Journal of Pharmacology, 2004. **486**(2): p. 141-150.

47. Xia, P., et al., *Tumor necrosis factor-α induces adhesion molecule expression through the sphingosine kinase pathway.* Proceedings of the National Academy of Sciences, 1998. **95**(24): p. 14196-14201.

48. *Disease Statistics*. 2012; Available from: http://www.nhlbi.nih.gov/about/documents/factbook/2012/chapter4.

49. Mozaffarian, D., et al., *Heart Disease and Stroke Statistics—2015 Update: A Report From the American Heart Association.* Circulation, 2015. **131**(4): p. e29-e322.

50. Libby, P., P.M. Ridker, and G.K. Hansson, *Progress and challenges in translating the biology of atherosclerosis.* Nature, 2011. **473**(7347): p. 317-325.

51. van Leeuwen, H.J., et al., *Lipoprotein metabolism in patients with severe sepsis.* Crit Care Med, 2003. **31**(5): p. 1359-66.

52. Martin, G.S., et al., *The epidemiology of sepsis in the United States from 1979 through 2000.* N Engl J Med, 2003. **348**(16): p. 1546-1554.

53. Riedemann, N.C., R.F. Guo, and P.A. Ward, *The enigma of sepsis.* J Clin Invest, 2003. **112**(4): p. 460-7.

54. Angus, D.C. and T. van der Poll, *Severe sepsis and septic shock.* N Engl J Med, 2013. **369**(9): p. 840-51.

55. Deanfield, J.E., J.P. Halcox, and T.J. Rabelink, *Endothelial Function and Dysfunction: Testing and Clinical Relevance.* Circulation, 2007. **115**(10): p. 1285-1295.

56. Aird, W.C., *The role of the endothelium in severe sepsis and multiple organ dysfunction syndrome.* Blood, 2003. **101**(10): p. 3765-3777.

57. Chien, J.Y., et al., *Low serum level of high-density lipoprotein cholesterol is a poor prognostic factor for severe sepsis.* Crit Care Med, 2005. **33**(8): p. 1688-93.

58. Tsai, M.H., et al., *Low serum concentration of apolipoprotein A-I is an indicator of poor prognosis in cirrhotic patients with severe sepsis.* J Hepatol, 2009. **50**(5): p. 906-15.

59. Navab, M., et al., *HDL and cardiovascular disease: atherogenic and atheroprotective mechanisms.* Nat Rev Cardiol, 2011. **8**(4): p. 222-232.

60. Singh, I.M., M.H. Shishehbor, and B.J. Ansell, *High-density lipoprotein as a therapeutic target: A systematic review.* Jama, 2007. **298**(7): p. 786-798.

61. Eggesbo, J.B., et al., *Different binding of 125I-LPS to plasma proteins from persons with high or low HDL.* Scand J Clin Lab Invest, 1996. **56**(6): p. 533-43.

62. Flegel, W.A., et al., *Inhibition of endotoxin-induced activation of human monocytes by human lipoproteins.* Infect Immun, 1989. **57**(7): p. 2237-45.

63. Van Lenten, B.J., et al., *The role of lipoproteins and receptor-mediated endocytosis in the transport of bacterial lipopolysaccharide.* Proc Natl Acad Sci U S A, 1986. **83**(8): p. 2704-8.

64. Murch, O., et al., *Lipoproteins in inflammation and sepsis. I. Basic science.* Intensive Care Med, 2007. **33**(1): p. 13-24.

65. Munford, R.S., *Detoxifying endotoxin: time, place and person.* J Endotoxin Res, 2005. **11**(2): p. 69-84.

66. Read, T.E., et al., *Chylomicrons enhance endotoxin excretion in bile.* Infect Immun, 1993. **61**(8): p. 3496-502.

67. Harris, H.W., et al., *Human very low density lipoproteins and chylomicrons can protect against endotoxin-induced death in mice.* J Clin Invest, 1990. **86**(3): p. 696-702.

68. Harris, H.W., et al., *Chylomicrons alter the fate of endotoxin, decreasing tumor necrosis factor release and preventing death.* J Clin Invest, 1993. **91**(3): p. 1028-34.

69. Lee, R.P., et al., *High-density lipoprotein prevents organ damage in endotoxemia.* Res Nurs Health, 2007. **30**(3): p. 250-60.

70. Yan, Y.-j., et al., *Beneficial effects of ApoA-I on LPS-induced acute lung injury and endotoxemia in mice.* Life Sciences, 2006. **79**(2): p. 210-215.

71. Imai, T., T. Fujita, and Y. Yamazaki, *Beneficial Effects of Apolipoprotein A-I on Endotoxemia.* Surgery Today, 2003. **33**(9): p. 684-687.

72. Levine, D.M., et al., *In vivo protection against endotoxin by plasma high density lipoprotein.* Proceedings of the National Academy of Sciences, 1993. **90**(24): p. 12040-12044.

73. Van Lenten, B.J., et al., *Influenza Infection Promotes Macrophage Traffic Into Arteries of Mice That Is Prevented by D-4F, an Apolipoprotein A-I Mimetic Peptide.* Circulation, 2002. **106**(9): p. 1127-1132.

74. Gupta, H., et al., *Inhibition of Lipopolysaccharide-Induced Inflammatory Responses by an Apolipoprotein AI Mimetic Peptide.* Circulation Research, 2005. **97**(3): p. 236-243.

75. Dai, L., et al., *The apolipoprotein A-I mimetic peptide 4F prevents defects in vascular function in endotoxemic rats.* Journal of Lipid Research, 2010. **51**(9): p. 2695-2705.

76. Zhang, Z., et al., *Apolipoprotein A-I mimetic peptide treatment inhibits inflammatory responses and improves survival in septic rats*. Vol. 297. 2009. H866-H873.

77. Moreira, R.S., et al., *Apolipoprotein A-I mimetic peptide 4F attenuates kidney injury, heart injury, and endothelial dysfunction in sepsis.* American Journal of Physiology - Regulatory, Integrative and Comparative Physiology, 2014. **307**(5): p. R514-R524.

78. Hubsch, A.P., A.T. Casas, and J.E. Doran, *Protective effects of reconstituted high-density lipoprotein in rabbit gram-negative bacteremia models.* J Lab Clin Med, 1995. **126**(6): p. 548-58.

79. Casas, A.T., et al., *Reconstituted High-Density Lipoprotein Reduces LPS-Stimulated TNFα.* Journal of Surgical Research, 1995. **59**(5): p. 544-552.

80. Pajkrt, D., et al., *Antiinflammatory effects of reconstituted high-density lipoprotein during human endotoxemia.* The Journal of experimental medicine, 1996. **184**(5): p. 1601-1608.

81. Anantharamaiah, G.M., et al., *Studies of synthetic peptide analogs of the amphipathic helix. Structure of complexes with dimyristoyl phosphatidylcholine.* Journal of Biological Chemistry, 1985. **260**(18): p. 10248-55.

82. Navab, M., et al., *Apolipoprotein A-I mimetic peptides and their role in atherosclerosis prevention.* Nat Clin Pract Cardiovasc Med, 2006. **3**(10): p. 540-547.

83. Di Bartolo, B.A., et al., *The apolipoprotein A-I mimetic peptide ETC-642 exhibits anti-inflammatory properties that are comparable to high density lipoproteins.* Atherosclerosis, 2011. **217**(2): p. 395-400.

84. Amar, M.J.A., et al., *5A Apolipoprotein Mimetic Peptide Promotes Cholesterol Efflux and Reduces Atherosclerosis in Mice.* Journal of Pharmacology and Experimental Therapeutics, 2010. **334**(2): p. 634-641.

85. Navab, M., et al., *Apolipoprotein A-I Mimetic Peptides.* Arteriosclerosis, Thrombosis, and Vascular Biology, 2005. **25**(7): p. 1325-1331.

86. Bloedon, L.T., et al., *Safety, pharmacokinetics, and pharmacodynamics of oral apoA-I mimetic peptide D-4F in high-risk cardiovascular patients.* Journal of Lipid Research, 2008. **49**(6): p. 1344-1352.

87. Watson, C.E., et al., *Treatment of patients with cardiovascular disease with L-4F, an apo-A1 mimetic, did not improve select biomarkers of HDL function.* Journal of Lipid Research, 2011. **52**(2): p. 361-373.

88. *Kos Reports on Promising Data Presented at AHA: New Compound Reverse-D4F, a Novel Apo A-I Mimetic Peptide, May Reduce the Progression of Atherosclerosis.*; Available from: http://www.businesswire.com/news/home/20051114005406/en/Kos-Reports-Promising-Data-Presented-AHA-Compound#.VF0-H_nF9HV.

89. Desseux, J.L., A.S. Schwendeman, and L. Zhu, *Apolipoprotein A-I mimics*, USPTO, Editor. 2013, Cerenic Therapeutics Holding SA: United States.

90. Wool, G.D., C.A. Reardon, and G.S. Getz, *Apolipoprotein A-I mimetic peptide helix number and helix linker influence potentially anti-atherogenic properties.* Journal of Lipid Research, 2008. **49**(6): p. 1268-1283.

91. Bielicki, J.K., et al., *A new HDL mimetic peptide that stimulates cellular cholesterol efflux with high efficiency greatly reduces atherosclerosis in mice.* Journal of Lipid Research, 2010. **51**(6): p. 1496-1503.

92. Dasseux, J.L., *Peptide/lipid complex formation by co-lyophilization*. 2001, Google Patents.

93. Dasseux, J.L., *Peptide/lipid complex formation by co-lyophilization*, USPTO, Editor. 2001, Esperion Therapeutics, Inc.: United States.

94. Nissen, S.E., et al., *Effect of recombinant apoa-i milano on coronary atherosclerosis in patients with acute coronary syndromes: A randomized controlled trial.* JAMA, 2003. **290**(17): p. 2292-2300.

95. Miles, J., et al. *Single-dose tolerability, pharmacokinetics, and cholesterol mobilization in HDL-C fraction following intravenous administration of ETC-642, a 22-mer ApoA-I analogue and phospholipids complex, in atherosclerosis patients*. in *Arteriosclerosis Thrombosis and Vascular Biology*. 2004.

96. Khan, M., et al. *Single-dose intravenous infusion of ETC-642, a 22-Mer ApoA-I analogue and phospholipids complex, elevates HDL-C in atherosclerosis patients*. in *Circulation*. 2003.

97. Tardif, J.-C., et al., *Effects of the high-density lipoprotein mimetic agent CER-001 on coronary atherosclerosis in patients with acute coronary syndromes: a randomized trial†.* European Heart Journal, 2014. **35**(46): p. 3277-3286.

98. Tardif, J., et al., *Effects of reconstituted high-density lipoprotein infusions on coronary atherosclerosis: A randomized controlled trial.* JAMA, 2007. **297**(15): p. 1675-1682.

99. Dasseux, J.L., A.S. Schwendeman, and L. Zhu, *Apolipoprotein A-I mimics*, USPTO, Editor. 2013, Cerenic Therapeutics Holding SA: United States.

100. Gille, A., et al., *CSL112 enhances biomarkers of reverse cholesterol transport after single and multiple infusions in healthy subjects.* Arterioscler Thromb Vasc Biol, 2014. **34**(9): p. 2106-14.

101. Nanjee, M.N., et al., *Acute effects of intravenous infusion of ApoA1/phosphatidylcholine discs on plasma lipoproteins in humans.* Arterioscler Thromb Vasc Biol, 1999. **19**(4): p. 979-89.

102. Keyserling, C.H., et al., *Abstract 15525: CER-001, a Synthetic HDL-Mimetic, Safely Mobilizes Cholesterol in Healthy Dyslipidemic Volunteers.* Circulation, 2011. **124**(suppl_21): p. A15525-A15525.

103. Bobillier, A., et al., *A single infusion of MDCO-216 (ApoA-1 Milano/POPC) increases ABCA1-mediated cholesterol efflux and pre-beta 1 HDL in healthy*

volunteers and patients with stable coronary artery disease. European Heart Journal - Cardiovascular Pharmacotherapy, 2015. **2**(1): p. 23-29.

104. *CSL Behring initiates AEGIS-II Phase III trial of CSL112.* . March 26, 2018; Available from: https://www.drugdevelopment-technology.com/news/csl-behring-initiates-aegis-ii-phase-iii-trial-csl112/.

105. Krause, B.R. and A.T. Remaley, *Reconstituted HDL for the acute treatment of acute coronary syndrome.* Curr Opin Lipidol, 2013. **24**(6): p. 480-6.

106. Kuai, R., et al., *High-density lipoproteins: nature's multifunctional nanoparticles.* ACS nano, 2016. **10**(3): p. 3015-3041.

107. Lerch, P.G., et al., *Production and characterization of a reconstituted high density lipoprotein for therapeutic applications.* Vox Sang, 1996. **71**(3): p. 155-64.

108. Spieker, L.E., et al., *High-density lipoprotein restores endothelial function in hypercholesterolemic men.* Circulation, 2002. **105**(12): p. 1399-402.

109. Bisoendial, R.J., et al., *Restoration of endothelial function by increasing high-density lipoprotein in subjects with isolated low high-density lipoprotein.* Circulation, 2003. **107**(23): p. 2944-8.

110. van Oostrom, O., et al., *Reconstituted HDL increases circulating endothelial progenitor cells in patients with type 2 diabetes.* Arterioscler Thromb Vasc Biol, 2007. **27**(8): p. 1864-5.

111. Shaw, J.A., et al., *Infusion of reconstituted high-density lipoprotein leads to acute changes in human atherosclerotic plaque.* Circ Res, 2008. **103**(10): p. 1084-91.

112. Calkin, A.C., et al., *Reconstituted high-density lipoprotein attenuates platelet function in individuals with type 2 diabetes mellitus by promoting cholesterol efflux.* Circulation, 2009. **120**(21): p. 2095-104.

113. *Safety, Tolerability and Pharmacokinetics of CSL112 in Healthy Volunteers.*; Available from: https://clinicaltrials.gov/ct2/show/study/NCT01129661?term=CSL112&rank=4.

114. *A Multiple Ascending Dose Study of CSL112 in Healthy Volunteers.*; Available from: https://clinicaltrials.gov/ct2/show/NCT01281774?term=CSL112&rank=3.

115. Easton, R., et al., *A multiple ascending dose study of CSL112, an infused formulation of ApoA-I.* J Clin Pharmacol, 2014. **54**(3): p. 301-10.

116. *A Single Ascending Dose Study Examining the Safety and Pharmacokinetic Profile of Reconstituted High Density Lipoprotein (CSL112) Administered to Patients.*

117. Michael Gibson, C., et al., *Safety and Tolerability of CSL112, a Reconstituted, Infusible, Plasma-Derived Apolipoprotein A-I, After Acute Myocardial Infarction: The AEGIS-I Trial (ApoA-I Event Reducing in Ischemic Syndromes I).* Circulation, 2016. **134**(24): p. 1918-1930.

118. Gibson, C.M., et al., *Rationale and design of Apo-I Event Reduction in Ischemic Syndromes I (AEGIS-I): A phase 2b, randomized, placebo-controlled, dose-ranging trial to investigate the safety and tolerability of CSL112, a reconstituted, infusible, human apoA-I, after acute myocardial infarction.* Am Heart J, 2016. **180**: p. 22-8.

119. Carlson, L.A., *Effect of a Single Infusion of Recombinant Human Proapolipoprotein a-I Liposomes (Synthetic HDL) on Plasma-Lipoproteins in Patients with Low High-Density- Lipoprotein Cholesterol.* Nutr. Metab. Cardiovasc. Dis., 1995. **5**(2): p. 85-91.

120. Eriksson, M., et al., *Stimulation of fecal steroid excretion after infusion of recombinant proapolipoprotein A-I. Potential reverse cholesterol transport in humans.* Circulation, 1999. **100**(6): p. 594-8.

121. Bisgaier, C.L.R., W. V.; Lalwani, N. D.; Hartman, D.; Johansson, J., *Pharmaceutical formulations, methods and dosing regimens for the treatment and prevention of acute coronary syndromes*, U. PTO, Editor. 2008.

122. Dasseux, J.-L.O., D. C.; Ackermann, R, *Lipoprotein complexes and manufacturing and uses thereof*, USPTO, Editor. 2012.

123. *Effect of CER-001 on Atherosclerosis in Acute Coronary Syndrome (ACS) Patients - Efficacy and Safety: The CHI SQUARE Trial.*; Available from: https://clinicaltrials.gov/ct2/show/NCT01201837?term=CER001&rank=2
.

124. *Effect of CER-001 on Plaque Volume in Homozygous Familial Hypercholesterolemia (HoFH) Subjects (MODE).* Available from: https://clinicaltrials.gov/ct2/show/NCT01412034?term=CER001&rank=1.

125. Hovingh, G.K., et al., *The effect of an apolipoprotein A-I-containing high-density lipoprotein-mimetic particle (CER-001) on carotid artery wall thickness in patients with homozygous familial hypercholesterolemia: The Modifying Orphan Disease Evaluation (MODE) study.* Am Heart J, 2015. **169**(5): p. 736-742.e1.

126. *Exploratory Study of Plaque Regression (EXPRESS).* Available from: https://clinicaltrials.gov/ct2/show/NCT01515241?term=CER001&rank=3.

127. *Esperion Begins Multiple-Dose Study of ETC-642 (RLT Peptide) In Patients with Stable Atherosclerosis.*; Available from: http://www.prnewswire.com/news-releases/esperion-begins-multiple-dose-study-of-etc-642-rlt-peptide-in-patients-with-stable-atherosclerosis-71438847.html.

128. Chien, J.-Y.M., et al., *Low serum level of high-density lipoprotein cholesterol is a poor prognostic factor for severe sepsis.* Critical Care Medicine, 2005. **33**(8): p. 1688-1693.

129. Guo, L., et al., *High density lipoprotein protects against polymicrobe-induced sepsis in mice.* J Biol Chem, 2013. **288**(25): p. 17947-53.

130. Dassuex, J.-L., et al., *Apolipoprotein A-I agonists and their use to treat dyslipidemic disorders.* 1999: US.

131. Guo, L., et al., *Scavenger Receptor BI Protects against Septic Death through Its Role in Modulating Inflammatory Response.* J Biol Chem, 2009. **284**(30): p. 19826-34.

132. Smith, C.K., et al., *Lupus high-density lipoprotein induces proinflammatory responses in macrophages by binding lectin-like oxidised low-density lipoprotein receptor 1 and failing to promote activating transcription factor 3 activity.* Annals of the rheumatic diseases, 2016: p. annrheumdis-2016-209683.

133. Schwendeman, A., et al., *The effect of phospholipid composition of reconstituted HDL on its cholesterol efflux and anti-inflammatory properties.* Journal of lipid research, 2015. **56**(9): p. 1727-1737.

134. Coetzee, G.A., et al., *Serum amyloid A-containing human high density lipoprotein 3. Density, size, and apolipoprotein composition.* J Biol Chem, 1986. **261**(21): p. 9644-51.

135. de Beer, M.C., et al., *ATP binding cassette G1-dependent cholesterol efflux during inflammation.* J Lipid Res, 2011. **52**(2): p. 345-53.

136. Smart, E.J., et al., *A detergent-free method for purifying caveolae membrane from tissue culture cells.* Proc Natl Acad Sci U S A, 1995. **92**(22): p. 10104-8.

137. Schrodinger, LLC, *The PyMOL Molecular Graphics System, Version 1.3r1*. 2010.

138. Monticelli, L., et al., *The MARTINI coarse-grained force field: extension to proteins.* Journal of chemical theory and computation, 2008. **4**(5): p. 819-834.

139. Marrink, S.J., et al., *The MARTINI force field: coarse grained model for biomolecular simulations.* The Journal of Physical Chemistry B, 2007. **111**(27): p. 7812-7824.

140. Marrink, S.J., A.H. De Vries, and A.E. Mark, *Coarse grained model for semiquantitative lipid simulations.* The Journal of Physical Chemistry B, 2004. **108**(2): p. 750-760.

141. López, C.A., et al., *Martini coarse-grained force field: extension to carbohydrates.* Journal of Chemical Theory and Computation, 2009. **5**(12): p. 3195-3210.

142. López, C.s.A., et al., *Martini force field parameters for glycolipids.* Journal of Chemical Theory and Computation, 2013. **9**(3): p. 1694-1708.

143. Denisov, I., et al., *Directed self-assembly of monodisperse phospholipid bilayer Nanodiscs with controlled size.* Journal of the American Chemical Society, 2004. **126**(11): p. 3477-3487.

144. Segrest, J.P., et al., *A detailed molecular belt model for apolipoprotein AI in discoidal high density lipoprotein.* Journal of Biological Chemistry, 1999. **274**(45): p. 31755-31758.

145. Shih, A.Y., et al., *Molecular dynamics simulations of discoidal bilayers assembled from truncated human lipoproteins.* Biophysical journal, 2005. **88**(1): p. 548-556.

146. Klon, A.E., J.P. Segrest, and S.C. Harvey, *Molecular dynamics simulations on discoidal HDL particles suggest a mechanism for rotation in the apo AI belt model.* Journal of molecular biology, 2002. **324**(4): p. 703-721.

147. Pronk, S., et al., *GROMACS 4.5: a high-throughput and highly parallel open source molecular simulation toolkit.* Bioinformatics, 2013: p. btt055.

148. Shih, A.Y., et al., *Coarse grained protein-lipid model with application to lipoprotein particles.* The Journal of Physical Chemistry B, 2006. **110**(8): p. 3674-3684.

149. Shih, A.Y., et al., *Assembly of lipoprotein particles revealed by coarse-grained molecular dynamics simulations.* Journal of structural biology, 2007. **157**(3): p. 579-592.

150. Kumar, S., et al., *The weighted histogram analysis method for free-energy calculations on biomolecules. I. The method.* Journal of computational chemistry, 1992. **13**(8): p. 1011-1021.

151. Hub, J.S., B.L. De Groot, and D. Van Der Spoel, *g_wham□A Free Weighted Histogram Analysis Implementation Including Robust Error and Autocorrelation Estimates.* Journal of Chemical Theory and Computation, 2010. **6**(12): p. 3713-3720.

152. Levels, J.H., et al., *Distribution and kinetics of lipoprotein-bound lipoteichoic acid.* Infect Immun, 2003. **71**(6): p. 3280-4.

153. Levels, J.H., et al., *Distribution and kinetics of lipoprotein-bound endotoxin.* Infect Immun, 2001. **69**(5): p. 2821-8.

154. Zhang, Z., et al., *Apolipoprotein A-I mimetic peptide treatment inhibits inflammatory responses and improves survival in septic rats.* Am J Physiol Heart Circ Physiol, 2009. **297**(2): p. H866-73.

155. Dai, L., et al., *The apolipoprotein A-I mimetic peptide 4F prevents defects in vascular function in endotoxemic rats.* J Lipid Res, 2010. **51**(9): p. 2695-705.

156. Hack, C.E. and S. Zeerleder, *The endothelium in sepsis: source of and a target for inflammation.* Critical care medicine, 2001. **29**(7): p. S21-S27.

157. Lee, W.L. and A.S. Slutsky, *Sepsis and endothelial permeability.* N Engl J Med, 2010. **363**(7): p. 689-691.

158. Morin, E.E., et al., *HDL in sepsis - risk factor and therapeutic approach.* Front Pharmacol, 2015. **6**: p. 244.

159. Al-Zaidawi, S., *Presepsis biomarker: high-density lipoprotein.* Critical Care, 2014. **18**(Suppl 2): p. P77-P77.

160. Trinder, M., et al., *Cholesteryl Ester Transfer Protein Influences High-Density Lipoprotein Levels and Survival in Sepsis.* American Journal of Respiratory and Critical Care Medicine, 2018.

161. Roveran Genga, K., et al., *Two-year follow-up of patients with septic shock presenting with low HDL: the effect upon acute kidney injury, death and estimated glomerular filtration rate.* Journal of Internal Medicine, 2017. **281**(5): p. 518-529.

162. Genga, K.R., et al., *CETP genetic variant rs1800777 (allele A) is associated with abnormally low HDL-C levels and increased risk of AKI during sepsis.* Scientific Reports, 2018. **8**(1): p. 16764.

163. Hubsch, A.P., et al., *A reconstituted, apolipoprotein A-I containing lipoprotein reduces tumor necrosis factor release and attenuates shock in endotoxemic rabbits.* Circ Shock, 1993. **40**(1): p. 14-23.

164. Cue, J.I., et al., *Reconstituted high density lipoprotein inhibits physiologic and tumor necrosis factor alpha responses to lipopolysaccharide in rabbits.* Arch Surg, 1994. **129**(2): p. 193-7.

165. Wang, L., W.-Z. Chen, and M.-P. Wu, *Apolipoprotein A-I inhibits chemotaxis, adhesion, activation of THP-1 cells and improves the plasma HDL inflammatory index.* Cytokine, 2010. **49**(2): p. 194-200.

166. Quezado, Z.M., et al., *Therapeutic trial of reconstituted human high-density lipoprotein in a canine model of gram-negative septic shock.* J Pharmacol Exp Ther, 1995. **272**(2): p. 604-11.

167. Moreira, R.S., et al., *Apolipoprotein A-I mimetic peptide 4F attenuates kidney injury, heart injury, and endothelial dysfunction in sepsis.* Am J Physiol Regul Integr Comp Physiol, 2014. **307**(5): p. R514-24.

168. Cockerill, G.W., et al., *High density lipoproteins reduce organ injury and organ dysfunction in a rat model of hemorrhagic shock.* Faseb j, 2001. **15**(11): p. 1941-52.

169. Casas, A.T., A.P. Hubsch, and J.E. Doran, *Effects of reconstituted high-density lipoprotein in persistent gram-negative bacteremia.* The American surgeon, 1996. **62**(5): p. 350-355.

170. Chen, Y., et al., *Compositions and methods for treating cardiovascular related disorders*, U. PTO, Editor. 2015.

171. McDonald, M.C., et al., *Reconstituted High-Density Lipoprotein Attenuates Organ Injury and Adhesion Molecule Expression in a Rodent Model of Endotoxic Shock.* Shock, 2003. **20**(6): p. 551-557.

172. DiPiro, J.T., et al., *Pharmacokinetics of reconstituted human high-density lipoprotein in pigs after hemorrhagic shock with resuscitation.* Crit Care Med, 1996. **24**(3): p. 440-4.

173. Fink, M.P. and H.S. Warren, *Strategies to improve drug development for sepsis.* Nat Rev Drug Discov, 2014. **13**(10): p. 741-758.

174. Navab, M., et al., *Monocyte transmigration induced by modification of low density lipoprotein in cocultures of human aortic wall cells is due to induction of monocyte chemotactic protein 1 synthesis and is abolished by high density lipoprotein.* J Clin Invest, 1991. **88**(6): p. 2039-46.

175. Rye, K.A., et al., *The metabolism and anti-atherogenic properties of HDL.* J Lipid Res, 2009. **50 Suppl**: p. S195-200.

176. Tardif, J.-C., T. Heinonen, and S. Noble, *High-density lipoprotein/apolipoprotein A-I infusion therapy.* Current Atherosclerosis Reports, 2009. **11**(1): p. 58-63.

177. Langmann, T., et al., *Molecular Cloning of the Human ATP-Binding Cassette Transporter 1 (hABC1): Evidence for Sterol-Dependent Regulation in Macrophages.* Biochemical and Biophysical Research Communications, 1999. **257**(1): p. 29-33.

178. Tardy, C., et al., *HDL and CER-001 Inverse-Dose Dependent Inhibition of Atherosclerotic Plaque Formation in apoE-/- Mice: Evidence of ABCA1 Down-Regulation.* PLoS One, 2015. **10**(9): p. e0137584.

179. Albrecht, C., et al., *ABCA1 expression in carotid atherosclerotic plaques.* Stroke, 2004. **35**(12): p. 2801-6.

180. Katz, A., et al., *Safety, Pharmacokinetics, and Pharmacodynamics of Single Doses of LXR-623, a Novel Liver X-Receptor Agonist, in Healthy Participants.* The Journal of Clinical Pharmacology, 2009. **49**(6): p. 643-649.

181. Hong, C. and P. Tontonoz, *Liver X receptors in lipid metabolism: opportunities for drug discovery.* Nat Rev Drug Discov, 2014. **13**(6): p. 433-44.

182. Kirchgessner, T.G., et al., *Beneficial and Adverse Effects of an LXR Agonist on Human Lipid and Lipoprotein Metabolism and Circulating Neutrophils.* Cell Metab, 2016. **24**(2): p. 223-33.

183. Rosenson, R.S., et al., *Dysfunctional HDL and atherosclerotic cardiovascular disease.* Nature Reviews Cardiology, 2015. **13**: p. 48.

184. Huang, Y., et al., *An abundant dysfunctional apolipoprotein A1 in human atheroma.* Nat Med, 2014. **20**(2): p. 193-203.

185. Vaisar, T., et al., *Inflammatory remodeling of the HDL proteome impairs cholesterol efflux capacity.* Journal of Lipid Research, 2015. **56**(8): p. 1519-1530.

186. Schwendeman, A., et al., *The effect of phospholipid composition of reconstituted HDL on its cholesterol efflux and anti-inflammatory properties.* J Lipid Res, 2015. **56**(9): p. 1727-37.

187. Guo, Y., et al., *Perhexiline activates KLF14 and reduces atherosclerosis by modulating ApoA-I production.* J Clin Invest, 2015. **125**(10): p. 3819-30.

188. Denis, M., et al., *Expression, regulation, and activity of ABCA1 in human cell lines.* Mol Genet Metab, 2003. **78**(4): p. 265-74.

189. Davidson, W.S., et al., *The Effect of High Density Lipoprotein Phospholipid Acyl Chain Composition on the Efflux of Cellular Free Cholesterol.* Journal of Biological Chemistry, 1995. **270**(11): p. 5882-5890.

190. Francis, G.A., R.H. Knopp, and J.F. Oram, *Defective removal of cellular cholesterol and phospholipids by apolipoprotein A-I in Tangier Disease.* The Journal of Clinical Investigation, 1995. **96**(1): p. 78-87.

191. Bochem, A.E., et al., *ABCA1 mutation carriers with low high-density lipoprotein cholesterol are characterized by a larger atherosclerotic burden.* Eur Heart J, 2013. **34**(4): p. 286-91.

192. Aiello, R.J., et al., *Increased atherosclerosis in hyperlipidemic mice with inactivation of ABCA1 in macrophages.* Arterioscler Thromb Vasc Biol, 2002. **22**(4): p. 630-7.

193. Joyce, C.W., et al., *The ATP binding cassette transporter A1 (ABCA1) modulates the development of aortic atherosclerosis in C57BL/6 and apoE-knockout mice.* Proc Natl Acad Sci U S A, 2002. **99**(1): p. 407-12.

194. Wang, M.D., V. Franklin, and Y.L. Marcel, *In vivo reverse cholesterol transport from macrophages lacking ABCA1 expression is impaired.* Arterioscler Thromb Vasc Biol, 2007. **27**(8): p. 1837-42.

195. Cuchel, M., et al., *Pathways by which reconstituted high-density lipoprotein mobilizes free cholesterol from whole body and from macrophages.* Arterioscler Thromb Vasc Biol, 2010. **30**(3): p. 526-32.

196. Lorenzi, I., et al., *Lipidation of apolipoprotein A-I by ATP-binding cassette transporter (ABC) A1 generates an interaction partner for ABCG1 but not for scavenger receptor BI.* Biochim Biophys Acta, 2008. **1781**(6-7): p. 306-13.

197. Arakawa, R., et al., *Phosphorylation and stabilization of ATP binding cassette transporter A1 by synthetic amphiphilic helical peptides.* J Biol Chem, 2004. **279**(8): p. 6217-20.

198. Kučerka, N., et al., *Cholesterol in Bilayers with PUFA Chains: Doping with DMPC or POPC Results in Sterol Reorientation and Membrane-Domain Formation.* Biochemistry, 2010. **49**(35): p. 7485-7493.

199. Yancey, P.G., et al., *High Density Lipoprotein Phospholipid Composition Is a Major Determinant of the Bi-directional Flux and Net Movement of Cellular Free Cholesterol Mediated by Scavenger Receptor BI.* Journal of Biological Chemistry, 2000. **275**(47): p. 36596-36604.

200. Ma, C.-I.J., et al., *Tweaking the cholesterol efflux capacity of reconstituted HDL.* Biochemistry and Cell Biology, 2012. **90**(5): p. 636-645.

201. Guo, Y., et al., *Synthetic High-Density Lipoprotein-Mediated Targeted Delivery of Liver X Receptors Agonist Promotes Atherosclerosis Regression.* EBioMedicine, 2018. **28**: p. 225-233.

202. Zhu, Y., et al., *Oxidized LDL downregulates ATP-binding cassette transporter-1 in human vascular endothelial cells via inhibiting liver X receptor (LXR).* Cardiovasc Res, 2005. **68**(3): p. 425-32.

203. Wang, Y. and J.F. Oram, *Unsaturated fatty acids phosphorylate and destabilize ABCA1 through a phospholipase D2 pathway.* J Biol Chem, 2005. **280**(43): p. 35896-903.

204. Schultz, J.R., et al., *Role of LXRs in control of lipogenesis.* Genes Dev, 2000. **14**(22): p. 2831-8.

205. Honzumi, S., et al., *Synthetic LXR agonist inhibits the development of atherosclerosis in New Zealand White rabbits.* Biochimica et Biophysica Acta (BBA) - Molecular and Cell Biology of Lipids, 2011. **1811**(12): p. 1136-1145.

206. Terasaka, N., et al., *T-0901317, a synthetic liver X receptor ligand, inhibits development of atherosclerosis in LDL receptor-deficient mice.* FEBS Lett, 2003. **536**(1-3): p. 6-11.

207. Joseph, S.B., et al., *Synthetic LXR ligand inhibits the development of atherosclerosis in mice.* Proc Natl Acad Sci U S A, 2002. **99**(11): p. 7604-9.

208. Lim, R.K., et al., *Targeted Delivery of LXR Agonist Using a Site-Specific Antibody-Drug Conjugate.* Bioconjug Chem, 2015. **26**(11): p. 2216-22.

209. Zhang, X.-Q., et al., *Nanoparticles Containing a Liver X Receptor Agonist Inhibit Inflammation and Atherosclerosis.* Advanced Healthcare Materials, 2015. **4**(2): p. 228-236.

210. Yu, M., et al., *Targeted Nanotherapeutics Encapsulating Liver X Receptor Agonist GW3965 Enhance Antiatherogenic Effects without Adverse Effects on Hepatic Lipid Metabolism in Ldlr(-/-) Mice.* Adv Healthc Mater, 2017. **6**(20).

211. Sanchez-Gaytan, B.L., et al., *HDL-mimetic PLGA nanoparticle to target atherosclerosis plaque macrophages.* Bioconjug Chem, 2015. **26**(3): p. 443-51.

212. Ou, X., et al., *Liver X receptor agonist T0901317 reduces atherosclerotic lesions in apoE-/- mice by up-regulating NPC1 expression.* Sci China C Life Sci, 2008. **51**(5): p. 418-29.

213. Kappus, M.S., et al., *Activation of liver X receptor decreases atherosclerosis in Ldlr(-)/(-) mice in the absence of ATP-binding cassette transporters A1 and G1 in myeloid cells.* Arterioscler Thromb Vasc Biol, 2014. **34**(2): p. 279-84.

214. Dai, X.Y., et al., *The effect of T0901317 on ATP-binding cassette transporter A1 and Niemann-Pick type C1 in apoE-/- mice.* J Cardiovasc Pharmacol, 2008. **51**(5): p. 467-75.

215. Boisrame-Helms, J., et al., *Endothelial dysfunction in sepsis.* Curr Vasc Pharmacol, 2013. **11**(2): p. 150-60.

216. Steyers, C.M., 3rd and F.J. Miller, Jr., *Endothelial dysfunction in chronic inflammatory diseases.* Int J Mol Sci, 2014. **15**(7): p. 11324-49.

217. *Cardiovascular Diseases (CVDs)*. 2017; Available from: https://www.who.int/news-room/fact-sheets/detail/cardiovascular-diseases-(cvds).

218. Dunbar Sandra, B., et al., *Projected Costs of Informal Caregiving for Cardiovascular Disease: 2015 to 2035: A Policy Statement From the American Heart Association.* Circulation, 2018. **137**(19): p. e558-e577.

219. Lagu, T., et al., *Hospitalizations, costs, and outcomes of severe sepsis in the United States 2003 to 2007.* Crit Care Med, 2012. **40**(3): p. 754-61.

220. Rajendran, P., et al., *The vascular endothelium and human diseases.* Int J Biol Sci, 2013. **9**(10): p. 1057-69.

221. Rye, K.-A. and P.J. Barter, *Cardioprotective functions of HDLs.* Journal of Lipid Research, 2014. **55**(2): p. 168-179.

222. Dasseux, J.L., *Peptide/lipid complex formation by co-lyophilization*. 2001, US PTO.

223. Gille, A., et al., *CSL112 (Apolipoprotein A-I [Human]) Enhances Cholesterol Efflux Similarly in Healthy Individuals and Stable Atherosclerotic Disease Patients.* Arteriosclerosis, thrombosis, and vascular biology, 2018. **38**(4): p. 953-963.

224. Yuan, Y., et al., *Synthetic high-density lipoproteins for delivery of 10-hydroxycamptothecin.* International journal of nanomedicine, 2016. **11**: p. 6229-6238.

225. Tang, J., et al., *Influence of route of administration and lipidation of apolipoprotein AI peptide on pharmacokinetics and cholesterol mobilization.* Journal of lipid research, 2017. **58**(1): p. 124-136.

226. Wilkerson, B.A., et al., *Sphingosine 1-Phosphate (S1P) Carrier-dependent Regulation of Endothelial Barrier: High density lipoprotein (HDL)-S1P prolongs endothelial barrier enhancement as compared with albumin-S1P via effects on levels, trafficking, and signaling of S1P1.* Journal of Biological Chemistry, 2012. **287**(53): p. 44645-44653.

227. Sattler, K., et al., *Defects of High-Density Lipoproteins in Coronary Artery Disease Caused by Low Sphingosine-1-Phosphate Content: Correction by Sphingosine-1-Phosphate—Loading.* Journal of the American College of Cardiology, 2015. **66**(13): p. 1470-1485.

228. Matsuo, Y., et al., *Newly developed reconstituted high-density lipoprotein containing sphingosine-1-phosphate induces endothelial tube formation.* Atherosclerosis, 2007. **194**(1): p. 159-168.

229. Qi, X., et al., *Sustained delivery of sphingosine-1-phosphate using poly(lactic-co-glycolic acid)-based microparticles stimulates Akt/ERK-eNOS mediated angiogenesis and vascular maturation restoring blood flow in ischemic limbs of mice.* Eur J Pharmacol, 2010. **634**(1-3): p. 121-31.

230. Zhang, Q., et al., *Porous nanofibrous scaffold incorporated with S1P loaded mesoporous silica nanoparticles and BMP-2 encapsulated PLGA microspheres*

for enhancing angiogenesis and osteogenesis. Journal of Materials Chemistry B, 2018. **6**(42): p. 6731-6743.

231. Wacker, B.K., et al., *Delivery of Sphingosine 1-Phosphate from Poly(ethylene glycol) Hydrogels.* Biomacromolecules, 2006. **7**(4): p. 1335-1343.

232. Williams, P.A., K.T. Campbell, and E.A. Silva, *Alginate hydrogels of varied molecular weight distribution enable sustained release of sphingosine-1-phosphate and promote angiogenesis.* J Biomed Mater Res A, 2018. **106**(1): p. 138-146.

233. Das, A., et al., *Delivery of S1P receptor-targeted drugs via biodegradable polymer scaffolds enhances bone regeneration in a critical size cranial defect.* Journal of Biomedical Materials Research Part A, 2014. **102**(4): p. 1210-1218.

234. Galvani, S., et al., *HDL-bound sphingosine 1-phosphate acts as a biased agonist for the endothelial cell receptor S1P1 to limit vascular inflammation.* Sci Signal, 2015. **8**(389): p. ra79.

235. Yanagida, K. and T. Hla, *Vascular and Immunobiology of the Circulatory Sphingosine 1-Phosphate Gradient.* Annual review of physiology, 2017. **79**: p. 67-91.

236. Jeffery, D.R., et al., *Fingolimod: a review of its mode of action in the context of its efficacy and safety profile in relapsing forms of multiple sclerosis.* Expert Rev Neurother, 2016. **16**(1): p. 31-44.

237. Park, S.-J. and D.-S. Im, *Sphingosine 1-Phosphate Receptor Modulators and Drug Discovery.* Biomolecules & therapeutics, 2017. **25**(1): p. 80-90.

238. Keul, P., et al., *The sphingosine-1-phosphate analogue FTY720 reduces atherosclerosis in apolipoprotein E-deficient mice.* Arterioscler Thromb Vasc Biol, 2007. **27**(3): p. 607-13.

239. Nofer, J.R., et al., *FTY720, a synthetic sphingosine 1 phosphate analogue, inhibits development of atherosclerosis in low-density lipoprotein receptor-deficient mice.* Circulation, 2007. **115**(4): p. 501-8.

240. Kimura, T., et al., *Role of Scavenger Receptor Class B Type I and Sphingosine 1-Phosphate Receptors in High Density Lipoprotein-induced Inhibition of Adhesion Molecule Expression in Endothelial Cells.* Journal of Biological Chemistry, 2006. **281**(49): p. 37457-37467.

241. Fink, M.P., *Animal models of sepsis.* Virulence, 2014. **5**(1): p. 143-153.

242. Lewis, A.J., C.W. Seymour, and M.R. Rosengart, *Current Murine Models of Sepsis.* Surgical infections, 2016. **17**(4): p. 385-393.

243. Dejager, L., et al., *Cecal ligation and puncture: the gold standard model for polymicrobial sepsis?* Trends Microbiol, 2011. **19**(4): p. 198-208.

244. Buras, J.A., B. Holzmann, and M. Sitkovsky, *Animal Models of sepsis: setting the stage.* Nature Reviews Drug Discovery, 2005. **4**: p. 854.

245. Emini Veseli, B., et al., *Animal models of atherosclerosis.* European Journal of Pharmacology, 2017. **816**: p. 3-13.

246. Lee, Y.T., et al., *Mouse models of atherosclerosis: a historical perspective and recent advances.* Lipids in health and disease, 2017. **16**(1): p. 12-12.

247. Whitman, S.C., *A practical approach to using mice in atherosclerosis research.* Clin Biochem Rev, 2004. **25**(1): p. 81-93.